A Numerical and Experimental Investigation of Glass Fibre Reinforced Epoxy Pipes

By

Pål Einar Aasrum

Department of Mechanical Engineering

McGill University

Montréal, Quebec, Canada

June 1999

A Thesis submitted to the Faculty of Graduate Studies and Research in partial fulfilment of the requirements for the degree of Master of Engineering (thesis option)

0-612-55014-1

ABSTRACT

The offshore oil industry is constantly seeking new and more cost efficient solutions to every aspect of their operations. In the later years, use of polymeric composite materials has proven to reduce cost and enhance reliability in several areas of oil operations. Several independent efforts, notably in Europe and in the US have targeted development of both spoolable and segmented fibre reinforced polymer pipe systems. These composite pipe systems have been designed for high internal pressure applications, with additional loads being both static and dynamic.

In this research, the short-term, high strain, cyclic bending fatigue of spoolable glass-fibre reinforced epoxy pipes designed for high-pressure static chemical injection line service (SSI) was investigated. Bending and torsion fatigue loading may occur during pipe laying operations. Bending (static and fatigue) of composite pipe was simulated experimentally using a self-designed four-point bending jig on a 25 metric ton MTS hydraulic testing machine. Comparisons between experimental results, simple analytical and numerical static solutions were executed. Numerical solutions for static analysis were found using I-DEAS Master Series 5.0 finite element analysis software. The research effort also attempted to utilise a finite element software developed at McGill University to predict fatigue behaviour of the composite pipe.

Findings in this research effort assist understanding of short-term, high strain, fatigue behaviour of spoolable composite pipes designed for static high pressure operations, as well as indicate the validity of the finite-element analysis efforts executed in this research.

RÉSUMÉ

L'industrie pétrolière est constamment à la recherche de solutions novatrices dans tous ses secteurs d'opération et ce, afin de réduire ses dépenses. Au cours des dernières années, il a été démontré que l'usage de matériaux composites à matrice polymérique permet une réduction des coûts d'exploitation tout en améliorant la fiabilité de plusieurs aspects opérationnels. Plusieurs programmes indépendants de développement, notamment en Europe et aux États-Unis, ont concentré leurs efforts sur les marchés de tuyaux en composite polymérique embobinable ainsi qu'en composite polymérique segmentée. Ces systèmes de tuyau en composite ont été conçus pour répondre aux besoins d'applications sous haute pression interne, les contraintes externes étant de l'ordre statique et dynamique.

Cette recherche vise l'étude de la fatigue cyclique de grande amplitude, i.e. au nombre de cycles réduits, de tuyaux embobinables en fibre de verre à matrice de résine époxyde. Ceux-ci sont conçus pour une ligne de service d'injection chimique sous haute pression statique. Des sollicitations de fatigue en flexion ainsi qu'en torsion peuvent être observées lors d'opérations de mise en service. Le phénomène de flexion statique et dynamique du tuyau de composite a été simulé en laboratoire à l'aide d'un montage à flexion en quatre points et d'une machine hydraulique à essai MTS de 25 tonnes. Les résultats expérimentaux ont été comparés aux solutions analytiques et numériques obtenues. Des solutions numériques relatives à l'analyse statique ont pu être obtenues à l'aide du logiciel d'analyse I-DEAS Master Series 5.0. Un logiciel d'analyse par éléments finis développé par M. Shokrieh de l'Université McGill a aussi été utilisé afin de prédire le comportement en fatigue d'un tuyau en composite.

Les conclusions de cette recherche contribuent à mieux comprendre le comportement de tuyaux en composites polymériques embobinables, lesquels ont été conçus pour des applications opérant sous haute pression et sous des contraintes statiques et de fatigue. En sus, la recherche permet de valider les logiciels d'analyse et techniques de modélisation par éléments finis.

Acknowledgements

The author would like to thank Prof. L.B. Lessard for his supervision throughout the thesis work.

A thanks also goes out to Prof. J. Nemes for his willingness to discuss concepts and issues related to the research.

Sincere thanks also to all the technicians in the Measurement Lab, Machine Tool Lab and the Undergraduate Lab for their help with the experimental part of the thesis.

Special thanks goes to all my fellow graduate students; Hamid Eskandari, Louis Brunet, Stephanie Lalonde, Tareck Horchani, Matthew Roy, John McDougall, Adnan Golubovic, Camille Mesikeh, Jihad Megdokrief, Marta Slanik, and numerous others for being both discussion partners and friends. Also, to several undergraduate students, most notably Todd, Marc-André and Edmond.

I am also in debt to the management of NAT Compipe AS for giving me leave of absence from my position to pursue a Masters. The willingness to provide pipe samples for testing is also acknowledged. Discussions with my colleagues at NAT Compipe, Bent Asdal and Per Arne Haug in particular were also of great help.

Thanks to Anna Cianci for putting up with my questions and always being very helpful.

Finally, my parents, family and friends in Norway should have their share of gratitude for always being there for me and supporting my when I needed it most.

Table of Contents

Table of Figures

List of Tables

1 INTRODUCTION & LITERATURE REVIEW

1.1 Introduction

Exploration of oil and gas in offshore environment has through the past three decades expanded to become one of the world's biggest businesses. There is almost no region on the earth that has not been touched by its growth in one way or another.

Between the late 1960s and the middle of the 1980s many of the North Sea offshore fields discovered were large and could together with the high oil price justify high initial capital investments. In the last 10 - 15 years the new fields discovered have been of marginal character and hence not exploitable with conventional technology. Based on this knowledge, a research program[1] involving several of the most important operating companies in the North Sea offshore market was initiated aiming to develop and qualify technologically, economically and environmentally viable solutions for small and marginal oil and gas fields. One of these technologies was the development of Static Spoolable Composite Injection Lines (SSI)[2]. The concept is based on the some times advantageous feature of composite materials not exhibiting plastic deformation. Composites have proven to be cost efficient on a total life-cycle analysis basis[3, 4, 5]. The latter is mainly due to the non-corroding feature of fibre reinforced polymer composites and the corrosive environment that can be found in both onshore and offshore oil field operations.

SSI can be produced in continuous lengths of up to 40 km. This adds another advantageous feature to the product, no couplings. Connectors on composite materials have traditionally been a problem, but with this new technology, the problem is minimised and limited to the end-connectors.

In order to place the SSI on the seabed, several methods are available. Fortunately, SSI does not require development of special laying methods, as conventional methods currently employed by cable and pipe laying companies can be adapted. Laying of pipe in an offshore environment involves the use of lay barges or vessels (Figure 1); thus the reduced weight of the pipe spool also becomes a positive factor. SSI can be laid as a single pipe or part of a larger structure. In the first case, and in some instances the latter case, the SSI pipe will be the main load bearing structure while suspended in the sea, before it touches the bottom. The pipe will take a shape in the water roughly described by a catenary equation[6]. Due to the nature of the environment, the pipe will experience short-term dynamic loads, approximately similar to those seen by offshore riser systems. This will involve combinations of axial, torsional and bending load cases. The effect of some of these load scenarios on the SSI with respect to laminate behaviour and selected failure criteria will be investigated in this thesis.

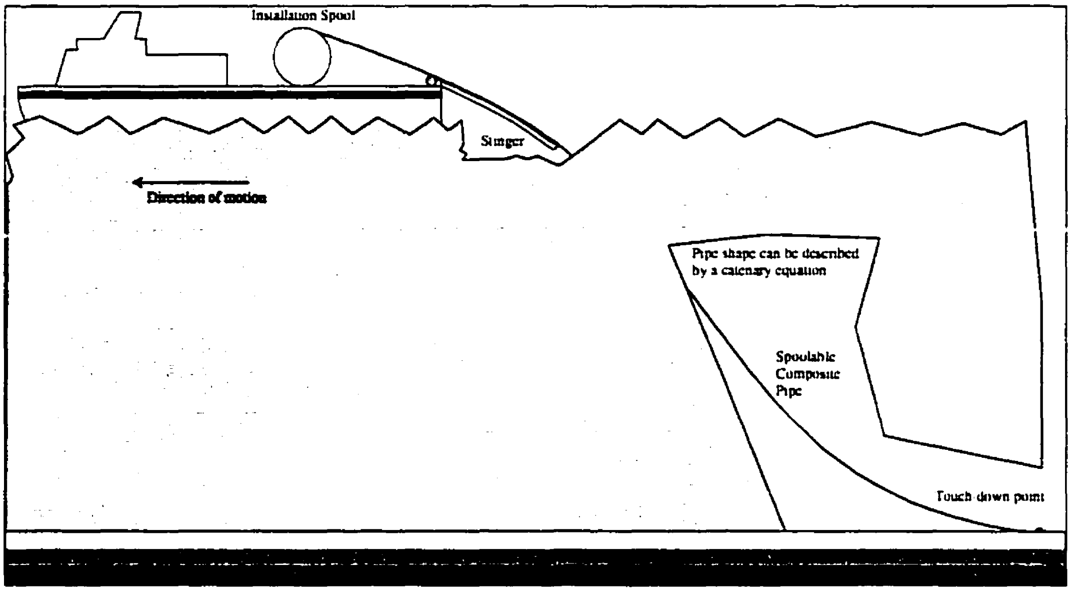

Figure 1 SSI Typical Laying Configuration

1.2 Literature Review

The concept of Spoolable pipe systems is roughly 45 years old. The very first use of spoolable pipe was by the allied forces during the Second World War. During landing operations in Normandy, a barge laid down steel pipes from the British coast to one of the landing beaches in Normandy. The pipelines were designed to carry fuel, and the concept was named PLUTO[7] (PipeLine Under The Ocean). This was the very first spoolable pipeline ever to be used.

Today, spoolable steel pipe is more or less a commodity in the oil industry. Pipelines of small to medium diameter are routinely laid down on the seabed, and coiled tubing[7] is routinely used to work over oil wells both onshore and offshore. The drive for increasingly cost efficient production and operational methods have made research and development efforts lucrative for the manufacturers of spoolable pipe systems.

In the last 10-15 years composite materials, more notably, polymeric composite materials have become increasingly interesting to the oil industry. This is due to the potential for weight and maintenance savings, directly transferable into increased cost efficiency. In 1979 a paper[8] outlining the use of spoolable composite pipes for the oil industry was published, focusing in particular on areas where the industry was operating offshore.

Since then, researchers world-wide, sponsored by most of the major oil companies, have looked into using composites for various components related to oil exploration. The use of composites in offshore oil operations currently includes simple walkway structures and other secondary structures, low pressure tanks and piping - including deluge systems for fire suppression, as well as high pressure tanks, vessels and pipes for both topside and subsea applications[9]. Companies like Lincoln Composites[17] have successfully designed, qualified and installed pressure vessels[10] with polymer composite structural laminates for operating pressures of 205 bar (3000 psi) and burst pressures of 1030 bar (15 000 psi). The same company, together with others such as Shell Oil Products Company, Conoco and Hydril has developed a composite production riser[i, 11, 12] and successfully tested the design according to thevarious oil operating companies requirements. Other developments include efforts to design and build drilling riser systems[13] to reduce top side weight and composite drill pipes[14] in order to be able to drill longer wells and hence reduce the need for subsea templates or even more expensive surface installations. A study by Conoco[15] identifies potential use and feasibility of composites on deep water platforms. It concludes that there are large potential cost savings through weight reductions and reduced maintenance. However, even though several systems are readily available for use now, more research is needed before composites can be used to their full potential.

Efforts more directly linked to the concept of spoolable composite pipes[16, 17] include the coiled tubing development effort by NAT Compipe AS in co-operation with Schlumberger Technology Services and the coiled tubing development by Fiberspar Inc[18] in co-operation with Haliburton Oil Field Services. Fiberspar have tested a 38.1 mm (1 1/2 inch) Outer Diameter (OD) composite hybrid pipe that can replace similar steel and titanium pipes currently being used for coiled tubing operations. The pipe sports an impressive burst pressure of 1120 bar (16250 psi), max tensile loading capacity greater than 7500 kg (16500 LBS), max compressive loading capacity of 5100 kg (11250 LBS) and is designed to operate safely for 5000 cycles of combined bending/pressure fatigue. NAT Compipe AS has successfully developed a 63.5 mm (2.5 inch) Inner Diameter (ID)[19] pipe for static applications, the SSI, with a service life of more than 20 years and an operating pressure of 380 bar (5000 psi). This corresponds to a virgin burst pressure of 1380 bar (20000 psi), an axial loading capacity in excess of 31600 kg. A static service and injection line is a static pipe that rests on the seabed. It can be a single line, or strapped together with, for example, a flowline. The pipe carries fluids to subsea templates and injects these into an oil well. These fluids may include

[i] A riser is a large diameter pipe going from the topside structure – the structure that is visible above the water line – to the seabed. These can be for operating purposes, when they carry well fluids etc, or have a multitude of smaller dimension pipes within carrying fluids to and from the sub-sea wells. All operations performed on the oil reservoir goes through these structures. Stiff and flexible riser systems exist. For an in-depth explanation refer to "Petroleum Engineering Handbook"

chemicals that, when injected enhance oil recovery, prevent hydrate formation, corrosion of metal pipes and valves etc. This pipe is now fully qualified to ASTM and operating companies standards. The first commercial contract for this pipe was received in January 1999 on 15 km pipe for the Åsgard field development in the North Sea. The pipe is available in inner diameters from 25.4 mm to 101.6 mm (1 – 4 inch), with ongoing efforts to increase the static long term pressure rating to above 500 bar. This is also the pipe that will be subject to investigation in this thesis report. In addition to these two areas of use for spoolable composite pipes, Compipe® pipes are being developed for Flowline and Dynamic Umbilical Composite Service and Injection Lines (DUCT). Dimension ranges from 101.6 to 254.0 mm (4 – 10 inch) ID for Flowlines to 63.5 mm to 101.6 mm (2.5 – 4 inch) ID for DUCT pipes. Flowlines are designed for well fluid transport; this includes crude oil and produced water, frequently H_2S, CO_2, acids from formation cracking as well as a multitude of other chemicals. DUCT pipes are designed for, for example, injection of methanol or glycol. While Flowlines are static pipes resting on the seabed, DUCT pipes may be part of a bundle of pipes and also often electro-hydraulic control lines, going from a production platform or floating operating and production ship to a sub-sea template. These DUCT lines will experience constant dynamic loading.

Fatigue of composite laminates has been investigated by numerous researchers[20, 21, 22] and continues to be a highly focused research area. Understanding fatigue is one of the key elements to making composite materials readily acceptable by the engineering community. Fatigue in multi-directional laminates, that is a laminate built up from several plies of unidirectional composite material has, in most cases, been found to be initiated by microcracks in the off-axis plies running parallel to the fibre direction. Formation of these cracks is a random occurrence, with the probability of their formation increasing with increasing transverse tensile stress, as described by Gao[23]. These micro-cracks cause loss of tensile and shear stiffness, but not immediate catastrophic failure. It is also interesting to note that the crack density reaches an asymptotic saturation state, the characteristic damage state (CDS), and exhibits rough regular patterns. A simple failure analysis using a ply level failure criterion is described by the Tsai-Hill theory[24]. The theory determines first ply failure to be matrix mode and subsequently assumes the transverse Young's modulus and axial shear modulus to be reduced to zero. Then a new stress analysis of the laminate is performed based on the reduced stiffness from the failed ply. The next ply to fail is then identified and a new reduced stiffness matrix calculated and so on. A more detailed description of the model presented by Gao[23] is included in the chapter dealing with fatigue (Chapter 5) where cumulative damage models will also be discussed. Other models that will be examined in Chapter 5 includes those presented by J. Lee et al[25], J. Botsis et al[26], Shokrieh et al[27].

Frost et al[28] examined the failure mechanisms of cyclic and static fatigue (by using internal pressure) of filament wound GRE pipes. They found that in all cases, failure was controlled by matrix cracking through a combination of through-thickness matrix cracking and ply delamination. Other researchers investigated failure of CFRP pipes due to combined compression and torsion and found the failure mechanism to be plastic micro-buckling[29]. Micro-buckling is defined as a plastic shear instability that occurs by rotation of initially misaligned fibres within a well defined band. Visual identification of failure mechanisms, such as matrix cracking and plastic micro-buckling will be attempted.

As will be come evident, the SSI pipe should be considered thick walled. Treatment of the SSI pipe as a thick-walled composite pipe would have enabled a more accurate numerical and analytical analysis of the pipe structure, as through thickness strains and stresses would have been accounted for. Analysis of thick-walled[30, 31, 32, 33] composites requires the use of more elaborate stress analysis descriptions as well as failure criterion[34, 35].

1.3 Summary of Objectives

The aim of this thesis is to investigate the effect of combined loads, in a quasi-fatigue mode on Spoolable Composite Line (SSI), simulating the relatively short-term exposure to dynamic loads as seen by the SSI pipe during laying. Short-term fatigue damage, with particular emphasis on selected failure mechanisms and investigation of crack growth in the laminate due to the selected loading scenarios, is examined. The goal is to aid understanding of fatigue behaviour of SSI pipes under multi-axial loading and give insight into design of pipes and tubes for use in dynamic applications.

The thesis is divided into three parts: initial analytical evaluations, numerical analysis and specimen testing. Initial analytical analysis is performed to obtain data on the composite pipe prior to starting numerical analysis. Numerical analysis is performed for selected static and fatigue cases. Static analysis is first done for a pipe structure using I-DEAS Master Series 5.0[36], followed by local analysis of selected critical sections using a Finite Element code developed at McGill[37]. Following static analysis, fatigue analysis of the critical section is performed, using a Finite Element code developed at McGill [37]. Test results are then used to corroborate the numerical analysis results.

2 PIPE STRUCTURE AND DATA

A number of pipe mechanical properties have been determined for the Compipe® pipe as part of the spoolable composite pipe SSI qualification program. The most relevant of these for this research effort are listed below (Table 1 and Table 2).

One of the basic design criteria for the SSI pipe is the maximum allowable axial strain at the surface of the composite pipe. This parameter is directly linked to the minimum allowable spooling diameter, and hence the size of the spool or reel that can be utilised. During the initial qualification program, this was set to 0.6% (in the axial direction of the pipe in the surface ply, equivalent of a spooling diameter of 15 m). Later developments and qualification programs by NAT Compipe AS has increased this allowable strain level to 1.0% (spooling diameter of 9.1 m)[38].

Pipe structure is $[0_{2.3mm} / \pm 78_{8.45mm}]_T$. Figure 2 provides a sketch of a generic spoolable composite pipe structure. Number of plies, their angles, thickness, material composition etc., can be varied. The pipe being investigated in this research has a total of 9 plies. The constituent materials are glass-fibre and epoxy, with the inner liner being cross-linked polyethylene.

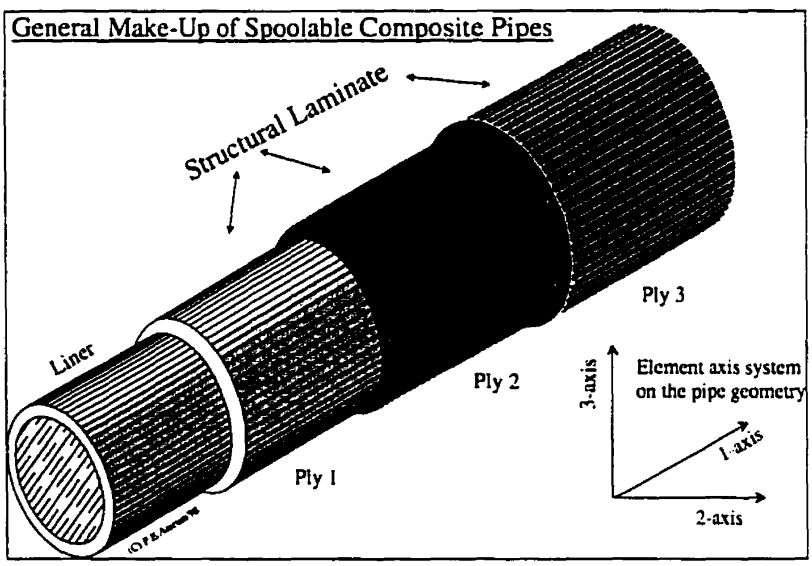

Figure 2 Typical Lay-Up of a Spoolable Composite Pipe.

Table 1 SSI Pipe Dimensional Properties

Pipe Dimensions:	34.75 mm	Inner radius (laminate) (IR)
	45.50 mm	Outer radius (laminate) (OR)

Table 2 SSI Selected Pipe Properties[39]

Hoop Tensile Modulus	35	GPa	API 15 HR, Appendix D
Axial Tensile Modulus	11.5	GPa	ASTM D-2105
Ultimate Axial Strength	>31[ii]	kN	ASTM D-2105
Glass fibre Content	60	% Vol	ASTM D-2584
Short Term Failure Pressure	1355	Bar	ASTM D-1599
Pressure Rating[iii]	350	Bar	ASTM D-2992 (Modified)
Poisson's Ratio (Hoop/Axial)	0.12 (@ 120 kN)	-	API 15HR. Appendix D
Poisson's Ratio (Axial/Hoop)	0.19 (@ 500 bar)	-	ASTM D-2105

As a precursor to testing of spoolable composite (GRE) pipes, a set of analytical calculations were performed to determine the effect of various load scenarios on the composite pipe. This is a first approximation of the behaviour of the pipe (prior to testing) and may limit risk to people and equipment.

Two *equivalent material* constants were determined analytically[40] for the laminated pipe as part of the initial work on the thesis. These include (Table 3):

Table 3 Analytically Determined Equivalent Material Constants for SSI pipe[40]

D_x (equivalent of EI_x)	31143[iv]	$Pa{*}m^4$	Bending Stiffness
GJ_{equiv}	20670[iv]	$Pa{*}m^4$	Torsional Stiffness

The values in Table 3 can now be used in beam equation calculations as found in any text on solid mechanics or mechanics of materials[41], or equivalent reference book[42].

For a review of the calculations leading to the equivalent bending stiffness, refer to APPENDIX B, and for torsional stiffness to APPENDIX C.

Terminology and definitions for the equations used can be found in APPENDIX E.

[ii] Attempts to pull the pipe to failure have so far been unsuccessful due to equipment limitations
[iii] 20 years service life
[iv] Material properties of uni-directional composite plies vary somewhat. This may in some cases give rise to range describing both bending and torsional stiffness.

3 BENDING OF PIPE

Four-point bend testing of SSI will be performed as part of this research. By exposing SSI specimens to four-point bending, a region with constant bending moment, and hence constant curvature is, in theory, created between the points of load application. Behaviour due to bending and bending radius is used by NAT Compipe AS as one of the basic design criteria for spoolable composite pipes, and is a parameter that can be compared with existing results.

3.1 Analytical Solution

Assuming that the SSI pipe can be treated as a thin composite tube and as a simple beam[40], the following set of equations can be used to obtain an analytical solution for bending of SSI. It was assumed that plane sections remain plane, and that the cross-section is uniform.

Equation 1[40]

$$M_1 = D_x \times k_1 = D_x \times \frac{1}{R}$$

The conventional version of Equation 1 can be found in any book on mechanics of materials[41], with D_x (Equation 1) exchanged for EI.

The induced stress at anyone point in the composite pipe structure, can then be determined using Equation 2 below.

Equation 2[40]

$$\sigma_1^k = Q_{11}^k \times \left(e_1^0 + x_3 \times k_1\right) = Q_{11}^k \times \varepsilon_1$$

In this case, we do not apply a load causing in-plane strain, hence the in-plane strain is ignored, and only strain induced from bending considered.

Bending axial surface strain can be found using the equation below:

Equation 3

$$\varepsilon_1 = \frac{Y}{R}$$

For a composite cylindrical pipe D_x is the equivalent bending stiffness (EI) engineering term[40]. D_x was found to be *31143* Pa*m^4 (Table 3). Assuming the second moment of inertia

(I) for a pipe section to be constant, we find the equivalent isotropic elastic modulus (E) for the pipe to be 14.0 GPa.

Table 4 Summary of Spoolable Composite Pipe Properties

D_x	31143	$Pa*m^3$
I	2.22*10-6	m^4
E	14.0	GPa

To find the induced off-axis stress in the surface of the pipe the following values where used:

Table 5 Values for strain and radius of curvature, related to Equation 3

ε_l	0.006	-
R	7.5	m
Y	45.5	mm

According to Equation 3, a pipe bending radius (R) of 7.5 m with the distance to the neutral axis (Y) being $45.5*10^{-3}$ m, gives an axial off-axis surface strain of 0.6%. By using the relevant Q^k_{11} values for off-axis stresses in the laminate can be found. These can in turn be transformed[46] to on-axis values and used to determine the stress state in each layer of the laminate.

Using beam theory for deflection of an elastic straight beam with the left end guided and the right end simply supported (see Figure 3), we find the following equations to hold[42]:

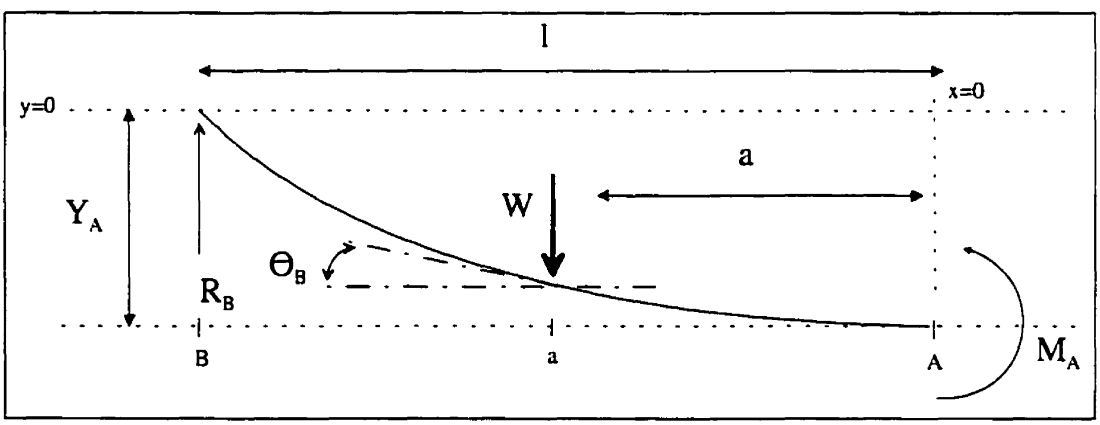

Figure 3 Illustration of a simply supported one side guided beam as depicted in Roraks[42]

Equation 4

$$Y_A = \frac{-W(l-a)}{6*EI} * \left[2*l^2 + 2*l*a - a^2\right]$$

By manipulating Equation 4 to find the deflection of the pipe at the point of load application a distance x from the guided, or maximum, deflection point we get Equation 5[42].

Equation 5

$$Y_a = Y_A + \frac{M_A * x^2}{2 * EI}$$

Equation 6[43]

$$M_A = W(l - a)$$

Y_a is measured experimentally and can be used to evaluate the accuracy of the analytical solution.

Letting Equation 1 be equal to Equation 6 it becomes possible to make use of the bending diameter and the equivalent bending stiffness (D_τ) to find the applied load for four-point bending.

Equation 7

$$\frac{EI}{W(l-a)} = R \Rightarrow W = \frac{D_\tau}{R(l-a)}$$

By using the equivalent engineering flexural modulus, D_τ for EI, we find the applied load, W, to be 12294 N for l = 0.45 m, a = 0.15 m and D = 15 m. The bending moment, M_A is then found to be 3688 Nm. From Figure 3, Equation 4 and Equation 5 we find the deflection at the point of load application to be Y_a = 8.9 mm, and at Y_A to be 10.2 mm.

Table 6 Summary of Calculated Data for SSI Pipe at Given Applied Load

R	7.5	m
L	0.45	m
A	0.15	m
M_A	3688	Nm
ε_l	0.607	%
W	12294	N
D	15.0	m
Y_A	10.2	mm
Y_a	8.9	mm

Using simple beam equations, as can be found in any mechanics of material[41] text book, the stresses in the top surface of the SSI can be estimated. The relationship used is:

Equation 8

$$\frac{M}{I}=\frac{\sigma}{Y}=\frac{E}{R}\Rightarrow\frac{EI}{R}=\frac{\sigma I}{Y}\Rightarrow\frac{D_x}{R}=\frac{\sigma I}{Y}\Rightarrow\sigma=\frac{D_x\times Y}{R\times I}$$

In short, like Equation 1[40] , the relationship between bending moment (M) and bending stiffness gives the bending radius:

Equation 9

$$\sigma_l = E * \varepsilon_l$$

By keeping D_x as 31143 Pam^{1}, and finding $I = 2.22*10^{-6}$ m^{4}, with R = 7.5 m and $Y = 45.5*10^{-3}$ m we get

σ_l = 85.1 MPa

We find the longitudinal axial strain to be ε_l = 0.607% corresponding to an axial stress of σ_l = 85.1 MPa in the top ply. This again corresponds to roughly 83.2 MPa on-axis stress in the y or matrix direction, and 17.7 MPa in the x or fibre direction. An outline of stress and strain transformations can be found in reference number 46.

These numbers will be compared with numerical analysis results in the preceding chapter.

3.2 Numerical I-DEAS[36] Analysis

Static numerical analysis of the SSI pipe was performed for four-point bending in order to obtain deflection, stress and failure index values that could later be compared with results from the Finite Element Analysis fortran code written by Mahmoud M. Shokrieh[37] as part of his PhD work.

A simple pipe section was created and meshed using the I-DEAS Master Series 5.0 software[36]. Simple four-node, thin shell elements with laminate properties were used.

3.2.1 Finite Element Model

A numerical solution was obtained from a map meshed pipe section corresponding to the size of the SSI section later to be used for experimental evaluation. The aim was to simulate a four-point bending situation hence it was necessary to use at the very minimum a pipe of 450 mm. This length corresponded to modelling of one half of a pipe exposed to four-point bending. Numerical simulation runs using a 1000 mm model was also executed.

A number of simulations where run at various loads to obtain data points to plot at curve. Not surprisingly the data points painted a straight line, as one would expect for a static linear analysis case.

An example is henceforth described: A force corresponding to bending moment expected to give a radius of curvature of 7.5 m (an axial (off-axis) strain of 0.6%) was applied over 12 nodes. The nodes where situated 150 mm from the far end (what would be the centre of a pipe in four point-bend) of the pipe section. The force applied was 1.02 kN on each of the 12 nodes (or a total of 12294 N). This corresponds to an applied load (total in four-point bending) of approximately 2506.42 kg.

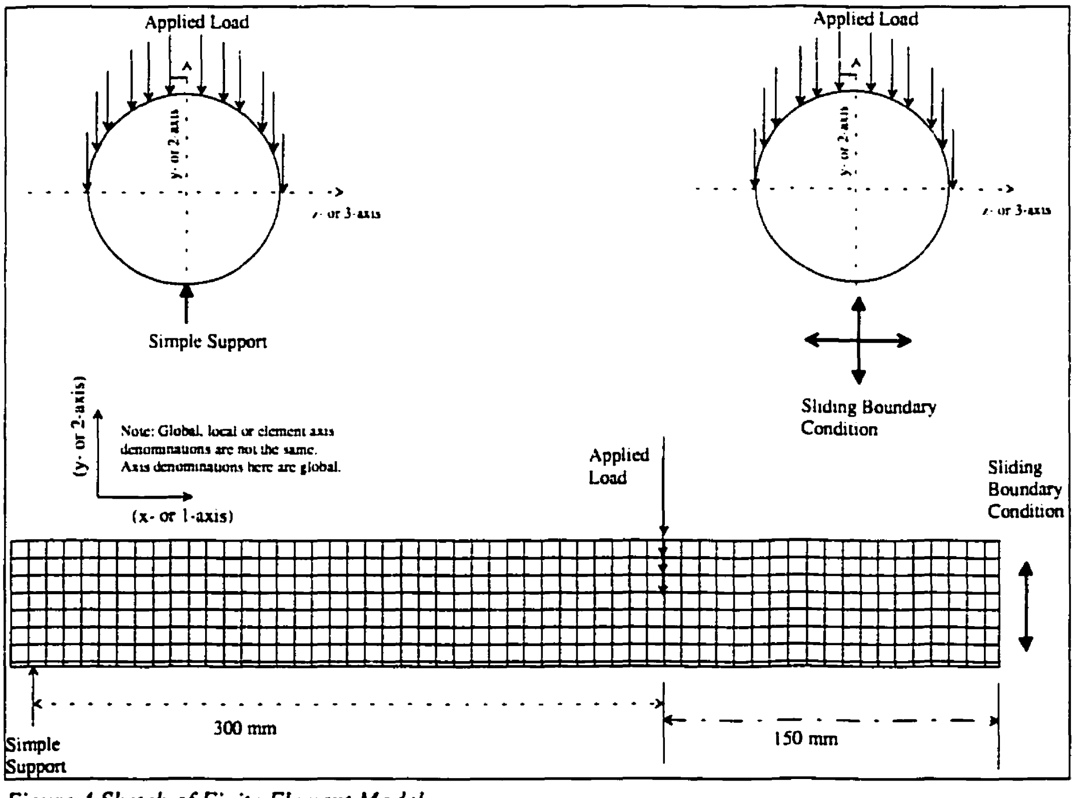

Figure 4 Sketch of Finite Element Model

A co-ordinate system was set by the FEA software so that the global z-axis was aligned with the longitudinal pipe axis, the x-axis defined the horizontal plane (x-z) and the y-axis such that it would define the vertical. The far end (centre of the pipe)of the pipe was restricted to move in any direction except the y-direction. The closed end was hinged (pin) about the lowest node (in the y-direction) to simulate a simply supported case. These boundary conditions should simulate a 900 mm long pipe, simply supported at the ends exposed to 4-point bending with a distance of 300 mm over which the bending moment and radius of curvature are constant (Figure 3).

By creating overlaying curves it is possible to examine the difference between the analytical and numerical analysis results.

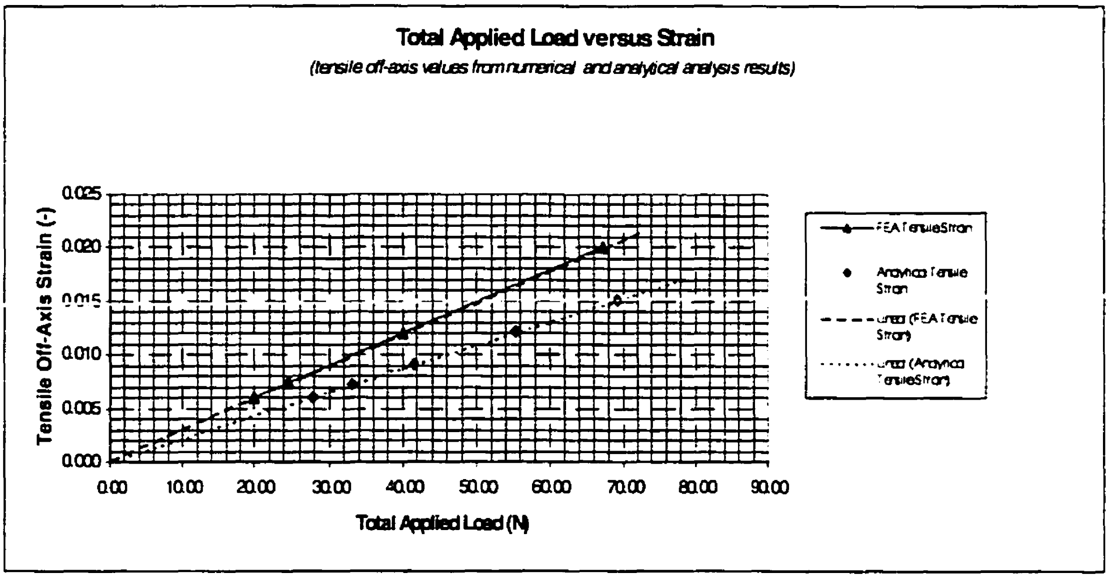

Figure 5 Total Applied Load versus Off-Axis Axial Strain at the Outer Most Surface of the Pipe

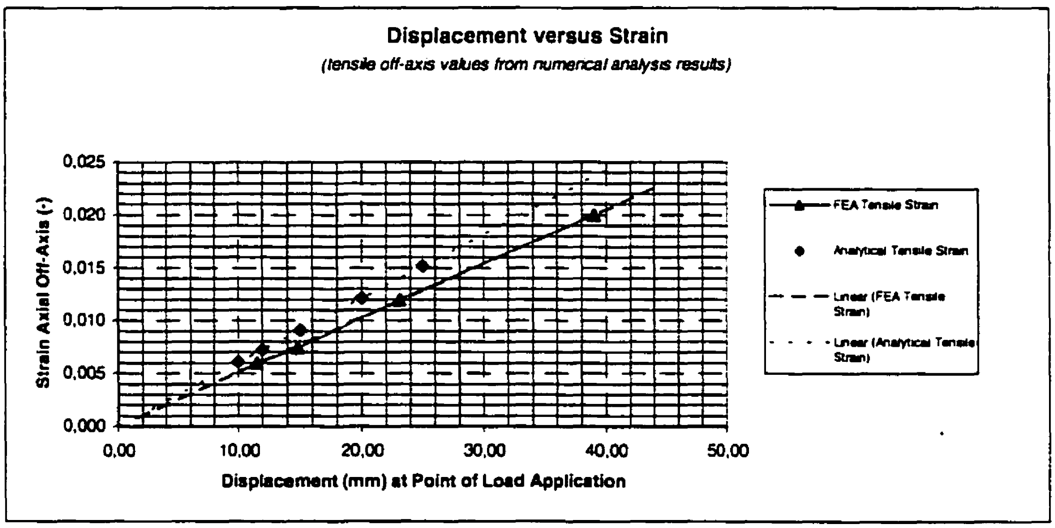

Figure 6 Displacement at Point of Load Application versus Tensile Off-Axis Axial Strain at the Outer Most Surface of the Pipe

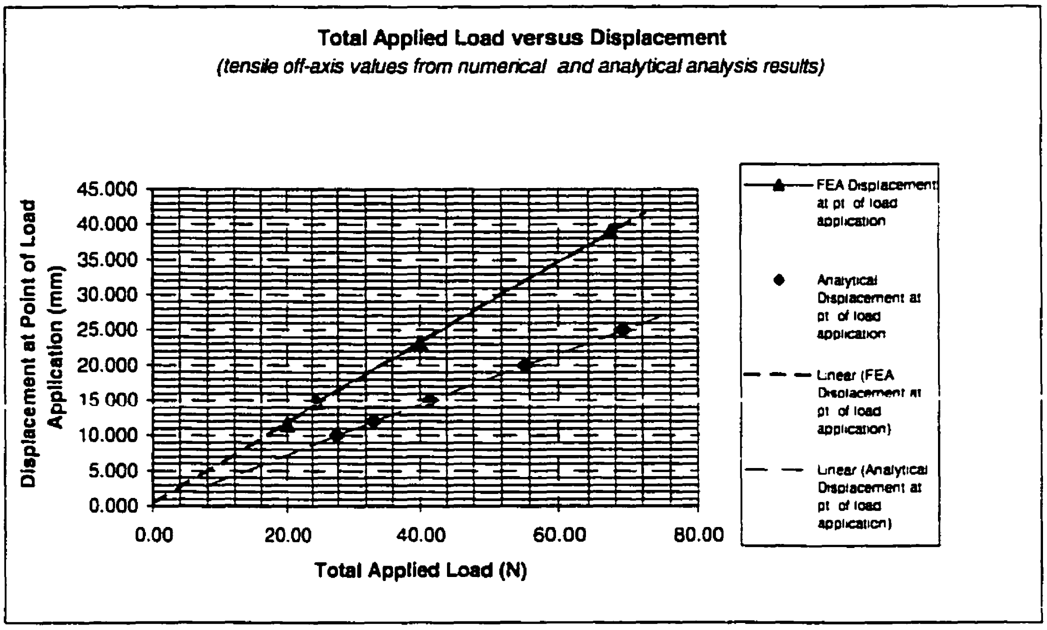

Figure 7 Total Applied Load versus Displacement at Point of Load Application for Analytical and Numerical Analysis

As we can see from the above curves (Figure 5 to Figure 7) and the table below (Table 7), there are noticeable differences between the analytical and numerical analysis results.

Table 7 Selected Values for Strain, Displacement and Total Applied Load from Analytical and Numerical Analysis.

Strain	Displacement (mm)			Total Load (kN)		
(-)	Analytical	FEA	Difference[v]	Analytical	FEA	Difference[v]
0.006	10.0	11.5	15%	28.0	20.0	-28.6%
0.010	16.5	19.5	18%	46.0	33.0	-28.3%

Numerical displacement is about 15% larger than the analytical, and the numerical total applied load 28% lower than the analytical value for a given off-axis surface strain.

Table 8 FEA Longitudinal Off-Axis strain values for pure bending @ 24.6kN applied load[vi]

Ply No.	Angle		ε_l (-)
9	78°	Top (compressive)	-0.0073
		Bottom (tensile)	0.0074

[v] Percentage difference calculated using the analytical analysis value as basis.
[vi] From numerical analysis result

The strain values in Table 8 are different on the 4^{th} digit after the decimal point. This difference in compressive and tensile pipe surface strain is most likely due to errors in the FE model and FE analysis. The difference is however so small, that it can be considered insignificant.

Table 9 FEA Off-Axis stress values for pure bending @ 24.6 kN applied load[i]

Ply No.	**Angle**		**σ_t (MPa)**
9	78°	Top (compressive)	-58
		Bottom (tensile)	59

Again, Table 9 shows off-axis stress values in the outer most surface of the pipe, as found from the numerical analysis results using I-DEAS[36]. The one MPa difference between the tensile and compressive pipe face surface stress is not significant, and can probably be contributed to small errors in the FE model.

On-axis stress and strain values can be used to determine the theoretical state of a laminate, or whether or not failure of lamina components has occurred. Several failure criteria are available for such analysis. The best known includes[40(Chapter 7)]:

- Maximum Stress
- Maximum Strain
- Tsai-Wu (Quadratic)
- Hashin

A section on failure analysis of the SSI pipe is included in the next section.

The FE analysis also gives the on-axis stresses and strains for any ply. Since the future experimental set-up only enable measurements of surface strains at best, only stresses and strains from the external/surface ply will be presented here (Table 10 and Table 11).

Table 10 FEA On-Axis strain values for pure bending @ 24.6 kN applied load

Ply No.	**Angle**		**ε_x (-)**	**ε_s (-)**	**ε_y (-)**
9	78°	Top	0.00036	0.0033	-0.0070
		Bottom	-0.00035	-0.0033	0.0070

Table 11 FEA On-Axis stress values for pure bending @ 24.586 kN applied load

Ply No.	Angle	σ_x (MPa)	σ_s (MPa)	σ_y (MPa)
9	78° Top	-0.5	11.5	-56
	Bottom	0.75	-11.5	56

From the above analysis efforts we can conclude that, although there are differences between analytical and numerical results, the data presented gives a reasonable description of the behaviour of the pipe in four-point bending. This with respect to both deflection (measured as displacement) and the induced stresses in the pipe structure.

Recognising that the correlation between numerical and analytical solutions are only reasonable, the following explanations are offered:

- Material properties of composite materials are different in different directions. Most notable is the higher compressive strength in matrix direction of a unidirectional ply[44,45]. As the pipe laminate consists of mostly hoop plies it is quite likely that the contribution from the matrix, which is not included in the analytical analysis affects the results.
- The pipe is modelled using thin shell elements. Examining the dimensions of the pipe, we find that the laminate is so thick (larger than 10mm) and the diameter sufficiently small, that use of orthotropic solid elements probably would have been more correct.
- Finally, the analytical set of equations used did not take into account shear effects in the laminate or induced through thickness stresses and strains due to four point bending.

In retrospective, a number of actions could have been taken to investigate the suitability of a thin shell model for the problem at hand. Firstly, a pipe of the same physical dimensions but with isotropic material properties should have been analysed. This would most probably have given numerical values to argue for the use of alternative element formulations. Numerical analysis using an isotropic material would also have allowed for optimisation of the mesh, and hence given a more effective solution process.

The thin shell model was chosen because the idea was to use these results as guidelines only for use in a more rigorous numerical analysis using a FE code developed at McGill[37] using solid orthotropic elements. The thickness of the pipe wall is such that through thickness effects should have been included in the calculations.

3.2.2 Failure Analysis

The Maximum Stress Criterion[40, 46] was utilised to identify failures in the pipe laminate due to the applied load.

Failure of the SSI pipe is clearly most plausible in the surface ply. Therefore Table.12 shows values for Maximum Stress Failure Criterion for ply number 9 only. The R_y-value is the smallest, indicating that the first onset of failure will be on the tensile face of the pipe as tensile matrix cracking. Ply 9 will fail in matrix tension in the bottom part of the pipe. Personal experience from bend testing of SSI pipe confirms this first initial failure mode. However, this constitutes by no means failure of the pipe as such. The SSI pipe is designed to operate with matrix cracking as an integral part of the structure. In real life, matrix cracks are induced when the SSI pipe is spooled during manufacturing, and when the SSI is spooled onto the transport spool. As will become apparent later, testing also revealed the SSI pipe to be able to survive surface strains in excess of 1%.

Table.12. Selected FEA Maximum Stress Criterion R-values @ 24.6 kN applied load

Ply no. / Top or Bottom	R_X	R_S	R_Y
9 (78°) Top	1220 (C)	5.2	2.1 (C)
9 (78°) Bottom	1467 (T)	5.2	0.89 (T)

We can henceforth conclude that although the Maximum Stress Criterion correctly identifies the mode of failure, failure sequence and, reasonably accurately, the stress in the laminate when matrix cracking is initiated, the Maximum Stress Criterion does not describe ultimate failure of the SSI pipe. Examination of the other available failure criteria renders the same result. This means for the SSI pipe, that matrix cracks, up to a certain size, are not the mode of damage that causes final failure of the SSI pipe. At this moment in time, no alternative failure criteria is known that correctly identifies the first onset of final failure of SSI pipes.

The idea of accepting matrix micro-cracks as part of a composite structure design is likely to be foreign to many, in particular the aerospace industry. However, the oil industry has accepted this as part of the inherent behaviour of composites and the increasing use of composites in the oil industry supports this[5].

3.2.3 Element Formulation Discussion

Thin shell elements assumes the structure to be thin in one direction. In this case, we have a pipe structure with a radius to wall thickness ratio of about 3.7, this does not constitute a thin wall. Thus, the assumptions done for thin shell elements[47]

- Through thickness stress is zero

- In the Kirchhoff formulation with shear deformations and a straight line perpendicular to the midsurface of the shell remains perpendicular during deformations

These assumptions ignores the presence of potential through thickness strain and stress, thus a numerical model will be unable to detect failures where through thickness effects are dominant. Further more, plane stress and plane strain elements assumes a two dimensional stress state to be present, that is, given that x-y describes the shell or membrane, zz, zx and zy components are zero. Obviously, in the case of a thick wall this is not the case. There will be through thickness strains and stresses in the SSI pipe.

An improved FE model would make use of elements where through thickness effects are taken into account, such as solid orthotropic elements. For a linear analysis, an 8 node three-dimensional element would have been appropriate. Such a model was attempted built, but the not successfully so due to computing power limitations. The I-DEAS FE software has a laminate shell element formulation that allows for building a shell model with a number of plies in one shell. This element made it possible to build the model, as described in this section, and still perform numerical analysis. Building a FE model with three-dimensional elements required at least double the number of elements, and the hardware proved unable to execute such analysis.

3.3 Summary

Although there are obvious differences between the analytical and numerical analysis results in the above chapters (3.1 and 3.2), the results are considered sufficient to continue on with further numerical analysis using non-linear static and fatigue analysis finite element codes.

More in-depth explanations for discrepancies between analytical and numerical analysis results, as well as differences between analytical, numerical and physical test results exist. In-depth explanations of are not part of the abstract for this research. For a comprehensive text on finite element analysis, refer to Bathe[47]. In brief, the analytical solution assumes that all loads and reactions are perpendicular to the axis of the beam, and lie in the longitudinal plane of symmetry. This allows for calculation of longitudinal axial stress and transverse shear. Shell elements include reactions due to for example bending in the longitudinal axial (or fibre direction), transverse (here referred to as matrix), and in-plane shear direction. In-plane refers to the plane in which the fibres are distributed. These are obvious differences between the beam formulation and the FE formulation.

Failure analysis is correct in identifying failure modes and their onset, but incapable of describing the severity of, in this case, micro-matrix cracking on the pipe structure as a whole.

4 DAMAGE MODELLING

4.1 Static and Progressive Fatigue

Two fortran codes were developed by Shokrieh[37] as part of his PhD research for modelling of fibrous composites failure behaviour. These codes were used to model the static and cyclicbehaviour of SSI under selected load cases.

Extensive efforts targeted modifications of the original codes in order to obtain a more versatile analysis tool. Unfortunately it was found to be impossible within the time frame and scope of work set forth in this thesis to pursue modifications enabling a full fledged three-dimensional finite element analysis code. Efforts were instead put into enabling loading in all three directions on a plate structure. Having successfully done so, for both the static and fatigue codes these were put into use performing analysis on critical segments of the structure as determined previously by I-DEAS analysis.

Both the static and fatigue codes use 20 node (parabolic) solid, orthotropic, brick elements in the analysis. Three-dimensional analysis is henceforth enabled for each individual element. This also required utilisation of a suitable set of failure criteria. Hashin-type criteria were found to be ideal for this purpose[37(Chapter 4)]. Hence, a quadratic polynomial stress based criterion based on Hashin, capable of distinguishing between different modes of failure, was developed by MMS et al[37]. For exact descriptions of these, the interested reader is referred to MMS Ph.D. thesis for a detailed review or to the following sub-chapter for a brief description. For now it suffices to say that the criteria are fully able to detect the following seven (7) defined failure modes:

- Fibre Tension
- Fibre Compression
- Fibre-Matrix Shearing
- Matrix Tension
- Matrix Compression
- Normal Tension
- Normal Compression

The modified Hashin failure criterion takes into account shear stress interaction, enables detection of various failure modes and allows for the use of strength degradation models.

4.2 Static Modelling

The static finite element modelling technique developed makes use of the following two components:

- Stress Analysis
- Failure Analysis

This technique is able to determine the ultimate static strength of a component.

4.2.1 Failure Modes

The following 4 sub-sections present the equations used to detect static failure of composites in the fortran code developed by MMS.

4.2.1.1 Fibre Tension and Compression

Failure of fibres due to high tensile or compressive loads (stresses). Any failure detected by the two equations below constitutes catastrophic failure and complete loss of all properties. The following quadratic polynomials detect failure.

Equation 10

$$e_{F^+}^2 = \left[\frac{\sigma_{xx}}{X_t}\right]^2 + \left[\frac{\dfrac{\sigma_{xy}^2}{2E_{xy}} + \dfrac{3}{4}\delta\sigma_{xy}^4}{\dfrac{S_{xy}^2}{2E_{xy}} + \dfrac{3}{4}\delta S_{xy}^4}\right] + \left[\frac{\dfrac{\sigma_{xz}^2}{2E_{xz}} + \dfrac{3}{4}\delta\sigma_{xz}^4}{\dfrac{S_{xz}^2}{2E_{xz}} + \dfrac{3}{4}\delta S_{xz}^4}\right]$$

Equation 11

$$e_{F^-} = \frac{\sigma_{xx}}{X_c}$$

4.2.1.2 Fibre-Matrix Shearing

Failure due to in-plane shearing between fibres and matrix. This type of failure does not constitute total loss of material properties, as does fibre failures. Failure results in the loss of the following properties:

$E_{xy} \Rightarrow 0$

$\nu_{xy} \Rightarrow 0$

$\nu_{yx} \Rightarrow 0$

$S_{xy} \Rightarrow 0$

With the remaining properties are kept unchanged.

Equation 12

$$e_{FM}^{2} = \left[\frac{\sigma_{xx}}{X_c}\right]^2 + \left[\frac{\dfrac{\sigma_{xy}^2}{2E_{xy}} + \dfrac{3}{4}\delta\sigma_{xy}^4}{\dfrac{S_{xy}^2}{2E_{xy}} + \dfrac{3}{4}\delta S_{xy}^4}\right] + \left[\frac{\dfrac{\sigma_{xz}^2}{2E_{xz}} + \dfrac{3}{4}\delta\sigma_{xz}^4}{\dfrac{S_{xz}^2}{2E_{xz}} + \dfrac{3}{4}\delta S_{xz}^4}\right]$$

This failure mode will not affect the compressive strength of the fibre as such, but it will reduce or totally remove lateral support for the fibres in the vicinity of the failure. Removing the lateral support on a fibre in compression will increase the possibility of the fibre buckling, hence failing. Fibre microbuckling has been investigated by P.M. Jelp et al[29].

4.2.1.3 Matrix Tension and Compression

Matrix cracking, either due to tensile or compressive stresses occurs long before catastrophic failure of any structure. Under most load scenarios matrix cracking occurs early during loading.

Matrix tension failure sudden degradation results in the following properties being set to zero:

$E_{yy} \Rightarrow 0$

$\nu_{yz} \Rightarrow 0$

$\nu_{yx} \Rightarrow 0$

$Y_t \Rightarrow 0$

With the rest of the material property values kept unchanged.

Matrix compression failure sudden degradation results in these properties being reduced to zero:

$E_{yy} \Rightarrow 0$

$\nu_{yz} \Rightarrow 0$

$\nu_{yx} \Rightarrow 0$

$Y_c \Rightarrow 0$

And with the remaining material property values kept unchanged.

Equation 13

$$e_{M^*}^2 = \left[\frac{\sigma_{yy}}{Y_t}\right]^2 + \left[\frac{\dfrac{\sigma_{xy}^2}{2E_{xy}} + \dfrac{3}{4}\delta\sigma_{xy}^4}{\dfrac{S_{xy}^2}{2E_{xy}} + \dfrac{3}{4}\delta S_{xy}^4}\right] + \left[\frac{\sigma_{yz}}{S_{yz}}\right]^2$$

Equation 14

$$e_{M}^2 = \left[\frac{\sigma_{yy}}{Y_c}\right]^2 + \left[\frac{\dfrac{\sigma_{xy}^2}{2E_{xy}} + \dfrac{3}{4}\delta\sigma_{xy}^4}{\dfrac{S_{xy}^2}{2E_{xy}} + \dfrac{3}{4}\delta S_{xy}^4}\right] + \left[\frac{\sigma_{yz}}{S_{yz}}\right]^2$$

4.2.1.4 Normal Tension and Compression

Normal tension or compression failure occurs due to stresses induced normal to (out of) the plane defined by the fibre-matrix directions.

Normal tension failure sudden degradation results in the following properties being set to zero:

$E_{zz} \Rightarrow 0$

$\nu_{zx} \Rightarrow 0$

$\nu_{yz} \Rightarrow 0$

$Z_t \Rightarrow 0$

And all other material properties kept unchanged.

Normal compression failure sudden degradation results in these properties being reduced to zero:

$E_{zz} \Rightarrow 0$

$\nu_{zx} \Rightarrow 0$

$\nu_{yz} \Rightarrow 0$

$Z_c \quad \Rightarrow \quad 0$

Again with all remaining properties kept unchanged.

Equation 15

$$e_{N+}^2 = \left[\frac{\sigma_{zz}}{Z_t}\right]^2 + \left[\frac{\frac{\sigma_{xz}^2}{2E_{xz}} + \frac{3}{4}\delta\sigma_{xz}^4}{\frac{S_{xz}^2}{2E_{xz}} + \frac{3}{4}\delta S_{xz}^4}\right] + \left[\frac{\sigma_{yz}}{S_{yz}}\right]^2$$

Equation 16

$$e_{N-}^2 = \left[\frac{\sigma_{zz}}{Z_c}\right]^2 + \left[\frac{\frac{\sigma_{xz}^2}{2E_{xz}} + \frac{3}{4}\delta\sigma_{xz}^4}{\frac{S_{xz}^2}{2E_{xz}} + \frac{3}{4}\delta S_{xz}^4}\right] + \left[\frac{\sigma_{yz}}{S_{yz}}\right]^2$$

From the above equations, it is obvious that complete characterisation of the composite material properties is necessary in order to make use of the failure analysis criteria as presented.

A simple "patch test" was performed to test the validity of the FE code. A flat plate was created using I-DEAS Master Series 5.0 and transferred to a format readable to the FE code. This enabled evaluation of the behaviour of the code when depicting failure modes for selected load cases.

The degradation rules employed here should be used with caution. Should an element fail in matrix tension, it would still be able to carry loads (sustain induced stresses) in compression. Reducing Y_t to zero makes sense. However, if an element fails in matrix compression and the load scenario involves cycling about zero, there would not be any load carrying capacity left in the element either in tension nor compression. In other words, both Y_t and Y_c should be reduced to zero. Since this is not incorporated in the fortran code developed, finite element analysis using this code is obviously limited to cases where the elements defining the structure being examined are kept in either constant tension or compression.

4.3 Progressive Fatigue Damage Modeling

The fatigue modelling technique consists of the following three components:

- Stress Analysis
- Failure Analysis

- Material Property Degradation Rules

Fatigue analysis simulates the fatigue life of a component for any given stress. The code is only able to determine the sequence of failure of the elements used to model the structure, and experience is needed before being able to determine the exact time of failure of the structure.

4.3.1 Failure Modes

The same set of equations as presented in chapter 4.2.1 are used for detection of failure during fatigue analysis with the following modifications:

All material properties (stiffness and strength parameters) are re-defined to be functions of number of cycles (n), stress state (σ) and stress ratios (κ or R in some literature). Thus

$X_t \Rightarrow \quad X_t(n, \sigma, \kappa) \quad \Rightarrow \quad R(n, \sigma, \kappa)$ – generalised case

$E_{xx} \Rightarrow \quad E_{xx}(n, \sigma, \kappa) \quad \Rightarrow \quad E(n, \sigma, \kappa)$ – generalised case

and so forth.

In order to make full use of the abilities presented by these equations it is necessary to perform a number of tests to determine the residual strengths and stiffness of uni-directional composite plates in 3-dimensions.

4.3.2 Material Property Degradation (Gradual)

Gradual material property degradation evaluation is based on a purely mechanistic approach and is a modified version of a model presented by Harris[25, 48, 49]. The normalised strength degradation equation[37(Chapter 5)] used is, as defined by MMS

Equation 17

$$R(n,\sigma,\kappa) = \left[1 - \left(\frac{\log(n) - \log(0.25)}{\log(N_f) - \log(0.25)}\right)^{\beta}\right]^{\frac{1}{\alpha}} (R_s - \sigma) + \sigma$$

Stress ratio (κ) is defined as:

Equation 18

$$\kappa = \sigma_{\min} / \sigma_{\max}$$

Similarly there exists a normalised stiffness degradation equation[37(Chapter 5)] as follows

Equation 19

$$E(n,\sigma,\kappa)=\left[1-\left(\frac{\log(n)-\log(0.25)}{\log(N_f)-\log(0.25)}\right)^{\lambda}\right]^{\frac{1}{\gamma}}\left(E_s-\frac{\sigma}{\varepsilon_f}\right)+\frac{\sigma}{\varepsilon_f}$$

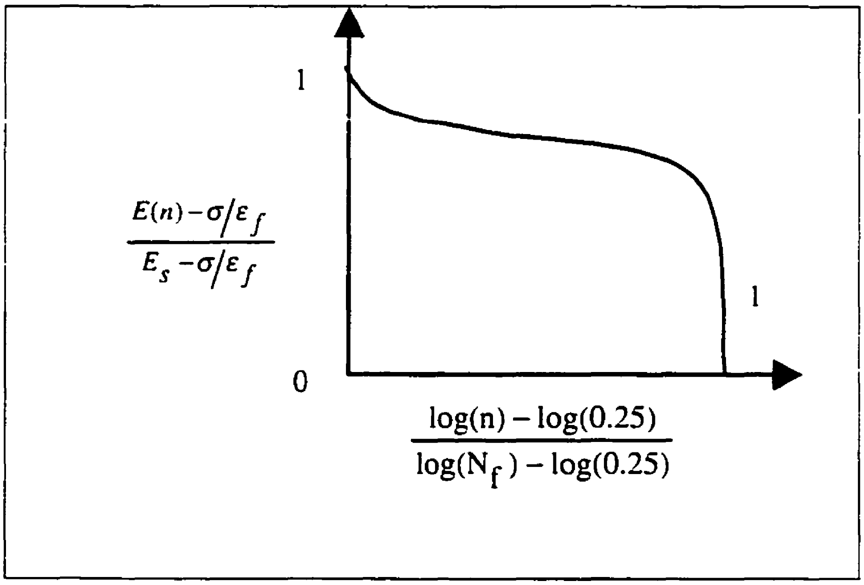

Figure 8 Sketch of Normalised Stiffness Degradation Curve

The figure above (Figure 8) illustrates how stiffness (and strength) degradation curves for differing stress states collapse to one single curve when making use of the normalisation technique.

As can be seen from Figure 8, stiffness degradation is very gradual, almost constant for most of the fatigue life until residual stiffness falls abruptly over the last 5-10% of the overall fatigue life.

N_f is a function of the stress state and the stress ratio, hence in theory an indefinite amount of tests would be necessary to fully characterise a material under varying fatigue conditions. In order to reduce the number of experiments necessary several researchers have sought to develop analytical models that accurately predicts the fatigue life for varying states of mean stress from a relatively modest number of experimental results. MMS uses a model based on work by Harris et al[48,49] presented briefly below

Equation 20

$$a=f\left[(1-q)(c+q)\right]^{A+B\log(N_f)}$$

Equation 21

$$q = {}^{\sigma_m}\!/_{\sigma_t}$$

Equation 22

$$a = {}^{\sigma_a}\!/_{\sigma_t}$$

Equation 23

$$c = {}^{\sigma_c}\!/_{\sigma_t}$$

Equation 24

$$\sigma_a = (\sigma_{max} - \sigma_{min})/2$$

Equation 25

$$\sigma_m = (\sigma_{max} + \sigma_{min})/2$$

Further manipulation of Equation 20 to Equation 25 leads to Equation 26 below

Equation 26

$$u = \frac{\ln\left({}^{a}\!/_{f}\right)}{\ln[(1-q)(c+q)]} = A + B\log(N_f)$$

With A and B being curve fitting constants. By knowing the stress state, stress ratio, the ultimate tensile and compressive strengths, u can be calculated. Having found u, and then plotting u (on the y-axis) versus N_f, gives A and B. In the event of simulating shear loading conditions, c is set equal to 1.

During the course of investigation it was found that in the cases where the ultimate tensile strength was less then the ultimate compressive strength Equation 26 would "blow-up". I.e. c would become larger than 1, in some cases as large as 4. This would give in numerical result where the numerator (the natural logarithm (ln)) would be a negative number divided by the denominator (natural logarithm (ln)) of a relatively small positive number, resulting in an overall negative number. Solving this for N_f would then yield a very small number indicating that the material being investigated would not be able to sustain any fatigue cycling at all. Given that the induced (or applied) stresses used to calculate a and q are small, less than 0.01 of σ_t say, this would obviously be wrong. In the modified fortran code this problem has been averted by using the absolute value of the numerical value found before taking the natural logarithm, and making use of various conditions to detect actual failure.

5 McGill FINITE ELEMENT MODEL CODE

The finite element analysis code developed by MMS is limited to using 3-dimensional 20 node quadratic iso-parametric solid element with an orthotropic material model. Stress analysis is 3-dimensional, enabling the use of three dimensional failure criteria as described in chapter 4. A users guide is available[50].

5.1 Patch Test:

In order to validate the static and fatigue finite element analysis codes a number of patch tests were performed. A square consisting of 9 orthotropic, solid, brick elements was created, given appropriate material properties and material directions. Carbon fibre material properties were used, as all parameters needed for numerical analysis were readily available from 37. The elements were appropriately constrained (clamped nodes) and material orientations for all nine elements set to 30°. Face pressures were applied to three faces opposite to the clamped nodes (magnitude 5 MPa).

Static analysis was executed to determine the ultimate static strength of the structure. Fatigue analysis for three different load cases was performed and the sequence of element failures recorded. The load ratios used were ~80%, ~75% and ~65% of static strength.

Table 13. Fatigue Analysis Patch Test Results

Load Ratio [%] / $\{\sigma_{app}/\sigma_{ult}\}$/Ratio	No. Cycles to Failure (of all elements) or Simulation End (No. failed elements)
80 / {15/130}/ 0.115	900 (all)
75 / {15/120} / 0.125	2000 (7)
60 / {10/100} / 0.1	6000 (6)

Complete failure defined as fibre fracture.

To further validate the fatigue analysis code a patch test with only one element loaded was executed. Static analysis was again performed first to determine the ultimate tensile strength of the structure for the particular load case, followed by a fatigue simulation using a load ratio of 0.1 (15/150) for an applied load of 80% of UTS. Given the boundary conditions it was found that the only three of nine elements had failed after 15000 cycles. This was expected and it was decided that until actual test results from SSI testing were available nothing further could be said about the accuracy of the static or fatigue predictions made by the finite element codes.

Figure 9 shows a sketch of the patch test set-up.

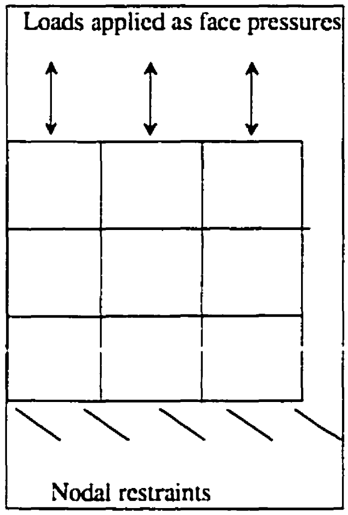

Figure 9. Sketch of patch test set-up

5.2 Finite Element Model

A 500 element, 2732 node model was created using I-DEAS appropriate loads and node translation restraints were applied, and the resulting finite element model exported as an universal file. Figure 10 is a sketch of the model created for FE modelling in the McGill[37] created fortran code. Four different load cases were examined; axial loading -, torsion -, bending-, and bending combined with torsion of SSI pipe.

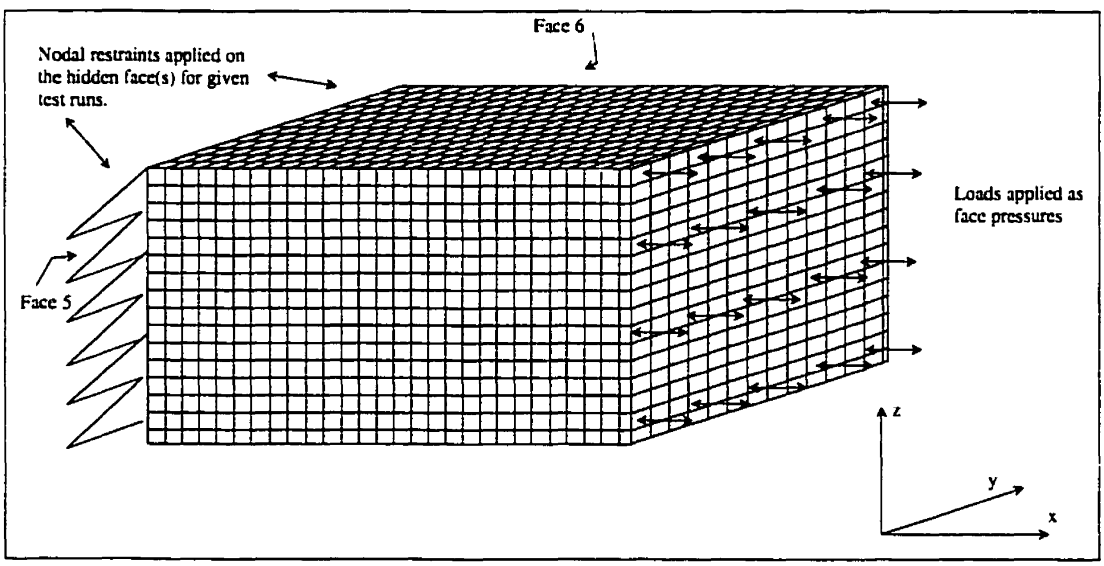

Figure 10 Sketch of full scale local FE code analysis model

Shear stresses were induced by face pressure applied perpendicular to global face. That is, shear was applied as face pressures in the volume of the elements, along the global edge of the plate structure. This obviously sets up an untrue stress state in the outermost elements, but provided the restraints are properly defined, the final stress and subsequently failure analysis should give good results.

Simulation of SSI torsion cases using MMS code required use of nodal restraints assuming plane sections remains plane. For most cases this assumption holds, and it is not believed to have caused large, undue errors in the final result sets.

5.2.1 Observations

While experimenting with the finite element code it was discovered that nodal restraints were of paramount importance. For instance, axial loading of the SSI pipe was attempted simulated with face 6 of the elements on one edge restrained from x translation and with face 5 of the elements on the corresponding perpendicular edge restrained from y translation as standard. The intersecting edge was restrained in a number of different ways each one yielding different ultimate axial tensile strengths.

The FE code is set-up to start the analysis at a given induced stress. It is possible to obtain an estimate of the strength of the structure, as the analysis is done in steps, with a (by the operator) constant increase in the induced stress being added for each analysis cycle. These increments are referred to as "*loadsteps*". The following were attempted (for given load cases) using 1/32th of the I-DEAS analysis stress results (section 3.2, Table 11 for bending) as the induced stress in each load step. The first induced stress was 1/32th of the mentioned I-DEAS stress results from the selected analysis cases.

The first case (a) exhibited a higher failure stress than (c). Case (b) resulted in numerical errors in the model, or less than 10 load steps to failure.

Upon examining the failure sequence of the elements, it was found that in some cases, notably (c), the only failed element was the same that had node 130 as the corner node. In other words, as soon as the node relating directly to the restrained element failed, the entire structure would experience mathematical large deformations/displacements and cause the code to define failure.

After a number of iterations with different restraining conditions it was found that clamping all the nodes on the far yz-surface gave the most accurate analysis results wrt. numerical versus test data for pure torsion. Indeed, in most of the cases analysed keeping the far yz-plane clamped gave the best correlation between test and numerical analysis data.

Table 14 Summary of Induced Stress Cases and Boundary Conditions from Numerical Analysis Using the Finite Element Analysis Code Developed by M.M. Shokrieh as part of his PhD work[37]

Boundary Condition	Axial loading No. of loadsteps to failure	Bending No. of loadsteps to failure	Torsion No. of loadsteps to failure
a) All nodes along edge clamped	59	25	24
b) Bottom node clamped (#. 130)	Numerical error	Numerical error	Numerical error
c) Bottom and top nodes clamped (#. 130 & 2732)	51	Numerical error	Numerical error
d) All nodes in yz-plane clamped	NA	NA	30[vii]

NA Not Available

Unfortunately, the failure stress as reported by the FE code was well below the expected for all the boundary conditions evaluated, and particularly low for the boundary condition cases set-up to simulate bending. The I-DEAS analysis stress results referred to earlier where all for low stress values, not sufficient to cause catastrophic failure of the pipe structure.

5.3 Finite Element Code Evaluation

Static and fatigue analysis performed using the code developed by MMS gave the following results:

The FE code is limited to analysis cases of flat plate structures, loaded by face pressures and with node translation restraints only.

The following suggestions for improvements are made:

- Conversion of the code from handling of plate structures, to full-fledged 3-D geometry analysis. This will, or should enable analysis of structures, such as pipes, with globally applied loads, thus resulting in more accurate analysis data.
- The above suggestion requires a new and more efficient solver to be programmed, as the current solver is too slow for such work.
- Another deficiency in the code that might be solved by a full 3-D geometry analysis is load transfer from failed plies/elements to non-failed plies/elements. An example is the simulation of axial SSI loading. Qualification testing of SSI pipe by NAT

[vii] Initial induced stress used was 1/8th of that found for a given applied load in I-DEAS

Compipe as has indicated[viii] a failure load capacity in excess of 31 metric tonnes[51]. The best numerical analysis result indicated failure at roughly 26 metric tonnes. This is at about 16% lower than the maximum value measured by NAT Compipe. The most probable reason for this is the fact that when the outermost plies (±78°) fail, load carrying capacity is lost and all loads are carried by the 0° plies (innermost plies). As the code stands today it is not able to perform such a load transfer effectively resulting in lower failure loads being indicated for the SSI (or any other structure).

- Attempts at simulation of bending revealed the code unable to execute such analysis satisfactory. This can be related directly to the limitations in boundary condition possibilities.

5.4 Summary on the Suitability of MMS FE Code for Current Research

The finite element code written by MMS proved unsuitable for local analysis of critical sections of a pipe subject to four point bending.

Reasons for its unsuitability are several, but the most important are listed below:

- Only translation restraints on nodes can be applied. Rotational restraints can not be applied.
- Loads can only be applied as face pressures. This means that bending moments have to be approximated as pressures on element faces.
- The code is not capable of performing analysis of three-dimensional geometries. This prevents usage of a complete pipe model, and forces use of a global ⇒ local approach where face pressures are taken as the element stresses found from a static finite element solution of a cylindrical thin shell model analysed in I-DEAS. Even so, a FEA performed using MMS FE code will not be accurate due to the lack of sufficient boundary condition options.

The rapid development of new features in commercial finite element software packages means that it is more efficient to develop modules for these commercial FE packages. Development of modules for prediction of static strengths of composites structures, and/or fatigue life and behaviour of composites using the mathematical formulations developed by MMS for commercial packages like NASTRAN, ABAQUS, ANSYS etc. is recommended. Making use of the interfaces provided in these codes also facilitates pre- and post-processing of models and the results.

[viii] Equipment limitations have prevented testing to failure of the SSI pipe

6 EXPERIMENTAL TEST RESULTS OF COMPOSITE PIPE

Numerical analysis of a pipe structure, like that of a spoolable composite injection line (SSI), must be backed-up by experimental work. In this research four-point static and dynamic fatigue bending was executed to allow evaluation of the theoretically predicted behaviour.

6.1 Method

To assure complete documentation of the experimental efforts, the following sections briefly describe the practical aspects of the experimental work.

6.1.1 Apparatus / Set-Up

A four point bending jig was designed allowing space for additional load applicators, like a torsional load applicator. The bending jig was designed for stiffness and modified from an existing design by Compipe AS. In order to obtain a surface strain of 0.6% a force of 39168 N (roughly 4 metric tonnes) had to be applied. This value also served as the initial design criterion for the bending test jig.

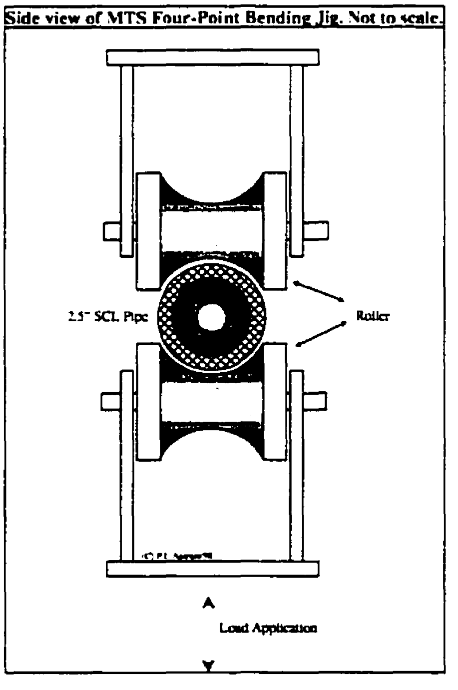

Figure 11. Looking along the axis of the four point bending jig.

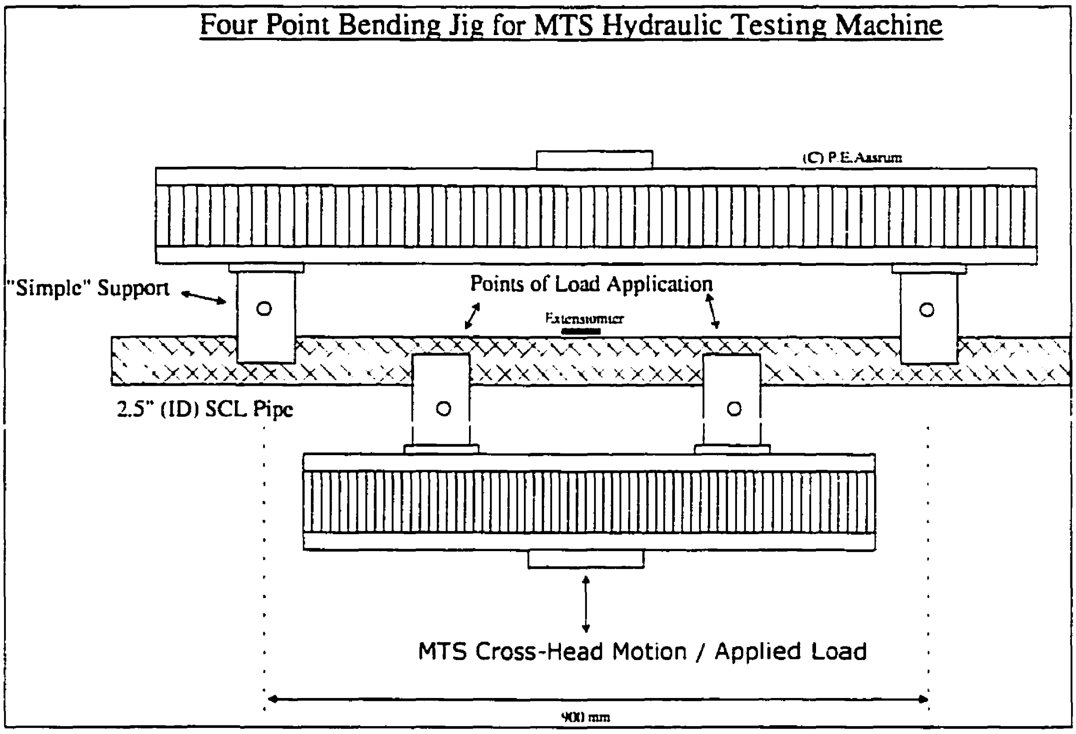

Figure 12. Four point bending jig

A MTS test machine with maximum capacity of 25 metric tonnes was used (Figure 13). Four-point bending was performed. Controller console and software was standard MTS: "458.20 Micro Console", and "Testlab Control Panel Version 2.0". Extensiometer data was collected using the standard MTS supplied extensiometer supplied with the testing machine.

6.1.2 Instrumentation

Selected pipes were instrumented with strain gauges and an extensiometer.

For four point bending tests, both static and fatigue, two (2) strain gauges and the extensiometer were utilised on selected specimens. For some static tests, the SSI was rotated 180 degrees between tests in order to get data from both the compressive and tensile face of the pipe. Damage, evident as matrix cracking, was visible from the first bending cycle any pipe was exposed to. The level of damage was not assessed as such. In 6.1.3 pre-conditioning of SSI pipes is described. Due to equipment (only four channels were available for strain gauges) and budget limitations, it was not possible to use a symmetric set-up of strain gauges with 3 gauges on both the tensile and compressive faces of the pipe (total of 6 strain gauges). The maximum number of strain gauges ever used on one pipe was three.

The surfaces on which the strain gauges were bonded to the SSI were carefully sanded down to provide a smooth surface. This was necessary in order to obtain a surface on which the strain gauges would bond and give accurate readings. Strain gauges are extremely sensitive to matrix micro-cracking. Creation of matrix micro-cracks results in sharp edges and large local deformations, subsequently causing pre-mature failure of, or loss of signal from, the strain gauge. Successful use of strain gauges is limited to static testing, this because increasing number of bending cycles increases the possibility of matrix cracks developing directly underneath the strain gauges.

The extensiometer provides excellent results in the longitudinal direction, provided it is properly aligned. It is not as sensitive to surface roughness as a strain gauge, although care must be taken to ensure that the extensiometer does not rest in an unstable position on the pipe surface. In most cases, the extensiometer will slide off a surface protrusion at some point during testing, resulting in discontinuities in the test data.

Strain Gauges:

Strain gauges used were from Measurements Group, Inc, Raleigh, North Carolina, type CEA-06-500UW-350. These are 350.0Ω ±5% strain limit gauges. Strain gauge measurements were registered through a Nicolet Pro40 digital oscilloscope. In most cases a maximum of three strain gauges could be used controlled via three quarter Weathstone 350Ω bridges.

6.1.3 Pre-Conditioning of Composite Pipe

Before exposing pipes to any load scenario described in this thesis, all pipes were pre-conditioned. Pre-conditioning simulates spooling of the composite pipe on a 10m diameter spool, equivalent of a surface strain of 1.0%, four times. Figure 13 shows a 2.5 inch SSI pipe exposed to four point bending.

Spooling of spoolable composite injection line pipe, indeed spooling of any spoolable composite pipe, induces matrix micro-cracks in the pipe. Four pre-conditioning bending cycles where employed. Between each bend cycle, the pipe was turned 90 degrees in order to initiate matrix micro-cracks all around the pipe. Bending to simulate spooling of continuous lengths of composite pipe precedes all qualification of spoolable composite pipe for oil field service and operations.

Composite pipes exposed to cyclic dynamic bending fatigue tests were also pre-conditioned as described above.

The philosophy of testing SSI pipes is to perform evaluation of SSI pipes in an as realistic state as possible. Therefore pre-conditioning is necessary. Apparent properties of virgin pipes in this respect is therefore not of great importance. However, Figure 29 and Figure 30 is included to show the initial change in bending stiffness on the first bending cycle of the pre-conditioning routine.

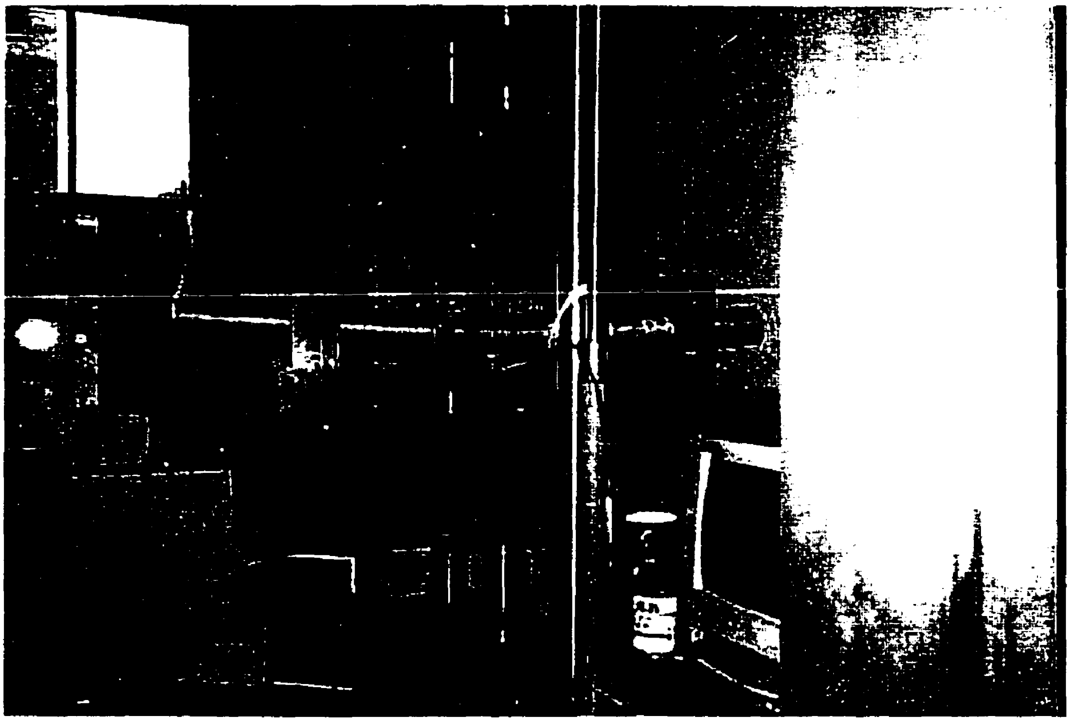

Figure 13 Picture of 2.5 inch SSI in Four-Point Bending Using 25 Metric Ton MTS Hydraulic Test Machine

6.2 Test Program

6.2.1 Static Bending

Static bend testing was necessary to find the required displacement and force to obtain a certain strain. The strain capacity of a composite, in this case, pipe is potentially indicative for the cyclic fatigue potential of the pipe. It is also interesting to compare the initial numbers with values obtained at a later stage in the test program after multiple cycles and various load combinations. Ultimate bending strength (UBS) of the SSI is thus found.

When spooled, the SSI experiences a surface strain of 0.6% due to bending onto the spool or reel[ix]. It is not expected that bending experienced during laying of the pipe will exceed this value. Hence the design case scenario wrt bending strains is equivalent to a bending radius of 7.5 m or 0.6% surface strain. In certain cases strains exceeding 0.6% may arise. Such situations may arise during laying operations if the weather takes a turn for the worse, or

[ix] After commencing research on this thesis, Compipe® SSI was certified for limited period exposure to larger spooling strains

handling of the SSI is not executed as described in the specification for spoolable composite injection lines as manufactured by NAT Compipe as. The test program therefore set-out to investigate the effect of high strain cyclic fatigue on the SSI. Later in the research it became clear that the end users of a product like the SSI desired smaller diameter reels and hence required a spoolable composite pipe with greater capacity to higher strain values. Activities investigating the effect of higher bending strains henceforth became of even more interest.

Table 15 Test Case Static Bending

CASE	No. Samples	Bending diameter (static) (m) / % ε_1	Comments
1	2	15 / 0.6% and to failure	Monitored wrt required load to desired deflection[x]

6.2.2 Dynamic Cyclic Fatigue Bending

During laying the pipe will experience a number of load cycles due to vessel movement caused by wave motion. The exact number of cycles is difficult to pin-point, but a reasonable approximation can be obtained based on the estimated annual number of wave cycles and the time span over which the pipe is exposed to these movements.

The annual number of wave cycles in the North Sea has been estimated to be roughly 5 000 000 (5 million cycles)[52]. This corresponds to a wave frequency (wf) of:

Equation 27

$$wf = \frac{no.waves / year}{\sec onds / year} = \frac{5000000}{365 * 24 * 60 * 60} = 0.15855(waves / \sec)$$

wf Wave frequency

The number of fatigue cycles used for pipe testing will be a function of wf and time exposure of the pipe to the cyclic fatigue. Several hours exposure is possible.

The magnitude of the constant amplitude (load) for cyclic bending was not decided prior to testing, but was decided upon as result of the first data from the test, and modified according to observations made during testing. During laying operations of conventional steel coiled tubing strains are not allowed to exceed yield. Hence, there is no direct line back to real life load scenarios. Should weather conditions change for the worse and wave motion increase to

[x] Compare values for load and cross-head deflection to bending strain, cross-head movement and measured surface strain with known and continue testing until failure or maximum capacity of MTS machine

critical levels, the pipe would be cut and left, for pick-up at a later time when weather conditions have improved.

Table 16. Test Cases Cyclic Fatigue Bending

CASE	No. Samples tested	Maximum bending load (cyclic) / % of UBS	Comments
2	2	47 (kN) / 74 (%)	To failure at constant maximum amplitude load
	1	48.6 (kN) / 76 (%)	
	1	50 (kN) / 79 (%)	
	3	55 (kN) / 86 (%)	
	2	60.3 (kN) / 95 (%)	

Samples tested 9

The total number of samples to be tested and test levels to be investigated changed during the execution of the test program. 2 to 3 specimens should ideally have been tested at each load level, thus repeatability of the results is not verified.

Due to a change in focus based on evaluation of the experimental set-up, a number of tests and the corresponding results where dismissed. A number of available samples were used, limiting the number of tests that could be done according to the above outline.

6.2.3 Static Torsion and Static Torsion and Four-Point Bending

Static torsion was also investigated in this research, and an experimental set-up devised.

Initial evaluations of the torsional capacity of the SSI pipe included estimation of the equivalent torsional stiffness GJ for the composite pipe using a relationship presented in McGill lecture course[40].This is a standard set of equations for estimating torsional rigidity of composite tubular structures. GJ (equivalent torsional stiffness) was found to be 20670 Pa*m^4. Refer to APPENDIX C for further explanation.

4 pipes were tested in static torsion and torsion combined with bending (both static). However, the experimental set-up proved to be limited, from a safety point of view, preventing application of sufficient torque to fail the pipe in torsion. The maximum applied torque on an SSI pipe was 431.6 Nm (applied as 75.85 kg on a 0.58m moment arm). This corresponds to a shear strain of approximately 0.1%, which is about 1/3 of the initially desired twist. The initial desired twist relates to a number given as a realistic value for twist in pipes during offshore laying operations. Figure 14 and Figure 15 are sketches of the experimental set-up devised for torsion related testing of SSI pipes.

With the values for torsional pipe rigidity and the applied torque, the pipe was estimated to twist about 0.0125 rad over the 0.6 m length. This corresponds to roughly 1.2 degrees per meter.

The mathematical relationships used are as follows:

Equation 28

$$\theta = \frac{T \times L}{G \times J}$$

Equation 29

$$\gamma_s = \frac{\theta \times r}{L}$$

Equation 30

$$\tau = G \times \gamma$$

By using the equations above, it is also possible to estimate the shear stress in the surface of the pipe. The value was found to be between 3.3 and 4.7 MPa when assuming the shear modulus to be between 3.5 and 5.0 GPa respectively. The range in shear modulus magnitude arises due to the laminate lay-up. Typically the shear modulus of an uni-directional glassfibre composite is about 3.5, but with the combination of angles in the SSI pipe, the value is most probably higher. Neither shear stress nor shear strain is close to values needed to cause noticeable damage to the pipe structure. Hence shear damage can be ignored for now.

The experimental set-up (see Figure 14) did not create an ideal torque on the pipe. Applying a load on a one legged moment arm on opposites side of the pipe also induced a bending moment in the pipe. The following simple equation[53] was used to estimate the bending deflection caused by the applied load:

Equation 31

$$\delta_d = -\frac{M \times l^2}{8 \times EI} = -\frac{F \times a \times l^2}{8 \times EI}$$

For a load 75.85 kg applied 0.15 m from the simple support, and with 0.9 m between the two simple supports, the maximum deflection should be 0.363 mm. By comparing this to the deflection values found and presented in section 6.3.1, we can conclude that the induced strain and stress are negligible.

Following static torque loading, the pipes where loaded in four point bending with the torque load maintained constant. Figure 15 outlines the torsion-bending set-up. All pipes where bent to the same measured cross-head deflection: 20 mm. The loads from the torque applicators and the bending load from the MTS machine induce opposite curvatures. A somewhat larger MTS load for a given MTS cross-head deflection was registered compared to those for a pipe loaded purely in four point bending. Surface damage observations of the pipe after combined torque-bending load were comparable with those from the pure bending case. Furthermore, pure cyclic four-point bending of the twisted and twisted-bent pipes yielded similar results to pipes exposed to bending only (6.3.3).

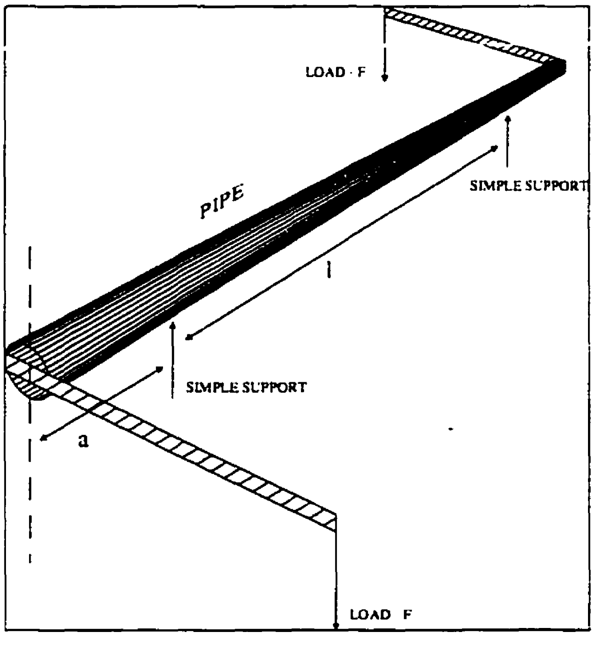

Figure 14. Sketch of experimental torsion set-up

The main reason for not pursuing the torsion load case was safety. Initial tests performed with the set-up revealed it to be unsafe. Space limitations did not allow for control and observation of testing from a safe distance, and application of a torque on the pipe put further limitations on the space available.

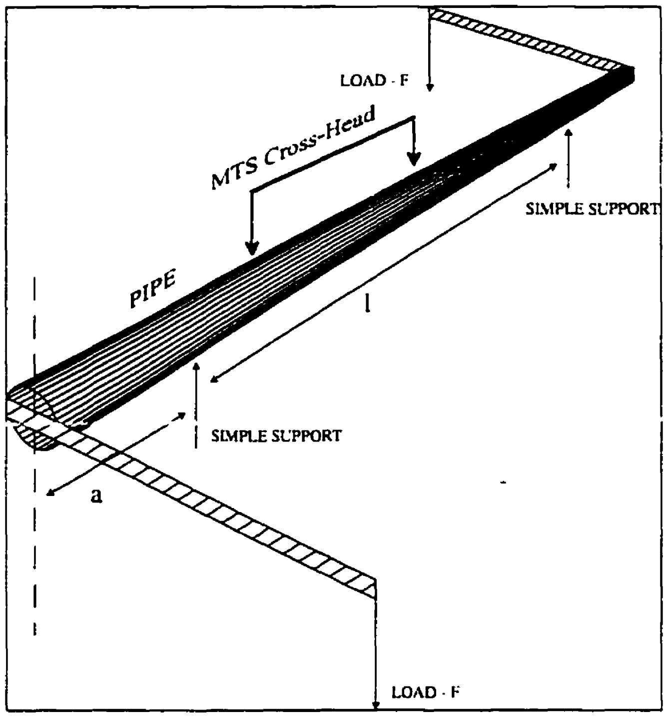

Figure 15. Sketch of static torsion-bending set-up

6.3 Results

Static and cyclic fatigue four point bending was performed in order to identify the behaviour of the SSI at high strain cyclic fatigue bending. Static torsion and static torsion combined with bending was executed for 4 specimens only (section 6.2.3), with a maximum load of 431.6 Nm.

Strain gauges were attempted used for both static and fatigue testing. Use of strain gauges gave good results for the first few static load events on a pipe. However it turned out to be difficult to obtain continuous reliable data readings during fatigue testing. The strain gauges "shorted out" at relatively small pipe strains after 10 – 20 fatigue cycles. This is due to strain gauge range limitations (the range is listed as ± 5% strain) and the emergence of micro-cracks directly underneath the strain gauges. The relative displacements caused by these micro-cracks are locally much larger than the measurement range of the strain gauge. This combined with the sharp edges of the cracks, result in premature failure of the strain gauges. The conclusion is that extremely careful surface preparations are necessary prior to adhesive bonding of strain gauges to composite pipe surfaces. By providing a surface as smooth as possible and avoiding areas with obvious sub-surface flaws, strain gauges can provide reliable data for a period of time, in general until pipe surface damage has grown to encompass the entire circumference of the pipe. An extensiometer will in general provide readings much longer than strain gauges. They are somewhat less accurate, are sensitive to surface contours and expensive, but reusable. The price of an extensiometer generally prohibits use in tests where the sample is poised to fail. Surface roughness may, in some cases cause the extensiometer to become detached from bump on the surface, and result in a discontinuity in the readings.

6.3.1 Static Bending

Two specimens were tested in static four point bending to failure and a third, instrumented with strain gauges, was tested statically prior to fatigue testing. The first pipe test was primarily executed in order to evaluate the set-up, but also contributed valuable information towards the test program.

Table 17 shows the registered failure loads or Ultimate Bending Strength (UBS).

Table 17 Static Failure Loads for 4-Point Bending

Specimen	TRAIL02	TRAIL03
Failure Load (kN)	64.7	62.7

Pipes were pre-conditioned according to section 6.1.3.

Average failure load in four point bending is 63.7 (kN).

In order to test pipes with damage simulating that caused by spooling and handling, no specimen was taken to failure as a virgin pipe (6.1.3).

One specimen was used to relate extensiometer readings to strain gauge readings. Data was collected from the tensile and compressive faces of the pipe. The specimen used was not taken to failure.

The equivalent bending stiffness (EI) was found using the relations described in Chapter 3.1. Using the same dimensional values (Table 1) for the pipe (Table 3), EI = 23936 (Pam^4), a 23% difference compared with the analytically calculated value. This is equivalent to an E-modulus of 10.6 GPa.

In Figure 16 absolute values are used. The MTS machine (Figure 13) is set-up to register the loads applied downwards as negative, as are cross-head movement in the same direction. The notations "Linear(Displacement)", "Linear(Strain)" in Figure 16 to Figure 19 relates to a linear fit of the data presented in the figures.

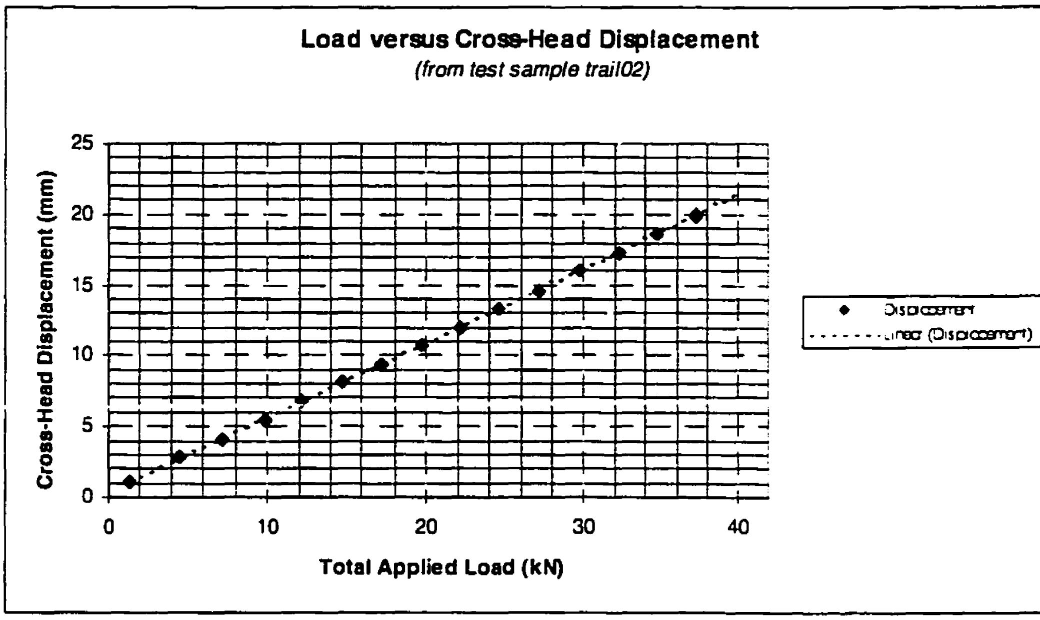

Figure 16 Static Four Point Bending Load versus Displacement Data from Sample Trail02

Figure 16 and Figure 17 above shows typical raw data curves for static four point bending. Figure 17 uses absolute values for both the measured compressive strain and total applied load.

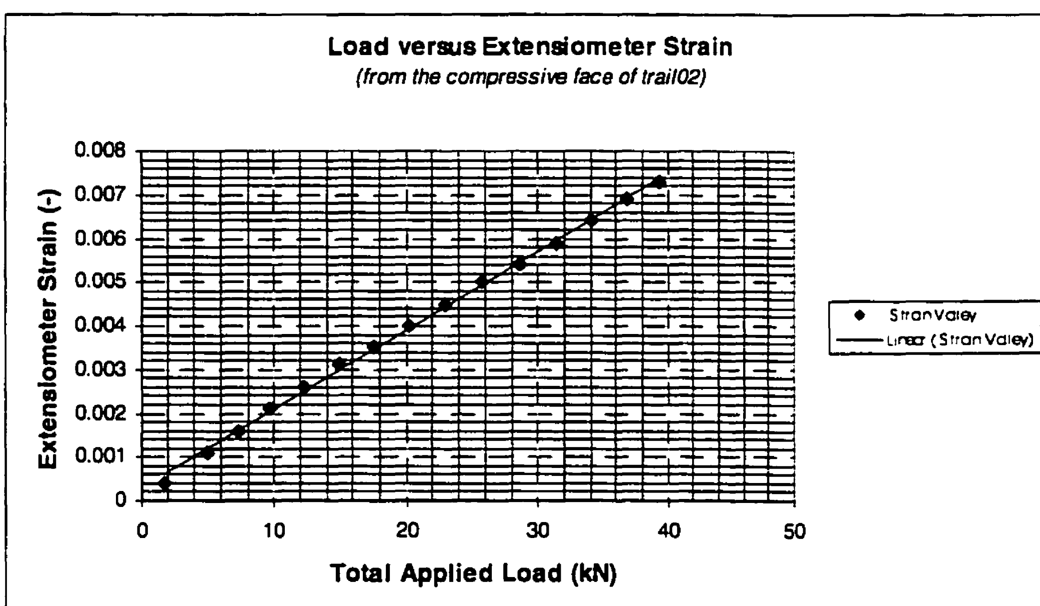

Figure 17 Static Four-Point Bending Load versus Extensiometer Strain on the Compressive Pipe Face.

From Equation 8, using the value for EI found based on experimental results (above), we find that the compressive on-axis stress (σ_1) is 64.67 MPa for a compressive on-axis strain (ε_1) of 0.006.

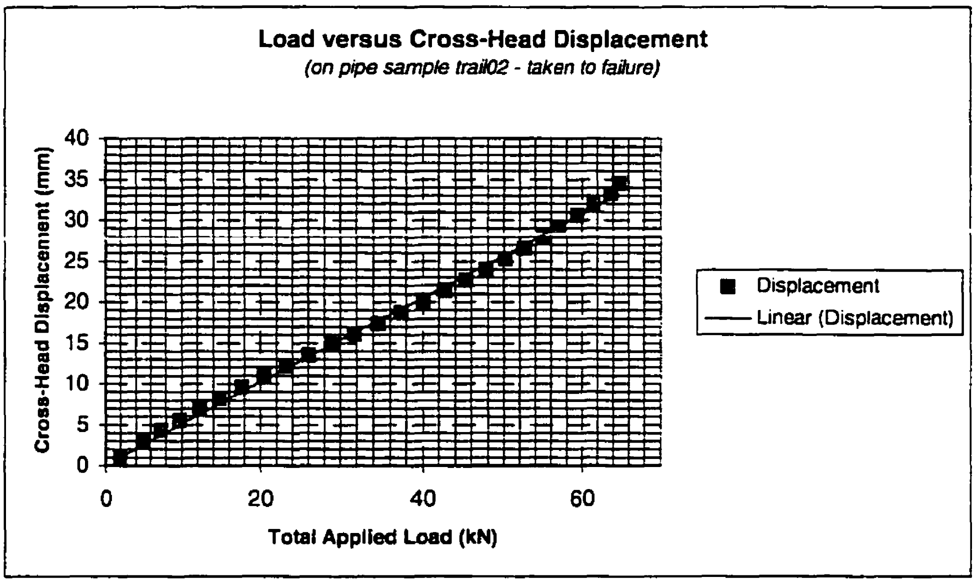

Figure 18 Static Four-Point Bending on Test Sample BS-001-trail-A, Data from Tensile Pipe Face

Figure 19 shows the relationship between load and strain on the compressive face of the SSI.

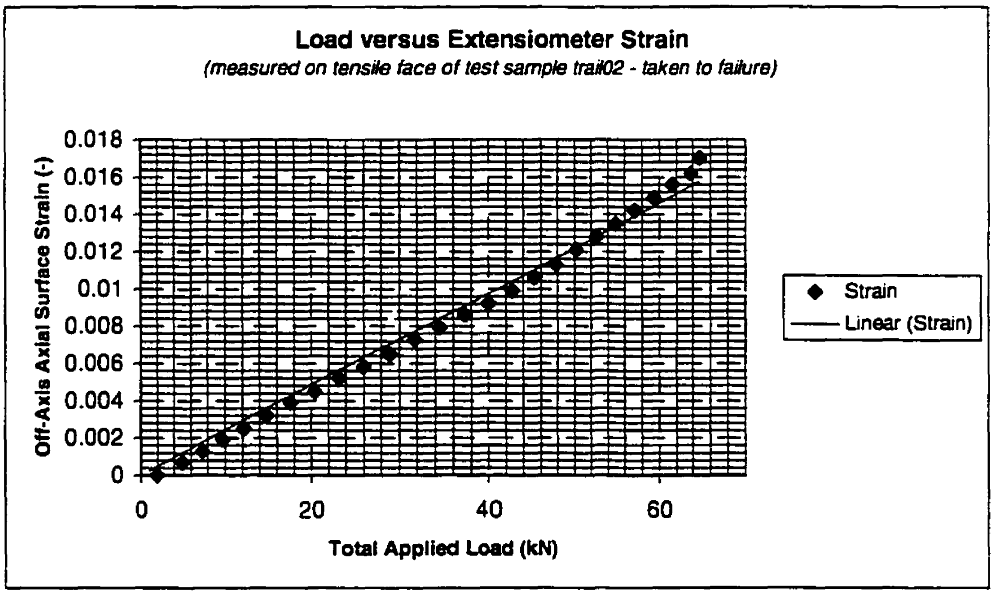

Figure 19 Static Four-Point Bending on Test Sample BS-001-trail-A, Data from Tensile Pipe Face

Using the value for EI calculated in this chapter, a linear development of off-axis axial compressive stress emerges (Figure 20)

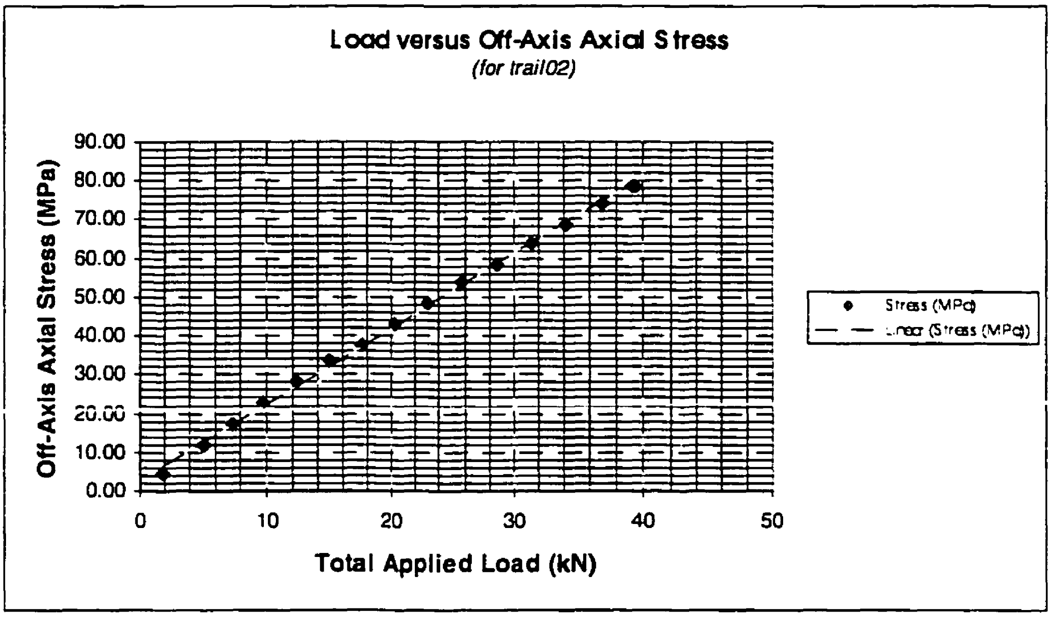

Figure 20 Off-Axis Compressive Axial Stress for Static Four Point Bend Test

In Figure 21, the change in bending radius of SSI with off-axis compressive axial strain is shown. The plot is created from experimentally measured off-axis axial surface strain used in Equation 3 with a known Y. This gives the radius of curvature of the pipe.

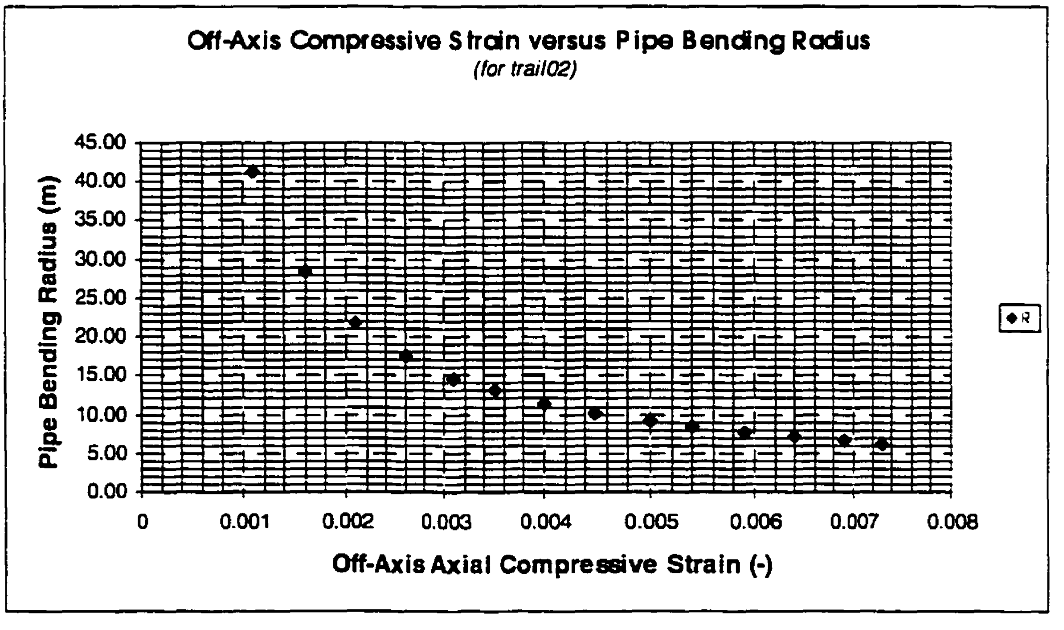

Figure 21 Change in Bending Radius with Off-Axis Axial Strain

In Figure 22 a difference in development of load versus strain for compressive and tensile pipe faces can be seen.

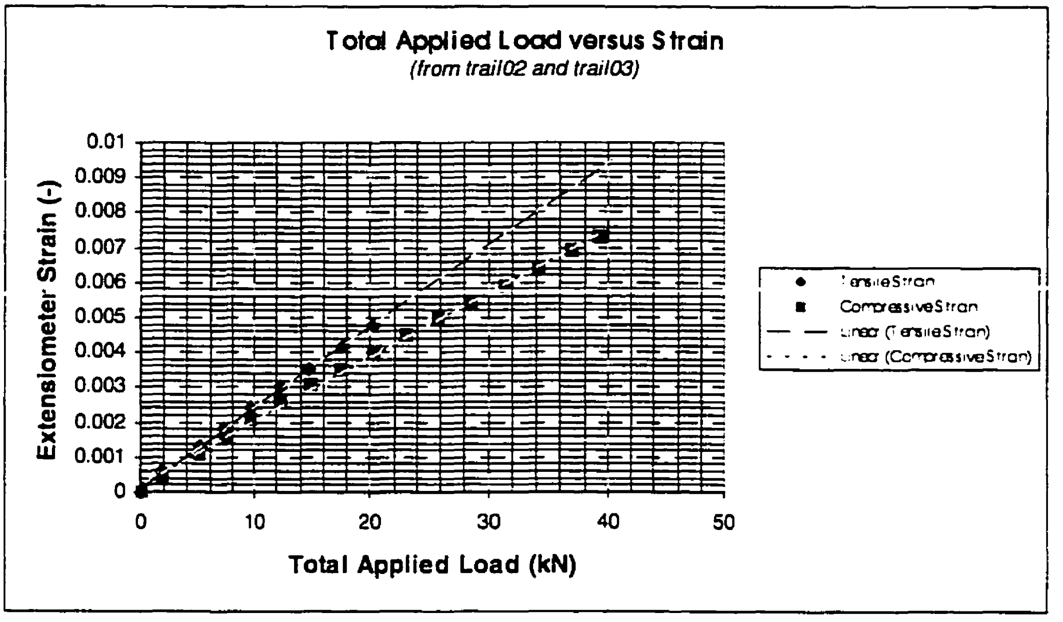

Figure 22 Comparison between Compressive and Tensile Bending Strains

For comparative reasons the compressive data points are shown as absolute values.

As can be seen from the curves in Figure 23 and Figure 24, the gradient is somewhat different for tensile and compressive surface strains. The tensile strain for a given MTS cross-head displacement is larger than the compressive strain for the same. This indicates a certain shift in neutral axis of the pipe (APPENDIX F), and hence a difference in bending stiffness for the compressive and tensile face of a composite pipe in bending. It could also be attributed to ovality induced in the pipe due to bending.

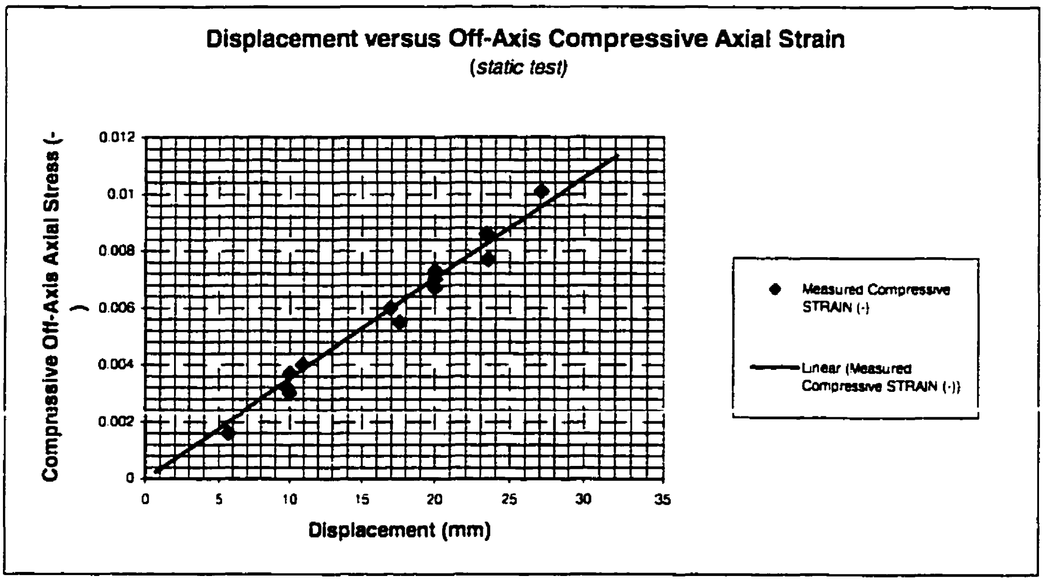

Figure 23. Relationship between Displacement and Strain for the Compressive Face of Composite Pipe under Four Point Bending

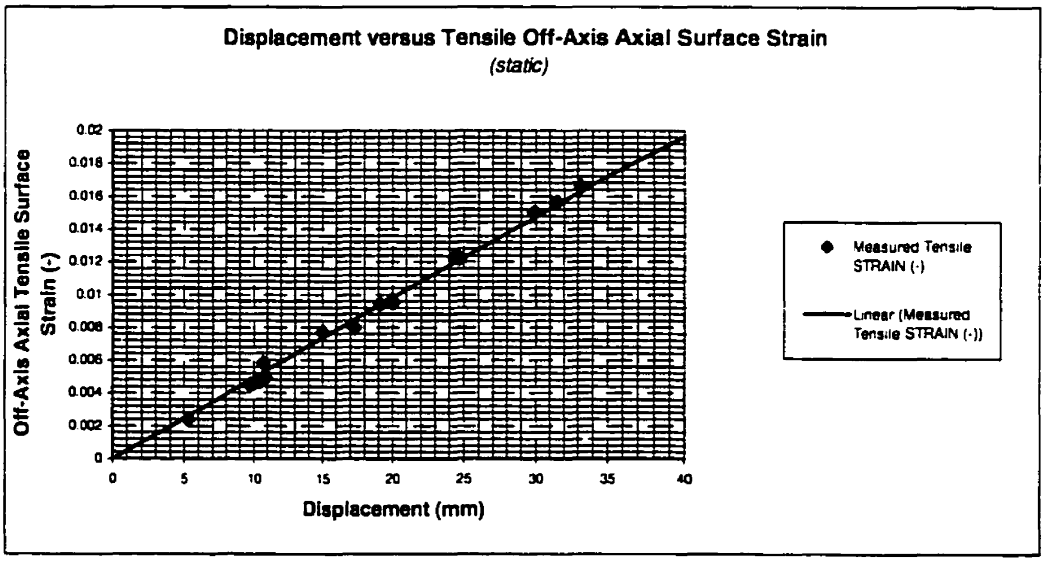

Figure 24 Relationship between Displacement and Strain for the Tensile Face of SSI under Four Point Bending

Fibre reinforced polymers often exhibits relatively large differences in material properties in different direction (anisotropy in the most extreme cases, but mostly assumed to be orthotropic). The most prominent example is the difference between compressive and tensile strength in the transverse direction (matrix direction). Compressive strength is commonly more than twice the tensile. Such differences can cause the neutral axis (APPENDIX F) of the pipe to shift, creating different bending stiffness and give rise to the variations in measured off-axis surface strain.

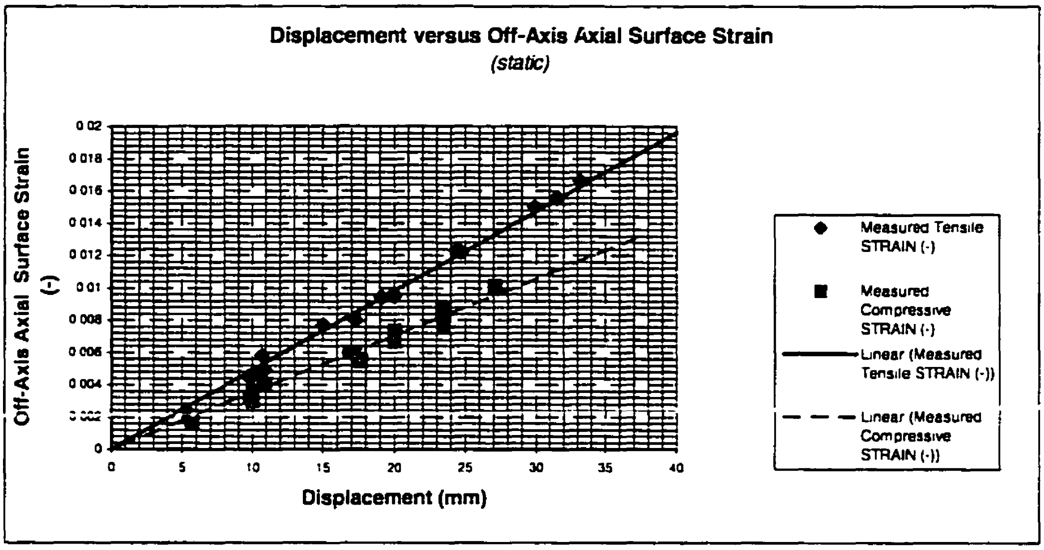

Figure 25 Relationship between Displacement and Strain for Tensile and Compressive Faces of SSI in Four Point Bending

MTS cross-head displacement relates to load according to the curve in Figure 26 below. Data presented in Figure 26 and Figure 27 is complied from several tested SSI pipes.

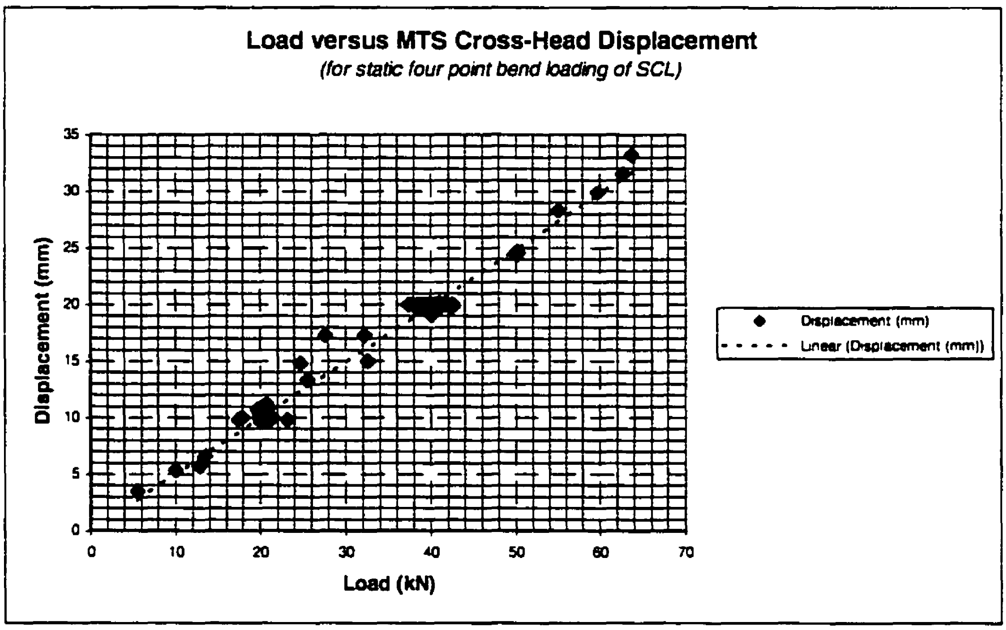

Figure 26 Relationship between Load and MTS Cross-Head Displacement for Composite Pipes under Four-Point Bending

A certain difference in load versus displacement values from experimental and analytical work is apparent in Figure 27.

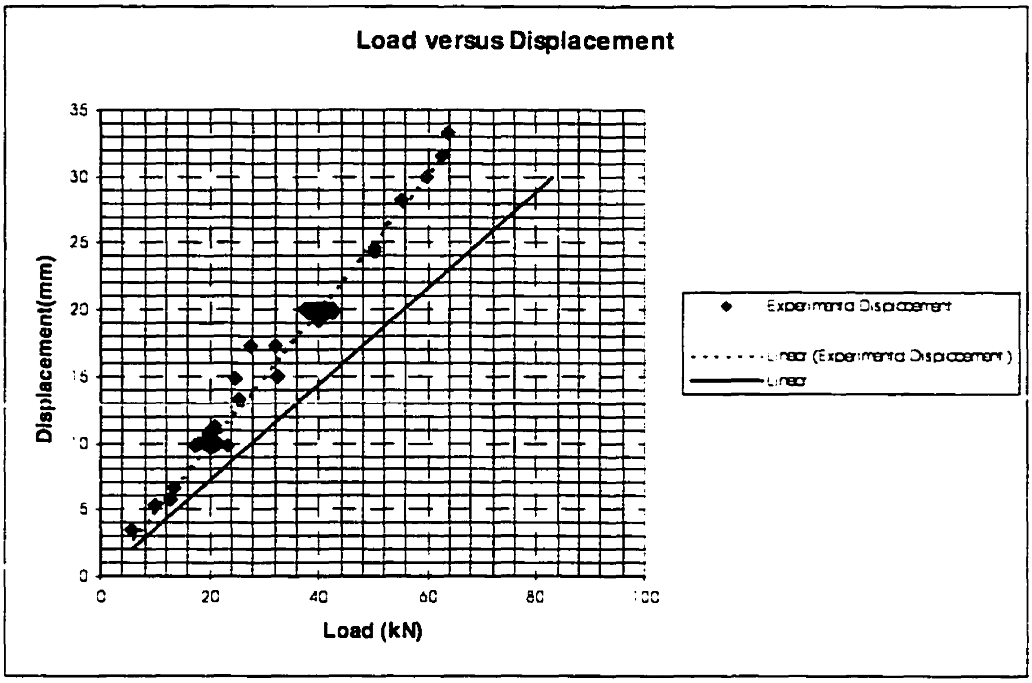

Figure 27. Relationship between Load and Displacement @ Point of Load Application for Composite Pipes under Four-Point Bending (Analytical and Experimental Values).

Through the strain values measured with extensiometer and strain gauge readings from the various tests, the equations relating displacement of the MTS cross-head at the points of load application on the pipe to strain was obtained. Equations for both the compressive and tensile faces of the pipe were found. Values from both static and selected conditioning cycles prior to fatigue testing were used for this purpose. The equation relating displacement to tensile strain was found to be

Equation 32

$$\varepsilon_1 = 4.9054 * 10^{-4} * Y_a$$

An R_{fit}^2 [xi] value of 0.994 with 1.00 being a perfect fit was found for the selected data.

Similarly for the compressive face, the equation was found to be

Equation 33

$$\varepsilon_1 = 3.5286 * 10^{-4} * Y_a$$

With an R_{fit}^2 [xi] value of 0.944.

[xi] R_{fit}^2-squared is not related to bending radius. Nor is it standard deviation. It is a measure of the accuracy of the curve fit to the data points. 1 would be a perfect match. APPENDIX D provides further explanation

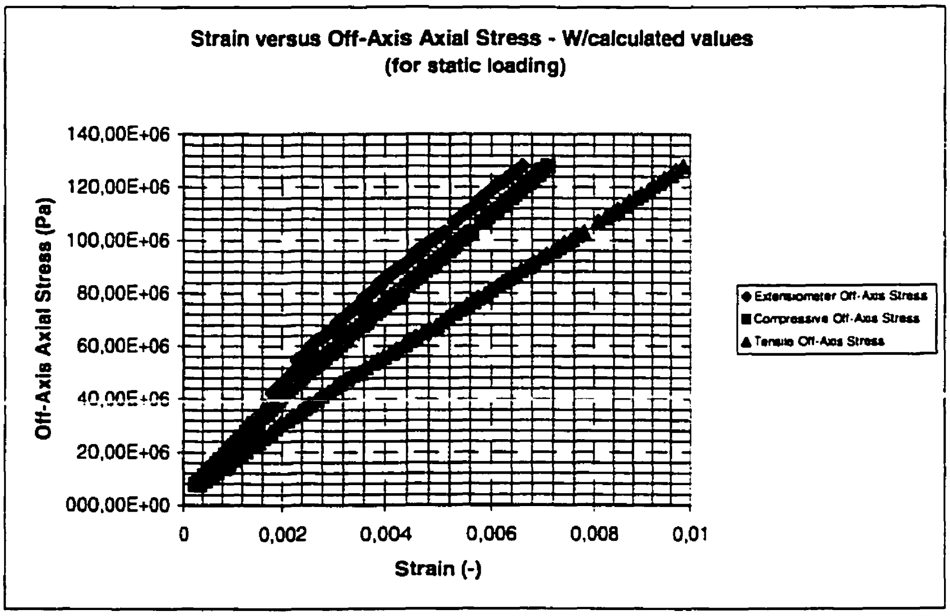

Figure 28. Comparative Development of Off-Axis Stress Plotted against Strain (Compressive and Tensile)

As can be seen above (Figure 28) compressive stress magnitudes increases faster than tensile stress values, indicating some effect causing shift in the neutral axis (APPENDIX F). The diamonds are for stress calculated from extensiometer measured compressive strain.

An equation relating MTS cross-head displacement to applied load was also sought. Only one equation was needed to describe the latter relationship. Load relates to displacement according to

Equation 34

$$Y_a = 4.9854 * 10^{-1} * W$$

The R_{fit}^2-squared[xi] value for this relationship was found to be 0.981.

In all of the above three equations (Equation 32 to Equation 34) absolute values have been used for total applied load and displacement. Off-axis axial strain (ε_1) is found for the tensile and compressive face of the pipe by using Equation 32 and Equation 33 respectively. This strain was then used to find the bending (spooling) radius (R) for the given MTS cross-head deflection using Equation 3. The value for spooling radius is then used in or Equation 7 to find the bending stiffness of the pipe. Finally, Equation 9 is used to find the off-axis axial stress (σ_1). Data series labelled "Compressive Off-Axis Stress" and "Tensile Off-Axis Stress" were found using this method. The data series labelled "Extensiomter Off-Axis Stress" was found from the extensiomter measured compressive strain, inputting the strain value into

Equation 3 and solving for R. The value found for the radius was then inputted into Equation 7 and the pipe bending stiffness determined. Then the off-axis axial stress was found from Equation 9.

As is apparent from Table 18, the bending stiffness is different for the compressive and tensile pipe faces. In lieu of the observed difference in measured off-axis surface strain (Figure 25) this is not surprising. In APPENDIX F, a short section on the effect of shift in the neutral axis as a result of different compressive and tensile material properties is presented.

Bending stiffness is found by:

a) inputting values for applied load and cross-head displacement at point of load application in to Equation 5

b) using measured compressive and tensile strains to solve for R in Equation 3 and substituting in for R in Equation 7.

These operations gave the following results for bending stiffness:

Table 18 Bending Stiffness (EI) of Composite Pipe from Experimental Data

Using W and Ya input values into Equation 5 - case (a) above. Bending stiffness (EI)		
EI (Pam4)	Standard deviation	95% Confidence
22637.0	406.0	240.0
Using measured tensile strain to find bending radius – case b) above. Bending stiffness (EI)		
EI (Pam4)	Standard deviation	95% Confidence
28036.0	1520.0	639.0
Using measured compressive strain to find bending radius - case b) above. Bending stiffness (EI)		
EI (Pam4)	Standard deviation	95% Confidence
39036.6	6858.0	3084.0

As can be seen from the curves in this chapter, the compressive strain found by using the mathematical relations, correlates fairly well with the directly measured strain values. In some cases the pipe appears to behave slightly non-linear when loaded statically. Unfortunately not enough samples were tested with instrumentation attached to the surface to confirm this.

While studying the curves describing compressive and tensile strains (Figure 23, Figure 24 and Figure 25) on the surface of the pipe, it is evident that the tensile strain is larger and growing at a faster rate than the compressive strain. The difference in compressive and tensile properties in the transverse ply direction (the matrix direction) most probably causes a shift in the neutral axis (APPENDIX F). Pipe samples that were taken to failure, failed on the compressive side by way of inter-ply de-lamination followed by fibre fracture in the hoop fibres in the outermost plies. This indicates large tensile through-thickness strains and stresses (de-lamination strains and stresses) on the compressive face of the pipe. Keeping in mind the large thickness of the hoop plies in the laminate, and the compressive matrix-direction properties, this is not entirely implausible.

It is also possible that the pipe became somewhat "out-of-roundness" as a result of bending, and the difference in compressive and tensile mechanical properties. This could have been investigated numerically, but when this effect was observed there was no more time available to do further experimental and numerical work. Ovality in pipe sections bent to their plastic limit is well known phenomena.

Figure 29 and Figure 30 shows the two general trends found with respect to development of E-modulus in SSI during static testing. In both cases the final value for the E-modulus approaches similar values for compressive (approximately 17 GPa) and tensile (approximately 12 GPa) modulus respectively. The trends show a reduction in apparent bending stiffness with decreasing bending radius and thus increasing surface strain.

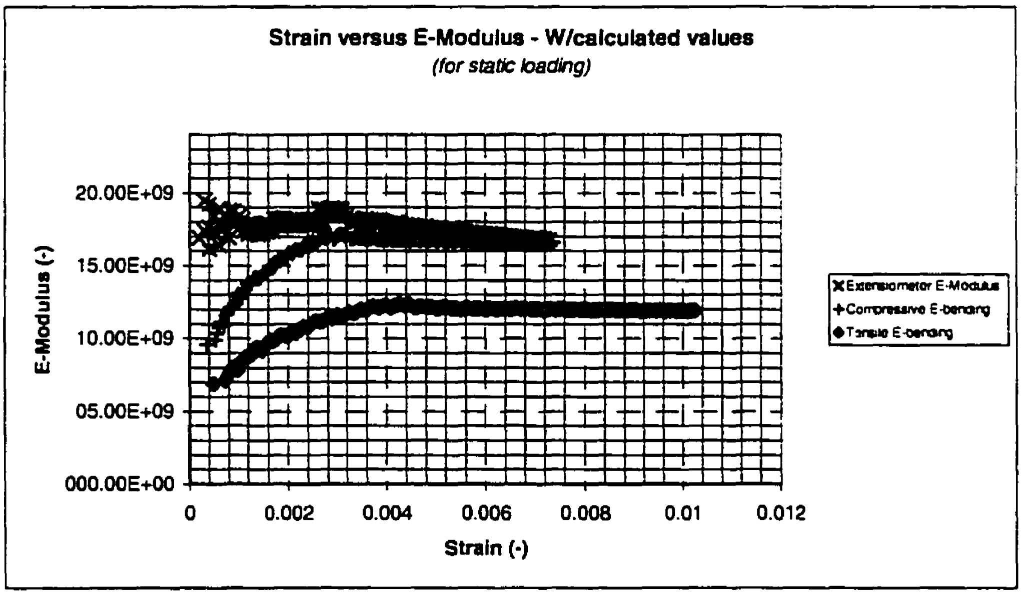

Figure 29 Strain versus E-Modulus for the Initial Conditioning Sequence in Static Four-Point Bend Tests

Figure 29 above, shows the first load cycle in the conditioning sequence for one of the test samples. Instead of bending stiffness (EI), elastic modulus is used on the y-axis. A second moment of inertia (I) of $2.221*10^{-6}$ was used to convert from bending stiffness to elastic modulus. Note the good correlation between the elastic modulus calculated from the measured extensiometer strain, and the compressive modulus found by using the measured cross-head deflection at the point of load application.

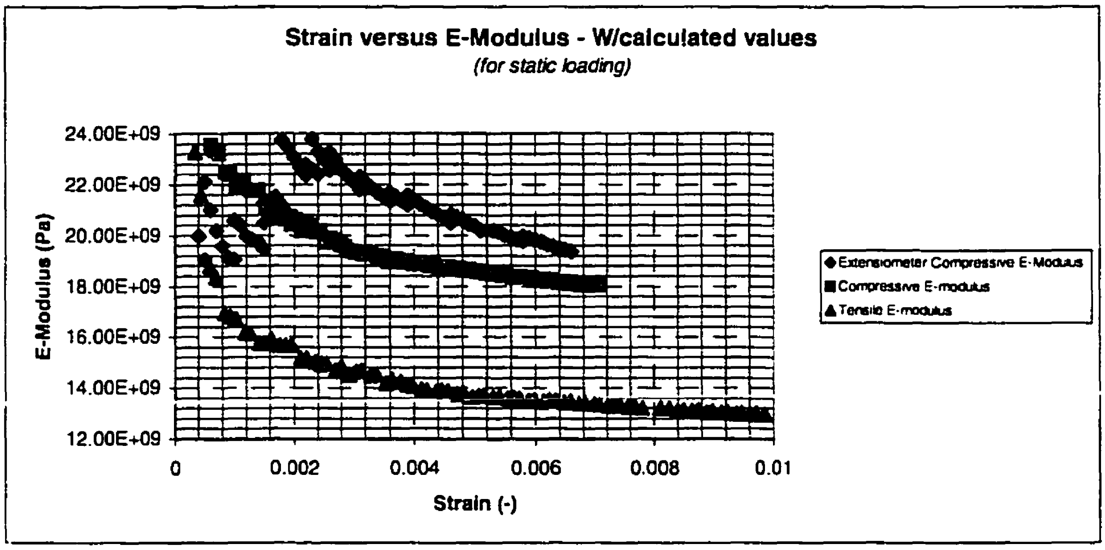

Figure 30 Strain versus Development in E-Modulus for the Initial Conditioning Sequence in Static Four-Point Bend Tests

In Figure 29 and Figure 30 the legends labelled "Extensiometer..." refer to data points found using measured strain (compressive). The measured strain, for a given load and cross-head deflection, is substituted into Equation 3 to find the bending radius of the pipe. Bending radius is then inserted into Equation 7, and the equation solved to find the bending stiffness. Knowing the second moment of area of the pipe cross-section, the elastic bending modulus is calculated. Legends starting with "Compressive..." or "Tensile..." refer to data points found using a known cross-head displacement in Equation 33 or Equation 32 respectively to find a strain value. Bending radius was then found using Equation 3, and the known applied load together with the bending radius substituted into Equation 7 to find the elastic bending modulus.

The difference in strain calculated, and cross-head displacement calculated elastic modulus for the compressive pipe face is larger in Figure 30 than in Figure 29. At present a satisfactory explanation for this can no be given. Possible explanations include differences in composite pipe properties and hence behaviour, inaccurate calibration of extensiometer and/or zeroing of cross-head displacement prior to test start.

The initial expected drop in modulus can be related to matrix cracking occurring in the initial stages of loading. It is also possible that non-linearity effects in the matrix material (epoxy) contribute towards the observed trend. However, Figure 31 indicates little or no non-linearity in the pipe. Particular attention should be paid to the part from time equals 2550 and onwards. A small amount of relaxation might take place just before the last bending test. Particular attention should be paid to the step trend in the measured strains after load release. The measured strain goes from zero to 0.0012 before the fourth conditioning event (section 6.1.3). The holding time at zero load is long enough to exclude large non-linearity effects from the matrix. In other words, the "residual" strain at zero load is due to matrix cracking.

Figure 31 also indicates how matrix cracks open up to produce large local strains with increasing number of conditioning event. The first two conditioning events have roughly the same end strain, whilst on the third event measured strain is peaking far above previously measured values. The strain gauge is still intact. This is obvious from it continuing to register data on the fourth and fifth loading events. These measurements were done during conditioning of the SSI pipes.

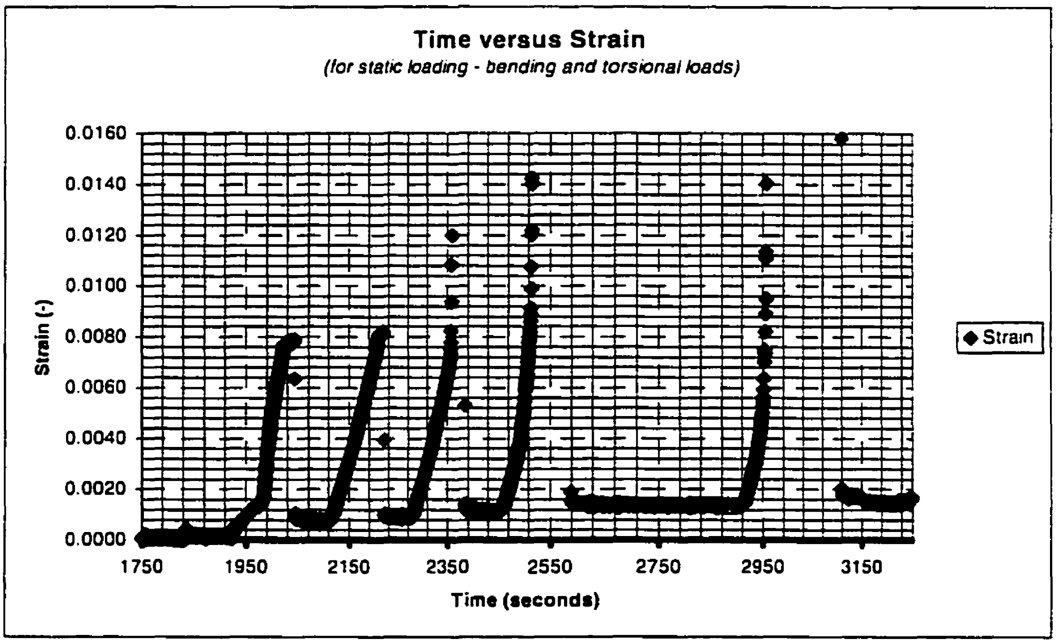

Figure 31 Strain Measured with Strain Gauges for 5 Bending Cycles of a Composite Pipe

Static failure of the tested composite pipes always occurred on the compressive face. This seems a little strange at first, as the measured tensile strains where larger than compressive for the same cross-head deflection. However, if we examine the possible explanation of shift in the neutral axis (APPENDIX F) a certain degree of clarity is obtained. Failure was preceded by large, wide circumferential cracks extending over roughly half the total circumference. The width of these cracks 2 mm approached in some cases. (Final failure often occurred close to the points of load application.) The first sign of final failure was whitening of the immediate surface followed by severe de-lamination of a strip 20 to 40 mm wide and stretching around ~1/3 of the pipe circumference. Once de-lamination had occurred, hoop fibres failed instantly, followed by catastrophic failure of the axial fibres, and hence of the pipe.

Table 19 is not what would be expected with respect to the relationship between strain and off-axis stress. In general one would assume the same absolute value for off-axis axial stress for the same absolute value of off-axis axial strain. Table 19 indicates that some mechanisms are in place that causes these variations. As has been suggested before, difference in material properties in compressive and tensile directions, causing a shift in the neutral axis of the pipe is at the moment the most plausible explanation (APPENDIX G). Other mechanisms may off course be in effect as well, with out these currently being obvious.

Table 19 Listing of Strains and Corresponding Stresses for Four Point Bending of SSI at the Middle of the Pipe Span, from Selected Test Results

Tensile Strain - ε_1 (-) 0.006 Off-Axis Axial Stress (MPa)		Tensile Strain - ε_1 (-) 0.01 Off-Axis Axial Stress (MPa)		Compressive Strain - ε_1 (-) - 0.006 Off-Axis Axial Stress (MPa)	
80		130		-110	
72 to 88		120 to 134		-102 to -118	
62 to 72		116 to 124		-100 to 104	
74 to 84		124 to 134		-104 to –114	
76 to 82		128 to 136		-106 to –114	
80 to 90		128 to 140		-108 to –120	
78 to 86		130 to 138		-108 to 116	
80 to 86		128 to 140		-100 to 116	
Average	Std.dev	Average	Std.dev	Average	Std.dev
79.333	7.106	130.000	6.890	109.333	6.436

By studying Table 20, we can see that the first mode of failure is matrix tension. The values found for matrix tensile failure indices are larger than 1, hence indicating failure[xii]. This failure mode is initiated at strains below the design strain of 0.6%. The failure indices calculated and presented in Table 20 are based on a modified version of those presented by Shokrieh[37]. No method for measuring data that could indicate through-thickness-strains (out-of-plane strains) was used. Hence, the equations describing the failure criteria are essentially those presented by Hashin, linear and in this case two dimensional.

The results should nevertheless not be cast away, as experimental observations support the predicted matrix tension failure as the first mode of failure. Experimental observations also indicate fibre-matrix shearing taking place at approximately the same pipe bending diameter as matrix failure initiation, indicating large out-of-plane stress, or larger shear stress to be present. Matrix failure on the compressive side is observed to initiate after matrix failure on the tensile side.

Final failure seems to be dominated by extremely large out-of-plane (normal) stresses. Delaminations of multiple plies are visible just prior to final failure. A complex three dimensional stress state is thus present in the pipe. The equations given in section 4.2.1 shows that the out-of-plane (normal) stresses would affect the failure mode predictions.

Table 20. Static failure indicies based on modified Ref 37 failure criteria

FAILURE INDICIES[xii]		
Static loading	*Tensile Strain - ε_l (-) 0.006*	
Fibre tension	Fibre-matrix shearing	Matrix tension
0.271	0.271	1.555
0.271	0.271	1.555
0.227	0.227	1.302
0.268	0.268	1.535
0.268	0.268	1.535
0.288	0.288	1.652
0.278	0.278	1.594
0.281	0.281	1.613
FAILURE INDICIES		
Static loading	*Tensile Strain - ε_l (-) 0.01*	
Fibre tension	Fibre-matrix shearing	Matrix tension
0.441	0.441	2.526
0.430	0.431	2.468
0.407	0.407	2.332
0.437	0.437	2.507
0.447	0.448	2.565
0.454	0.454	2.604
0.454	0.454	2.604
0.454	0.454	2.604
FAILURE INDICIES		
Static loading	*Compressive Strain - ε_l (-) -0.006*	
Fibre compression	Fibre-matrix shearing	Matrix compression
0.008	0.373	0.953
0.008	0.373	0.953
0.007	0.346	0.884
0.008	0.370	0.944
0.008	0.373	0.953
0.008	0.386	0.988
0.008	0.380	0.970
0.008	0.366	0.936

[xii] Values large than 1 (FI > 1) indicates failure

6.3.2 Bending Fatigue

Fatigue testing was performed in the same way as for static four-point bending, using the same equipment and set-up (Figure 12 and Figure 13).

A constant load was applied until failure of the pipe. Some pipes where tested to the point where surface fibre fracture were visible, others where fatigued until a certain cross-head displacement was reached. The stress ratio (load ratio), K, varied between -0.45 and -0.5. The variation was due to inherent software control inaccuracies. The pipes were cycled at a frequency of 0.5Hz.

The stress ratio is defined as the ratio of minimum applied stress to maximum applied stress (Equation 18). The pipe was not cycled around the zero point (neutral position). As a constant load was applied, and a stress ratio would require estimation of the induced stresses due to the applied loads, load (P_{min} and P_{max}) was used to find the stress ratio – K

A typical curve showing number of cycles versus cross-head deflection, is expected to have a relatively rapid initial increase in cross-head displacement, followed by a longer period of constant and slower increase in cross-head displacement. Finally an accelerated stage is reached. At this point, catastrophic failure is inevitable (Figure 32). Increase in measured cross-head displacement for a fixed applied load can be related to decrease in pipe bending stiffness.

The shapes of the slopes of observed curve(s), are potentially important. The initial drop in bending stiffness can be related to matrix cracking and possibly fibre-matrix shearing. During the slower middle phase, the initiated cracks grow, and some fibre fracture may take place. Inter-laminate de-laminations are also initiated and grow, indicating presence of relatively large through-thickness strains and stresses. The final stage is reached when matrix cracks and fibre-matrix shearing, combined with de-lamination growth reaches a critical level. At this point, inter-laminate de-lamination starts to grow, and fibres failing faster. Final failure is now only a few cycles away. Figure 32 shows a typical curve with maximum and minimum cross-head displacement versus number of cycles to failure. The figure also clearly shows the various stages of the fatigue process, initial, long intermediate and the rapid final failure stage.

Final failure unfortunately frequently occurred close to one of the points of load application. These areas have maximum shear and maximum bending moment. However, observations of the pipe surface indicate matrix crushing taking place at the top (compressive) face of the pipe. Matrix crushing would affect the final mode of failure. Future work should look at ways of distributing the loads at the points of load application more. One possibility is to use inserts for reinforcement of the pipe under the points of load application.

All specimens used for bending fatigue experiments were conditioned (6.1.3) prior to fatigue testing commencement. The samples were bent four times to an MTS cross-head displacement of 20 mm, corresponding to about 0.98% tensile and 0.71% compressive off-axis axial strain (measured). After each bend cycle, the samples were twisted 90 degrees in order to initiate damage around the circumference of the pipe. Fatigue testing always started on the same face as the first conditioning cycle.

A total of 8 specimens were tested at various load levels for the case of pure four point bending. An S-N curve was obtained. Due to time limitations and availability of a limited number of test specimens, only loads larger than 70% of the measured static bending strength were used for testing.

A number of specimens were also exposed to torsional loading before bending fatigue. Torsion testing in it self was not entirely successful. However, when comparing the number of cycles to failure at the loads selected for pure bending with the number of cycles to failure for specimens twisted and bent before fatigue testing, little or no difference was observed. This is not surprising considering the small twist induced through the set-up for torque application.

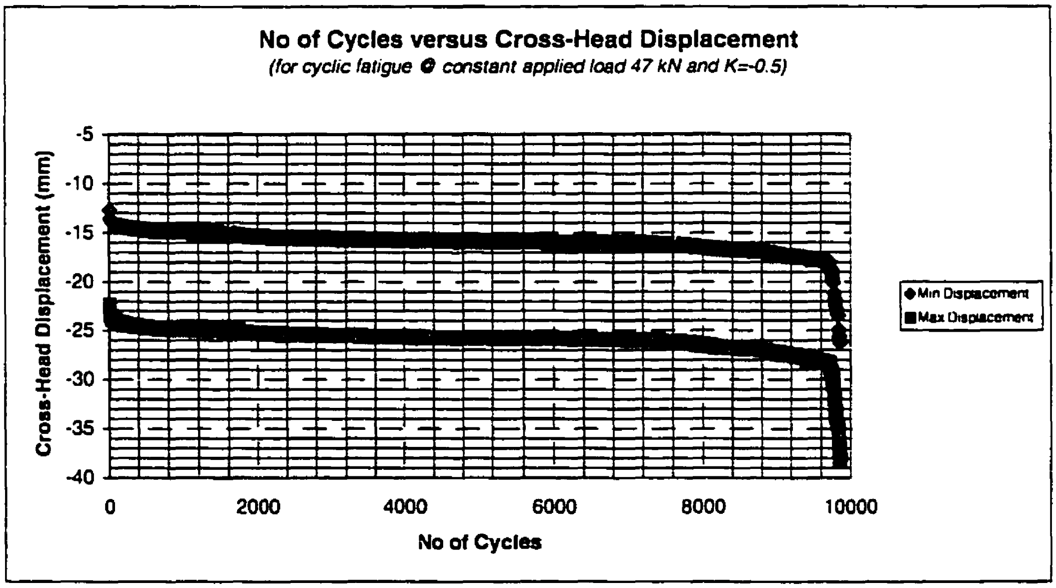

Figure 32 Minimum and Maximum Cross-Head Displacement for a Constant Applied Load of 47 kN

Another curve, Figure 33 (from a different test), shows the maximum cross-head displacement with the measured off-axis axial surface strain as an overlay. Note the similar shape of the two curves. The staggered appearance of the curves is due to the MTS applied load for some reason "adjusting" itself towards the end of the pipe fatigue life. As mentioned, all fatigue experiments where done using constant amplitude maximum load. But in this test, which was left alone with a guard to prevent cross-head deflection exceed a certain value, the applied load was reduced by the software, or the machine was for some reason unable to keep the applied load constant at the pre-set value. This resulted in a longer fatigue life for the specimen being tested. This behaviour was only observed for one test. The "adjustment" occurred after final failure of the pipe would be inevitable. Thus, including this result in the total result discussion did not skew the results.

Both Figure 32 and Figure 33 exhibits the same curve shapes with respect to the development of cross-head displacement development. The curves are from two different tests (pipes).

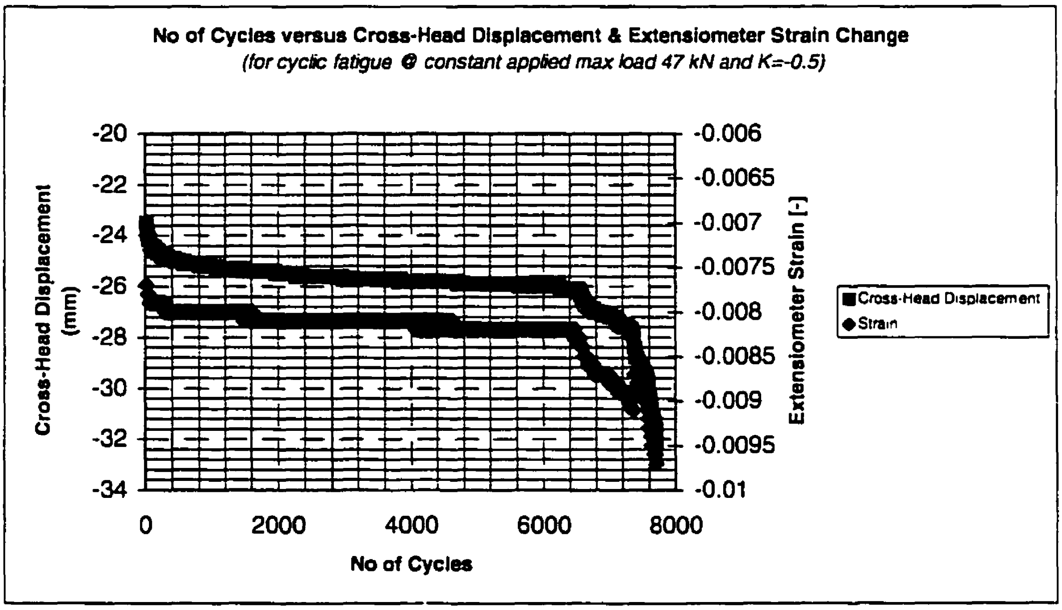

Figure 33 Softening of SSI Exposed to Constant Amplitude Fatigue Load (47 kN). Cross-Head Displacement and Extensiometer Strain Shown.

From Figure 33 we can observe that a reduction in applied load at a point before catastrophic failure is initiated prolongs the fatigue life of the SSI pipe. By being alert for such abrupt changes at medium high cyclic strain fatigue loads, it might be possible to prevent catastrophic failure of SSI. This off course requires that the load applying device, or scenario in itself is capable of reacting to an abrupt change in deflection while loading the pipe. In this test case this happened only because the MTS machine somehow failed to maintain the pre-set load pattern. In a real life case this is unlikely to happen. The observation also supports an idea of it being possible to use a Miner-Palmgren cumulative damage rule[54] to find residual fatigue life of a composite pipe having been exposed to a known fatigue loading scenario.

Comparing the total number of cycles to failure in Figure 33 and Figure 32 (for the same applied load), it becomes obvious that there is a relatively large scatter wrt. fatigue life of SSIs'.

Initial damage, matrix micro-cracking, and possibly fibre-matrix cracking (Figure 33 and Figure 32), is rapid and occurs over the first 400 cycles of the fatigue life. A relatively "quiet" period follows where the matrix and fibre-matrix cracks develop and grow whilst the reinforcing fibres gradually loose stiffness and strength. Fibre failure also occurs at this stage. Final failure occurs rapidly and within the span of a few hundred cycles. This last stage is dominated by the reinforcing fibres accelerated loss of structural integrity and inter-ply de-lamination growth.

Figure 34 is presented with log-log scale in an attempt to more clearly identify damage mechanisms and the transition between these during fatigue testing of the SSI pipes.

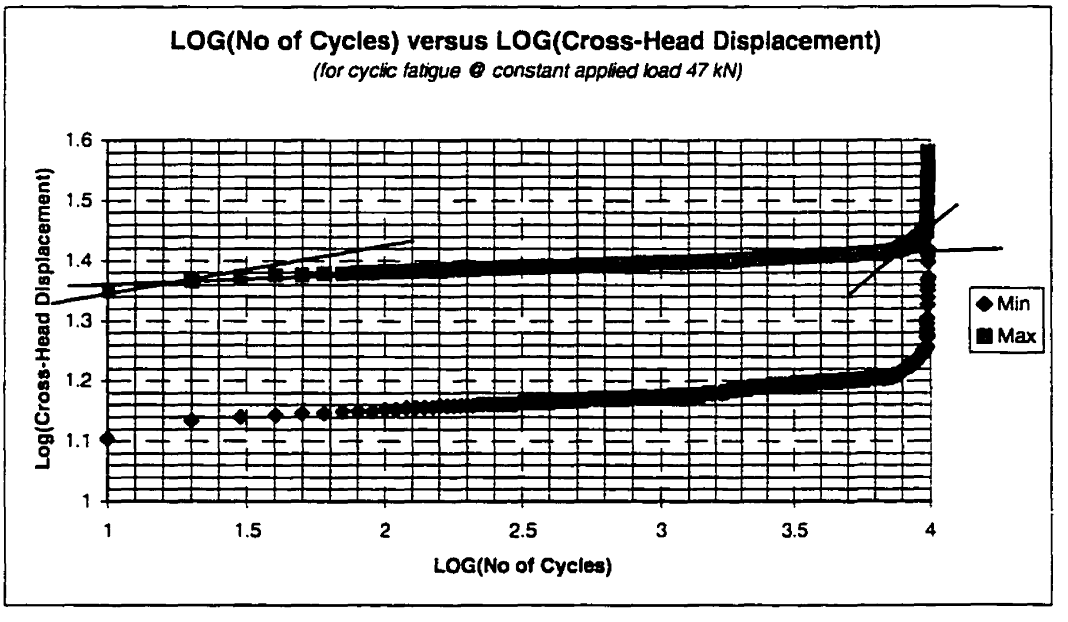

Figure 34 Log-Log values for Constant Applied Load of 47 kN using No. of Cycles and Cross-Head Displacement

In Figure 34, it is possible to identify three to four different failure mechanisms/modes of failure. Between x-values 1.0 - 1.3 matrix micro-cracking and fibre-matrix (shearing) cracking will be the dominant mechanisms. Then follows matrix and fibre-matrix crack growth, and slow decrease in stiffness and strength of the reinforcing fibres. From x-values 3.8 to 4.0 severe matrix cracking and tensile de-laminations separating individual plies occurs, before catastrophic failure of the pipe takes place due to complete tensile separation of plies and fracture of axial fibres. The last two failure sequences take place rapidly. After onset of the severe tensile de-lamination stage, the pipe has effectively lost all its structural integrity and will fail.

A material or structure can have its fatigue life characterised through a series of tests eventually resulting in the S-N curve (Figure 35). The S-N curve shows the number of cycles to failure on the x-axis with the load or stress represented on the y-axis. Sometimes log scales are used to give a better overview of the fatigue characteristics.

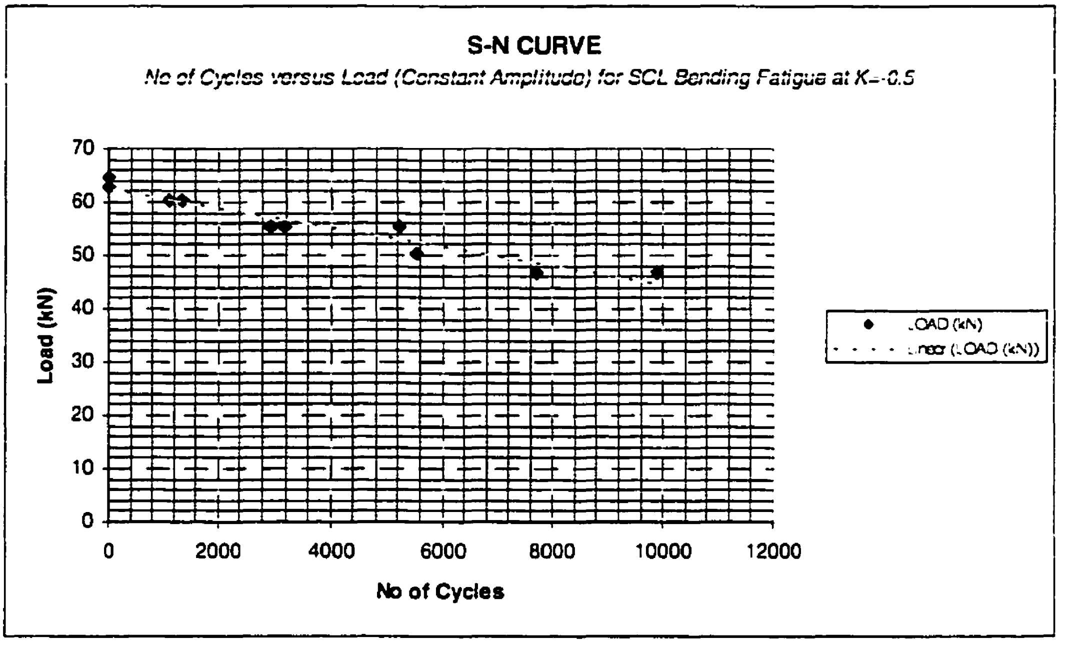

Figure 35 Predicted Number of Cycles to Failure for Various Load Levels for SSI Bending Fatigue

The data points in Figure 35 are nicely gathered on a straight line.

Figure 36 is shows the same data as Figure 35, only zooming in on the data points, and using log scales on both the x- and y-axes. A fairly nice straight line emerges. A linear trend fit predicts a bending failure load of about 62 kN for virgin pipe. This is not far from the values measured during static testing (Table 17) of 63.7 kN. The curve suggests that the SSI pipe should be able to sustain almost 1000 cycles for applied bending loads just a few kN below virgin failure load. Based on the experimental data obtained for bending loads of 60.3 kN, equivalent of 95% of ultimate static bending strength, this would seem to correlate well. For lower loads however, the number of cycles to failure drops faster than would be expected. The linear curve predicts that for an applied bending load of 10 kN number of cycles to failure is around 32 000.

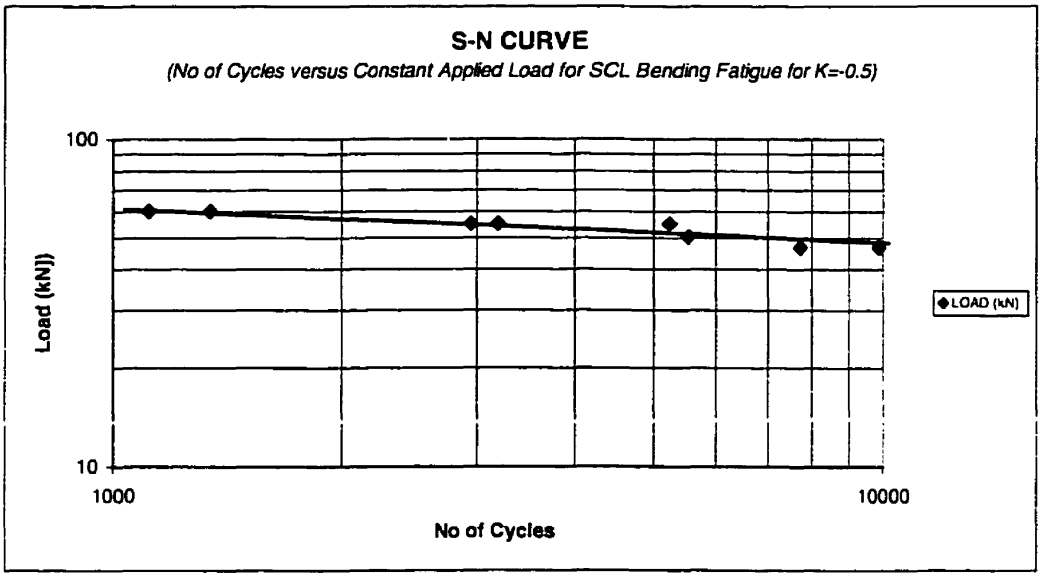

Figure 36 S-N Curve for Four Point Bending Fatigue of 2.5" SSI

The trendlines that can be obtained from and plotted in Figure 35 and Figure 36 are extremely conservative, as one would normally expect to find a plateau value for applied load (induced stress), where the fatigue life would approach infinity. In this research, fatigue life at low stress levels was not investigated, hence such a plateau was not found.

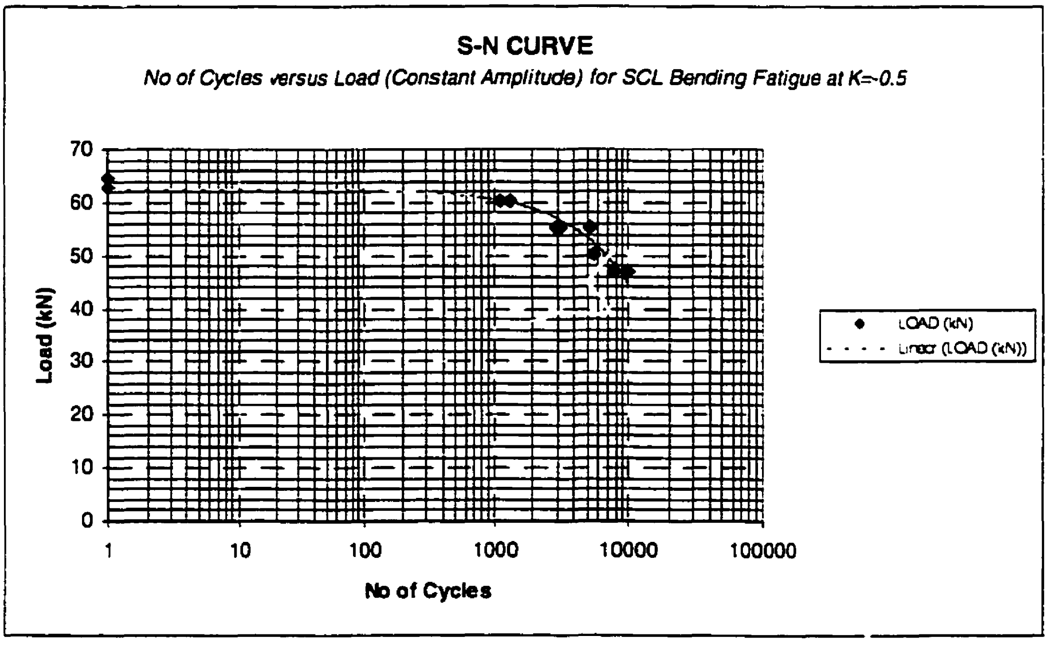

Figure 37 S-N Curve for Four-Point Bending of Composite Pipes with Extrapolated Linear Curve-Fit Included (linear curve if seen in a linear-linear graph)

The curve fit of experimental data is a linear least square approximation. In Figure 37 the curve fit would appear non-linear, but this is due to the use of a logarithmic scale on the x-axis. Figure 37 is similar to Figure 35 except for the use of a logarithmic scale on the x-axis.

The equation for the linear curve fit of the S-N curve is:

Equation 35

$$F(X) = -1.81 * 10^{-3} \times X + 62.4$$

with an $R_{fit}^2 = 0.92$

The projected curve in Figure 35 and Figure 37 shows that the pipe can not sustain fatigue bending loads to such an extent as to qualify for use in long term dynamic load scenarios. Regardless of the accuracy of the projected curve (Equation 35), the design philosophy behind the SSI was governed by internal static high pressure. Literature has several times shown glass fibre composites to have a shorter fatigue life than to carbon fibre composites.

Table 21 Summary of Compressive Stress, Strain, Applied Load and Displacement for Cyclic Fatigue of SSI.

ID	Applied Load (kN)	Induced stress - σ_l (MPa)	ε_l start (-)	ε_l end (-)	Cross-Head Displ (mm) start	Cross-Head Displ (mm) end
BF009	47	-143.94	-0.0078	-0.0097	23.9	32.2
BF009	47	-143.94	-0.0083	-0.0114	23.9	32.2
BF010	47	-144.1	-0.0083	-0.0119	23.6	32.5
BF008	48.5	-149.32	-0.0087	-0.0096	24.5	28.2
BF003	50	-154.5	-0.0087	-0.0124	24.6	32.2
BT006[xiii]	55	-169.02	-0.0104	-0.0119	27.5	31.5
BT006[xiv]	55	-169.08	-0.0098	-0.0112	27.5	31.5
BF004	55	-169.43	-0.0099	-0.0111	28.1	31.0
BF005	55	-169.33	-0.0097	-0.0115	27.5	31.6
BF006	60	-185.5	-0.0111	-0.0129	31.3	34.7
BF007	60	-185.17	-0.0111	-0.0124	31.4	35.2

The radius of curvature was found using Equation 3. Then from the relation (Equation 7 solved for D) below the change in stiffness with number of cycles was found. From the simplified assumption in Equation 9 the off-axis axial stress was estimated.

[xiii] The two values for off-axis axial stress was calculated using two different approaches

Table 22 Summary of Tensile Stress, Strain, Applied Load and Displacement for Cyclic Fatigue of SSI.

ID	Applied Load (kN)	Induced stress - σ_1 (MPa)	ε_1 start (-)	ε_1 end (-)	Cross-Head Displ (mm) start	Cross-Head Displ (mm) end
BF009	47	143.94	0.0115	0.0158	23.9	32.2
BF010	47	144.1	0.0116	0.0165	23.6	32.5
BF008	48.5	149.32	0.0120	0.0134	24.5	28.2
BF003	50	154.5	0.0121	0.0173	24.6	32.2
BT006	55	169.02	0.0136	0.0155	27.5	31.5
BF004	55	169.43	0.0138	0.0155	28.1	31.0
BF005	55	169.33	0.0135	0.0159	27.5	31.6
BF006	60	185.5	0.0154	0.0180	31.3	34.7
BF007	60	185.17	0.0154	0.0173	31.4	35.2

Equation 36

$$E = \frac{D * W * \left(l^2 - a^2\right)}{(l + a) * 2 * l}$$

By using the classical relationship between off-axis and on-axis stress and strain values it is possible to estimate stresses in the fibre, matrix and shear directions[46] and use these in failure criteria calculations.

Examining the data in Table 21 and Table 22, we can see that the initial strain values, both for tensile and compressive pipe faces, falls on a nice straight line. Failure strains show larger scatter. The scatter can possibly be explained from a statistical point of view. This research did not include efforts using statistical analysis to better fit measured data to mathematical models. From the nature of polymeric composite materials we know that there will be statistical[55] differences, local flaws, points of stress concentration in particular on the surface of the pipe etc., contributing towards differences in observed properties and behaviour.

Figure 38 presents the experimental data using a log scale on the x-axis, and off-axis axial stress on the y-axis. The curve also has the measured static failure stress plotted at approximately 195 MPa.

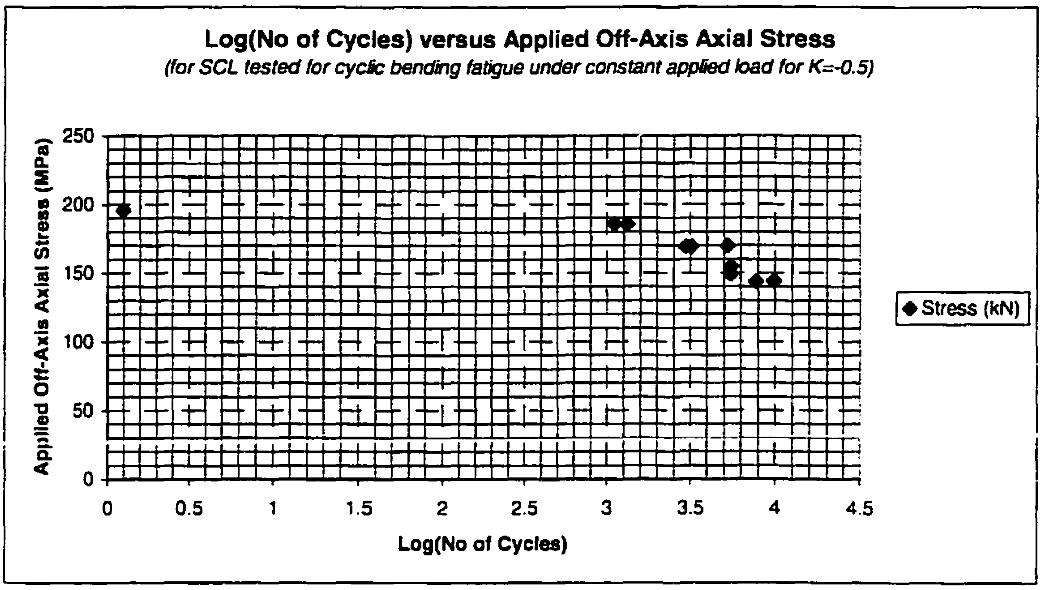

Figure 38 Log of number of cycles to failure versus applied load

As can be seen from Figure 38, an approximate straight line can be drawn through the data points for the fatigued pipes. Looking into literature for research on fatigue of composites under constant-amplitude loading using a stress ratio of 0.5, a paper by Gathercole et al[49] gave interesting information. Their research was performed on flat carbon fibre reinforced laminates. By disregarding the number of cycles to failure and the applied stresses, and using only the shape of the curves, their figure 4, peak stress versus Log(N_f), has a curve for K = 0.5 that looks very much like the shape predicted by the data points presented in this thesis.

Somewhere between the measured static strength and the first data point depicting a fatigued SSI pipe, there is a transition in failure mechanism. The static bending strength is decided by the fibre strength of the pipe, while the fatigue life is much more influenced by the matrix properties of the structure. That is not to say that it is the matrix which fully decides the fatigue life of the pipe, only that it plays a much more important role in cyclic fatigue than in static bending strength tests.

As discussed earlier, using constant applied load results in a constant degradation in stiffness, visible in the raw data as an increase in MTS cross-head displacement with progressing number of cycles. Change in bending stiffness was estimated using the mathematical relationships in Equation 3 and Equation 7 as described in b) on page 59, and the resulting bending stiffness plotted against number of cycles (Figure 39).

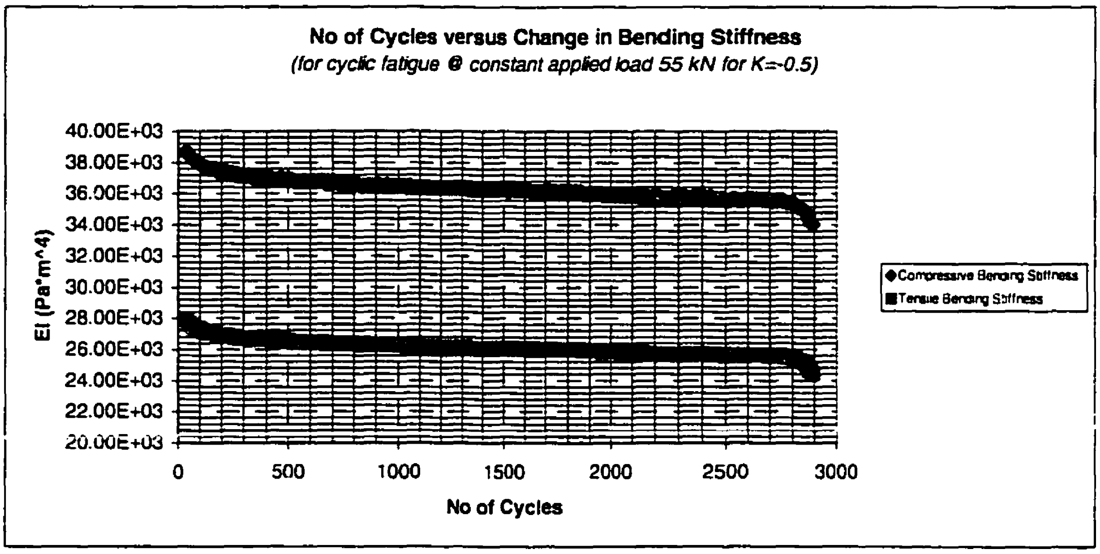

Figure 39 Reduction in Bending Stiffness with number of Cycles for Constant Applied Load

In Figure 39 the reduction in bending stiffness, represented as drop in EI, is obvious. Note the initial rapid drop in stiffness over roughly the first 100 - 400 cycles. Next comes the constant linear slow reduction in bending stiffness followed by fast failure occurring over the last 100 cycles or so. The linear slow stiffness reduction part and the last drop towards final failure are easier to see in Figure 40. Here, reduction in elastic modulus has been used to represent drop in pipe stiffness. Representation of the progress towards fatigue failure with change in surface off-axis axial strain is done in Figure 41. This figure corresponds well with the observations of Perreux et al[56]. The experimental work in reference 56 is different from that presented in this thesis, but the general shapes of the curves are similar. Note that absolute values for strain have been used.

Comparing Figure 40 and Figure 42, which are plots from two different tests, it is clear that both have a linear region from a point after the initial damage sequence is terminated to final failure initiation. It is however, more difficult to find the initial damage sequence section in these two plots. Figure 41 and Figure 39 show the initial damage sequence section much better.

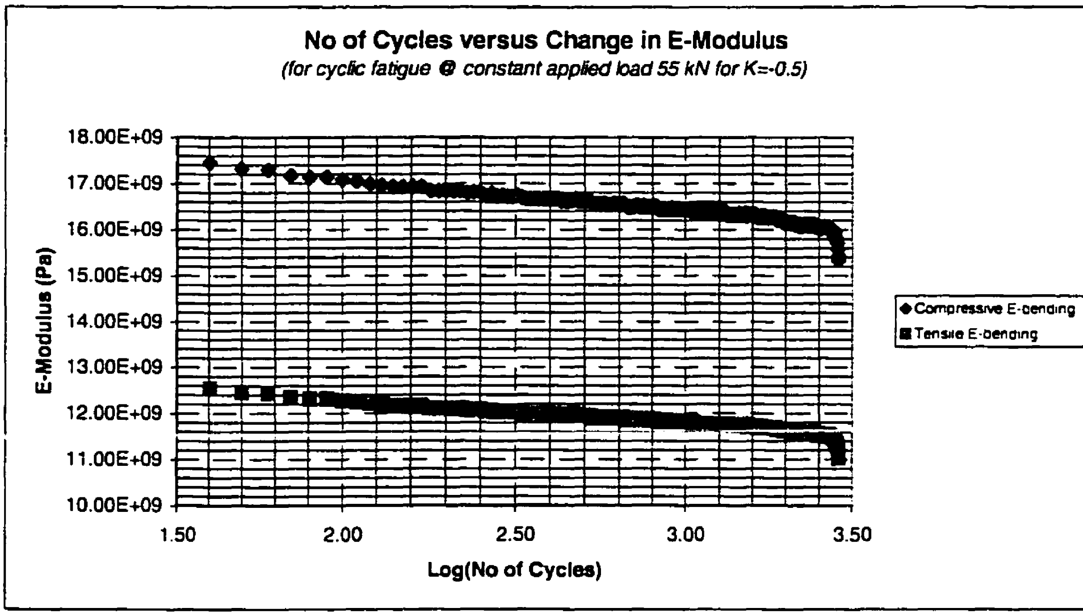

Figure 40 Reduction in Bending Elastic Modulus for SSI under constant applied load represented using log(no of cycles) on the x-axis

Another interesting property to examine is the retained or residual stiffness just prior to the point of failure of the composite pipes.

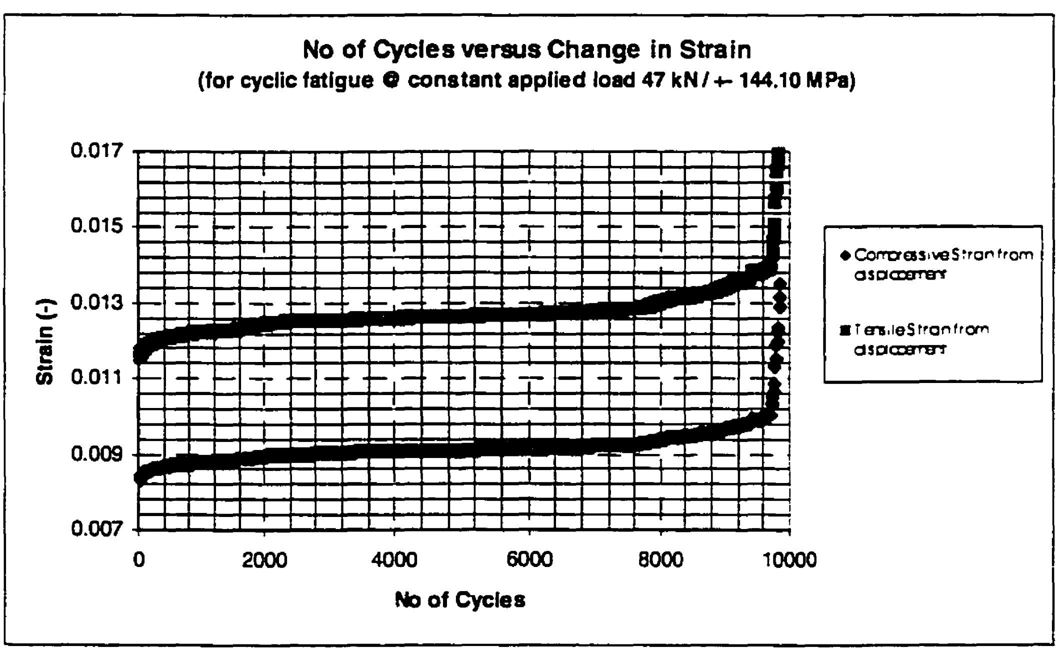

Figure 41 Change in Off-Axis Axial Strain as a function of No. of cycles to Failure.

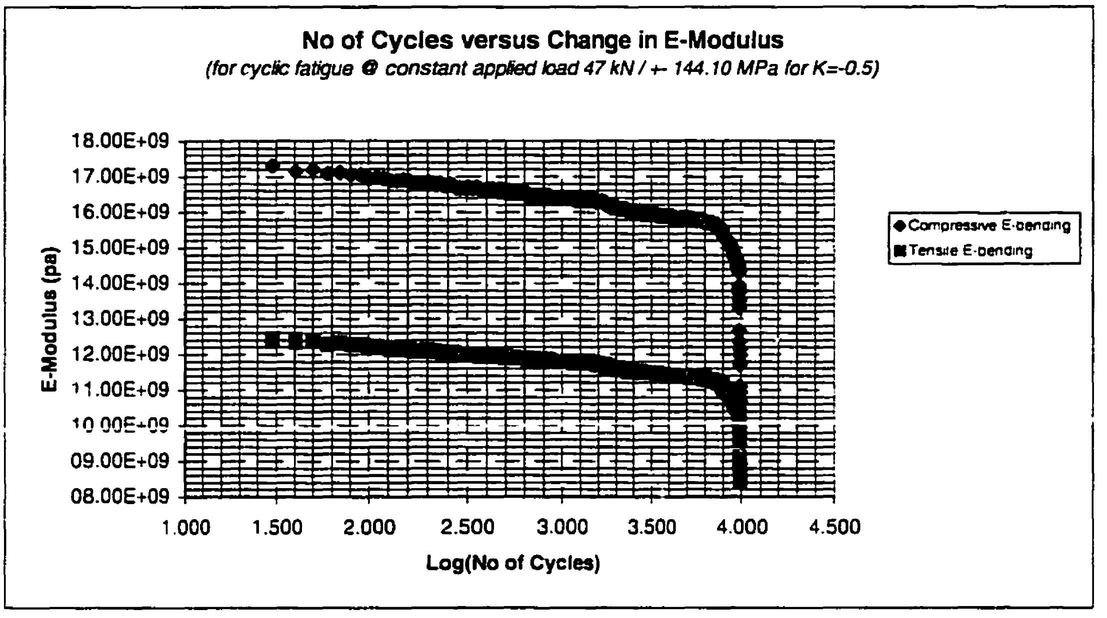

Figure 42. Log(No of Cycles) versus Reduction in Stiffness Represented as Drop in Elastic Modulus.

Figure 43 shows the stiffness just before failure of SSI pipes exposed to constant amplitude (load) bending fatigue. Both tensile and compressive face "stiffness" is plotted. Data points are average values obtained from the tests executed.

From Figure 43 we can see that the residual stiffness of the SSI pipe at just prior to final fatigue failure increases with the applied load, and hence induced off-axis axial stress in the pipe. The trend indicated by the data points above looks non-linear. No attempt to identify an equation describing the development of residual stiffness to normalised applied load was performed. The reason being insufficient data for low bending fatigue loads.

The curve shown by the data points in Figure 43 indicates that, at high off-axis axial stresses (equivalent to high applied loads), the pipe retains much more bending stiffness just before the point of failure than at lower stress cycling. This should mean that at higher loads the dominant failure mechanism (or mode) is fibre failure, and that hoop fibres play a less important role. At lower cyclic stresses, the most important damaging mechanism (mode) is matrix cracking and fatiguing of the matrix. Table 23 shows the data used to create Figure 43 prior to normalisation. Note the larger reduction in residual stiffness prior to final failure for the lower load amplitudes.

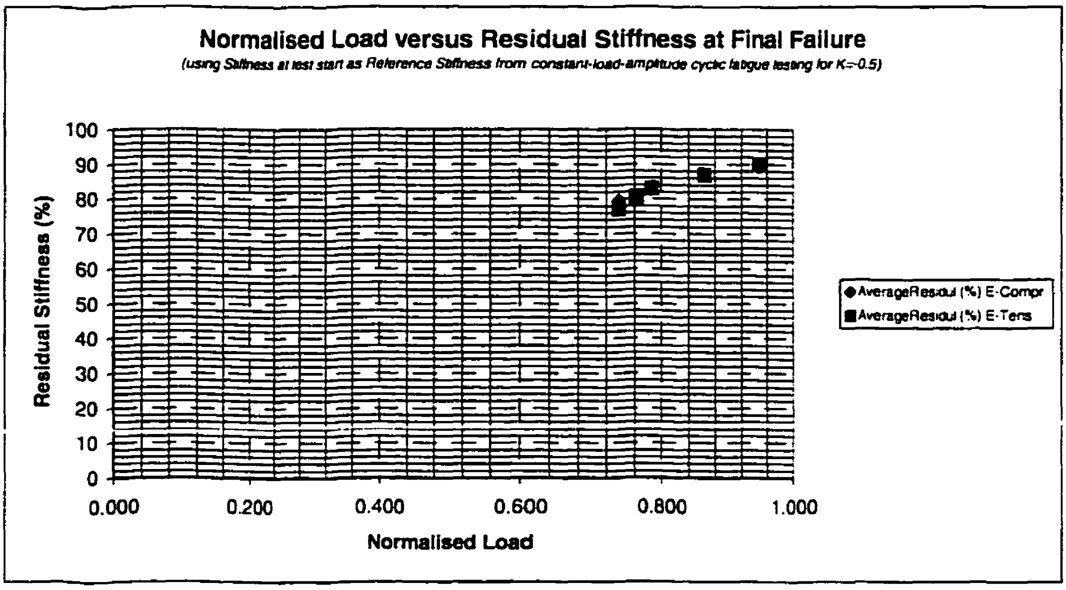

Figure 43. Normalised Load versus Average Residual Stiffness from All Tests

Table 23. Elastic Bending Modulus at start and Failure of SSI

Loading Cases		Bending Compressive E-Modulus		Bending Tensile E-Modulus	
Applied Load (kN)	Applied Load / Max Load	Start (GPa)	Failure (GPa)	Start (GPa)	Failure (GPa)
47	0.74	17.42	13.3	12.53	9.57
47	0.74	17.27	13.44	12.42	9.67
48.5	0.76	17.28	13.92	12.43	10.02
50	0.78	18	14.96	12.95	10.76
55	0.86	17.23	15.21	12.39	10.94
55	0.86	17.45	14.66	12.55	10.54
55	0.86	17.11	15.12	12.31	10.88
60	0.95	16.75	15.06	12.05	10.83
60	0.95	16.7	14.89	12.01	10.71

6.3.3 Bending Fatigue of Torsion Loaded Pipes

As mentioned in chapter 6.3.2, pipes exposed to static torsion and torsion-bending are expected to behave similarly to those only exposed to static bending. Three pipes were twisted and bent prior to fatigue testing. The results are presented as part of an S-N curve where fatigue results from chapter 6.3.2 also are included.

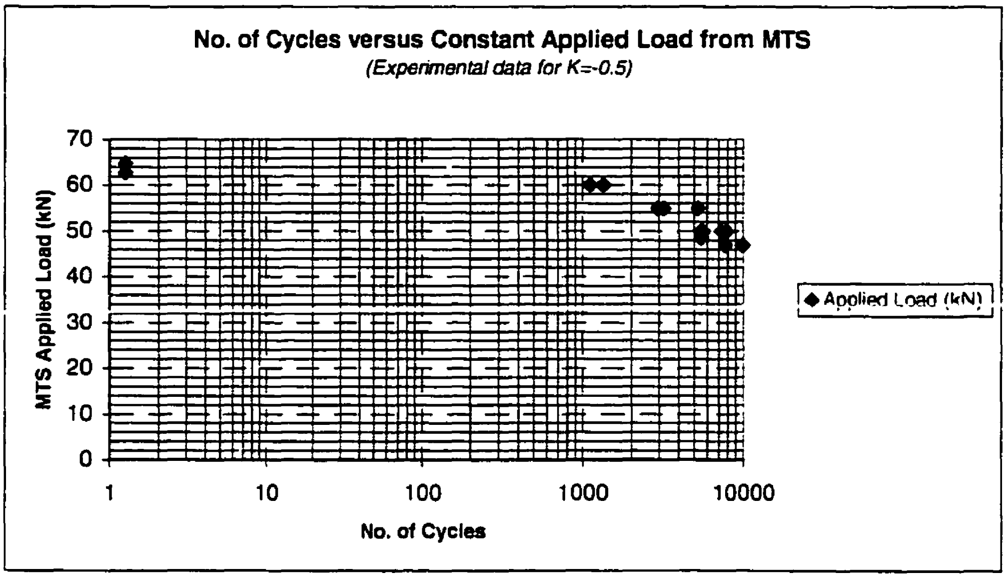

Figure 44 S-N curve including pre-twisted pipes

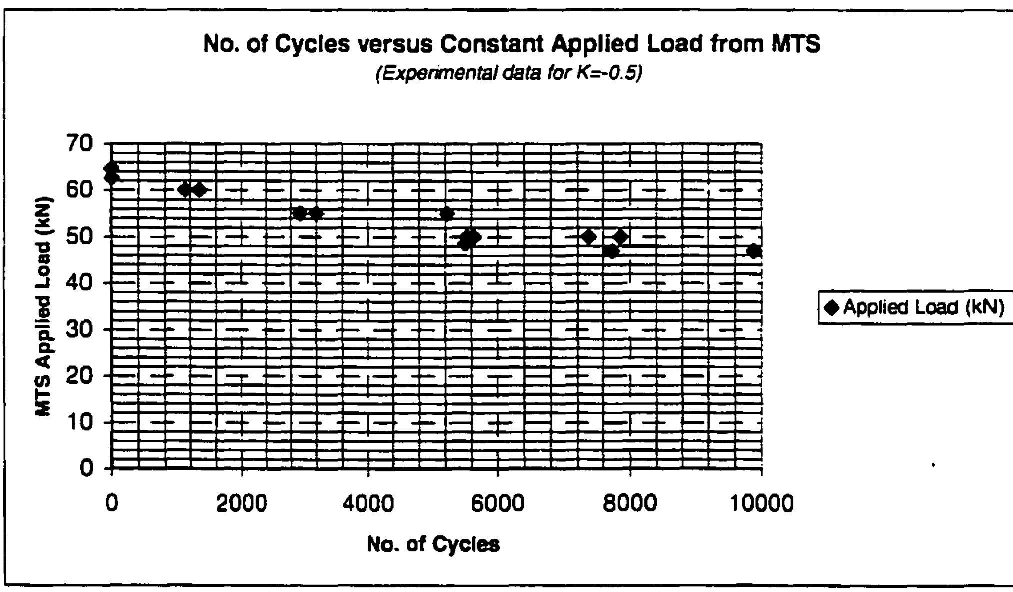

Figure 45 S-N curve including pre-twisted pipes on linear scales

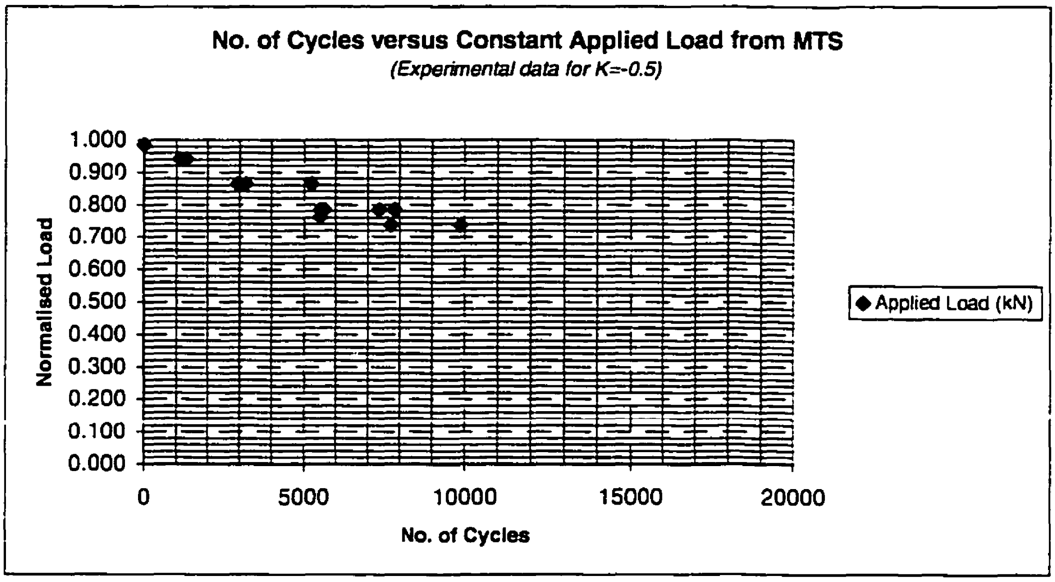

Figure 46 Number cycles versus of normalised load including pre-twisted pipe results

From Figure 44 to Figure 46 it can be seen that the points on the S-N curve follow the same trend as in Figure 35. Hence, the pre-twisting of the pipes did not reduce fatigue capacity of the SSI. The points that were included were all for 50 kN applied MTS load tests (about 78% of measured maximum bending load).

7 Visual Observations

All final failures visible on the exterior of the pipe have the same appearance: Tensile de-lamination that causes immediate fibre failures in the top two or three hoop plies, followed by rapid fibre failures of the axial ply. These final failures all originates from two of the circumferential matrix cracks initiated in the first few bending cycles.

Pipes that were not taken to complete failure all exhibited extensive surface damage visible as matrix cracking, in some cases extending around the entire circumference of the pipe. Most of the pipes had one or two very wide cracks extending around about 2/3 of the circumference. These cracks were approximately 1 to 2 mm in width. Figure 47 is a sketch of a typically failed pipe.

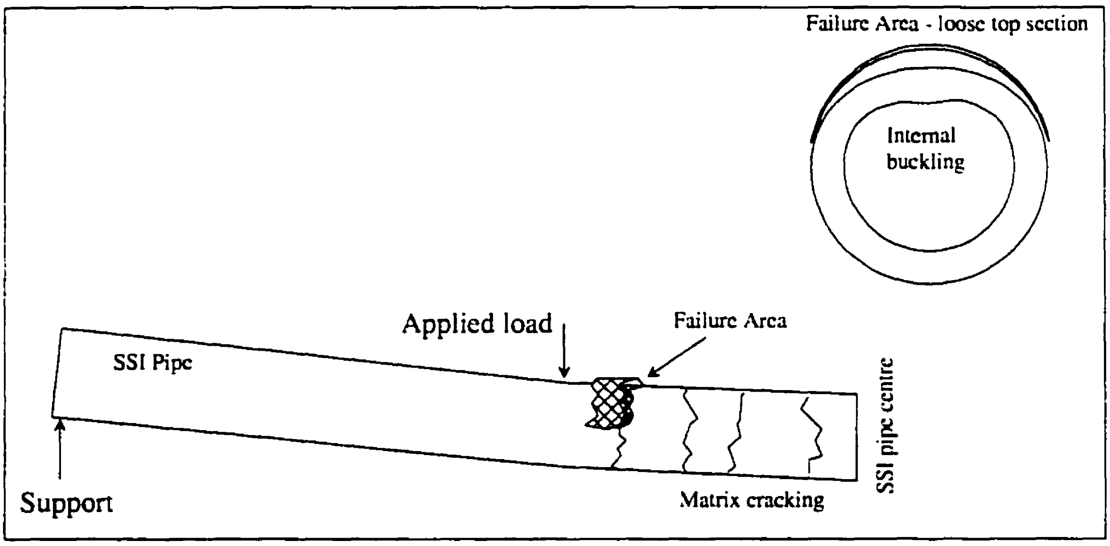

Figure 47 Sketch of SSI Pipe Failure.

A systematic effort to register the density of the cracks was not initiated, but typical surface crack spacing was between 10 and 40 (mm).

Fatigue failure saw growth of what appeared to be matrix or fibre-matrix cracks on both the compressive and tensile faces of the pipe. It is unknown whether or not these cracks initiated or caused failure of hoop fibres throughout the laminate as no microscopy or pressure testing was performed after fatigue testing.

Internal examination of failed pipes revealed the liner on the compressive side to have a discontinuous angle just underneath the point of failure. The tensile side was smooth and continuous. This observation indicates buckling having taken place on the compressive side of the pipe. Considering the lay-up of the laminate it is very plausible that the axial fibres have buckled into the liner. The liner is much less stiff than the reinforcing glass fibres, and hence prone to inward buckling in the current pipe design.

The observed differences in bending stiffness of the composite pipes, as differences in measured surface compressive and tensile surface strain, indicates either:

- Difference in material properties, either initially, or a as a result of damage
- Geometrical effects from, say, the pipe not being round, either initially, or due to the high bending strains
- Both of the above

8 DISCUSSION

8.1 Comparison of Analytical, Numerical and Physical Test Results

Static bending modelled by I-DEAS master series correlates well with experimental observations only for tensile strain-displacement results. The same is true for experimental-analytical, as would be expected. Load-strain relationship is good for tensile data when comparing analytical and experimental results. Although reasonable results for strain-displacement analysis and experimental work were obtained for the tensile cases, complete success was not accomplished. Results from the experimental part of the research diverge from the analytical and numerical solutions found in several respects. A summary is presented in Table 24.

Table 24. Summary of analytical, numerical and experimental results for static loading cases.

	Analytical - Experimental		Analytical – Numerical	Experimental – Numerical	
	Tensile	Compressive	Tensile & Compressive	Tensile	Compressive
Strain – Load	-8% to – 11 %	14% to 18%	-28% to –29%	-19% to – 22%	-36% to – 39%
Strain – Displacement	20 to 24%	70% to 79%	15% to 18%	-4% to –5%	-32% to – 34%
Load – Displacement	33% to 39%		53% to 61%	15% to 16%	

The best explanation for the differences found with respect to the numerical analysis and the solutions for analytical as well as experimental work are the use of thin shell elements to model the pipe. Differences between analytical and numerical results can also be partly contributed to the use of thin shell elements. The laminate is in reality a thick shell, requiring solid elements for proper modelling in the I-DEAS FEA software. A pipe in isotropic material is considered thin walled when the ratio of wall thickness to pipe radius is about 1:20[57].

It is also worth noting the differences between tensile and compressive face values. These differences can be contributed to geometrical and material effects. Geometrical differences can be related to the test set-up, but should be small. Material differences from a claim that composites have inferior tensile matrix dominated properties to compressive. The pipe studied (SSI pipe) has a laminate consisting of a majority of hoop plies. In other words when being bent, the pipe will tend to have a higher E-modulus on the compressive face than the tensile face. A consideration of neutral axis shift in the composite pipe is included in APPENDIX F. The shift in neutral axis is assumed to be mainly due to material properties.

Attempts to make use of the McGill developed static strength and fatigue analysis FE code was successful for flat plate cases. Results comparable with those presented by the programmer[37] were obtained. The failure to model fatigue of the SSI pipe using the McGill developed FE code was due to the code having insufficient boundary condition alternatives. It was also found that if the tensile properties of the material were lower than the compressive, as is the case for matrix dominated properties (Table 25), the mathematical relation (Equation 27) used in the FE code had inherent discontinuities under these conditions. Detection of the discontinuity required a small induced stress in the analysed structure.

An experimental technique for four-point bending of composite pipe was successfully developed. Results from the experimental work were found to be consistent and repeatable. Some scatter is evident, but this can most probably be contributed to statistical variations in composite material properties or pipe[55]. Statistical differences arise from, among other things, the manufacturing process, but also the constituent materials themselves have such variations.

The Maximum stress criterion was successfully used to identify the first failure mode. It is however unable to identify final failure correctly, as a proper material property reduction routine was not included. Initial matrix cracking is considered to be inherent to the SSI pipe, and taken into account during the design phase of the pipe. The McGill developed FE code had features enabling identification of the various stages of failure for a composite material. The code lacked the ability to analyse proper three-dimensional geometries, but for flat plates with three-dimensional stress state present, it was shown to correctly identify the failure sequence[27]. Future work on failure analysis of composite pipe should look into using strain based failure criteria, and reforming of the relevant constituent matrices based on reduction in properties after first failure mode detected.

Composite materials are of nature at least orthotropic and have a more complex stress-strain relationship than isotropic materials. The complexity combined with the difference in loading capacity in the various directions of the pipe, gives rise to the observed complex mode of failure. Both for static and fatigue bending, tensile de-laminations (normal through thickness stresses) were clearly present. As mentioned in be preceding paragraph, better analysis tools for SSI pipes are possibly strain dependent failure criterions. The reason being that we can measure surface strains, at least axial, hoop and shear strains directly, whilst it is necessary to calculate stress magnitudes using either measured or theoretically determined material properties. Statistical differences in material properties will contribute towards scatter and differences in apparent stress values within the SSI pipe. The use of simple beam equations means that three-dimensional stresses are not reported.

Reported bending stiffness, and the derived elastic bending moduli have also been estimated using a simplified approach. The values are consistent and repeatable. More accurate bending stiffness figures would have been possible to find if strain gauges measuring surface hoop and shear strains had been included. But as mentioned in the previous paragraph, final failure suggest high through thickness stresses and strains being present, and as no method of measuring these was used, their contribution is unknown. It is the belief of the author that through thickness stresses play a significant role in the failure sequence of SSI pipes, both for static and dynamic fatigue cases.

The fatigue capacity of the SSI pipe at high applied loads (high strains) was very good. For an applied load of 95% of ultimate static bending strain, the pipe proved capable of sustaining about 1200 bending cycles before failure. At lower load levels, 75% of ultimate static bending strain, 10 000 cycles seemed to be the upper limit (Figure 46). This is a very good result if we look at the conditions and limitations put on pipe laying operations. The ability to sustain high strains over as many as bending 1000 cycles is also positive with respect to the always present possibility of operational errors resulting in overloading. A note of caution is in place however, this research did not include post fatigue pressure testing. Without having pressurised pipes exposed to a given number of bending cycles and a given load or strain level, it is difficult to give a reliable estimate of the residual pressure capacity of the SSI pipe.

As has been mentioned several times previously, there is a consistent measured difference in off-axis axial surface strain between the compressive and tensile pipe faces for the same applied load (measured MTS cross-head displacement). In APPENDIX F, this is illustrated graphically. At present, the most plausible is difference in material properties, notably for matrix dominated behaviour, possibly combined with geometrical effects. The geometrical effects may not be apparent initially, but rather become more pronounced with increased bending loads (in static cases) and number of bending cycles (for fatigue cases). When bent, the pipe will no longer be perfectly round. However, at what level of bending strains this out-of-roundness becomes an important factor is currently unknown. The combination of these effects results in a shift in the neutral axis. As is obvious in Figure 49 and Figure 50, the neutral axis moves towards the compressive pipe face.

From the measured surface strain differences and the work in APPENDIX F, the data shows that the compressive modulus must be higher than the tensile modulus for the pipe structure. This must be the case in order for the structure to be stable; the compressive bending stiffness must be equal in magnitude to the tensile bending stiffness of the pipe structure. As can be seen in Figure 49 and Figure 50, the area of the pipe structure apparently kept in tension is larger than that maintained in compression.

The experimental part of the research also showed very good repeatability and consistent difference in retained stiffness at final fatigue failure dependent upon the applied load. Pipes exposed to higher loads had more retained bending stiffness at point of failure than pipes exposed to lower loads (Figure 42). This is most probably due to differences in failure mode. High loads, thus high strains, have failure modes synonymous with fibre failures, whilst lower loads allows for matrix crack growth and most importantly inter-ply de-lamination growth.

From static testing with strains measured using strain gauges it was found that the pipe structure largely behaves linearly in four-point bending (Figure 31). In reality there are two mechanisms involved giving rise to the curves in Figure 31: visco-elasticity and matrix cracking. Visco-elasticity is responsible for the non-linear behaviour, whilst matrix cracking causes the permanent set seen on the curve. This is called the hysterisis effect. Literature generally suggests that fibre reinforced composites behave non-linearly[37] but as can be seen in Figure 31 the SSI pipe show limited non-linear behaviour. Particular attention should be made to relaxation after maximum load release. This is a largely linear region. During loading the curves have indications of non-linearity. Closer examination of the curves and the pipe after testing suggest matrix crack opening to be the culprit for this observed behaviour. The permanent strain measured and seen in Figure 31 after load release is due to matrix cracking.

Examination of curves showing change in bending stiffness, for example Figure 32 or Figure 39, shows three different (possibly four) stages in fatigue failure. The first stage is initial matrix cracking and fibre-matrix shearing. This stage lasts for a limited number of cycles, dependent upon the applied load. Large loads mean a shorter initial damage sequence. Next comes the longest stage. This lasts for most of the fatigue life of the pipe, and has a constant rate of decrease in bending stiffness. During this stage matrix cracks grow and de-lamination is initiated and grows. Limited fibre fracture may also take place. The final stage is rapid, and takes place over approximately the same amount of time as the initial stage. Here, rapid and extensive de-lamination, as well as fibre fracture, are the dominant modes of failure.

9 Conclusions

The SSI has limited high strain bending fatigue capability, although it behaved surprisingly well in testing, with more than 1000 cycles completed at 95% of ultimate bending strength.

SSI has sufficient dynamic fatigue capability to survive high dynamic strain events. As no pressure testing was performed on fatigued although not failed pipe, it is not possible to conclude anything with respect to pressure handling capacity of the pipe after fatigue loading. Indications are however that for the strains expected during normal installation and operating conditions, fatigue will not cause undue damage to the pipe.

Visual inspection of failed pipes suggests an alternative to complete removal of axial fibres may be put forward. The buckling mode towards the centre of the pipe through the softer liner can possibly be prevented by moving the axial ply inside the laminate where it is more restrained from the observed buckling mode.

Future tests should be performed using instrumented pipes. For long term cyclic analysis, extensiometers on both the compressive and tensile faces of the SSI should be considered used. Strain gauges may give good results for static tests in cases where surface preparations have been optimal.

Surface finish of the SSI can affect the position of matrix cracking initiation. Observations suggest matrix cracking to be initiated in the valleys on the surface. The topography is a result of the dimensions of the fibre tow bundles used to manufacture the pipe. Finer (smaller) fibre bundles will yield smoother surface finish, as will refinement of the manufacturing process.

Differences in apparent bending stiffness for the compressive and tensile faces of the pipe can be contributed to:

a) geometrical effects. These can be inherent to the pipe, a result of the experimental set-up or combination of the two.

b) difference in compressive and tensile matrix properties of composites also contribute towards this apparent difference in compressive and tensile bending stiffness.

The test set-up should possibly be modified if further experimental work is to be performed. Notably changing the roller material to a softer polymer to reduce matrix crushing underneath the rollers should be considered. Evaluation of the support span and the distance between the two points of load application should also be performed.

Experimental and numerical findings only show limited correlation.

For static analysis on I-DEAS the correlation is not bad. The differences can be contributed to the following factors:

- The pipe was modelled using thin-shell elements. These are best suitable for thin walled pipes. The SSI has a thick laminate wall.
- I-DEAS did not modelled the shift in the neutral axis, hence predicted equal but opposite stress and strain results on the compressive and tensile faces of the pipe.
- Finite Elment analysis should have been performed with element formulations capable of three-dimensional analysis.

The finite element code developed by MMS[37] proved unable to model pipes structures.

- It lacked the necessary transformation routines for three-dimensional geometries.
- The boundary conditions available were limited to "loads" applied as element face pressures, and node translation restrictions. This was insufficient for global – local numerical analysis using I-DEAS for global and MMS code for local numerical analysis.

Attempts on experimental analysis of torsion loading were not successful. The loads that could safely be applied did not initiate damage in the pipe. The set-up was also deemed unsafe for fatigue experiments with a constant applied torque.

10 Recommendations for Further Work

The spoolable composite injection line pipe is designed for internal static pressure only. Bending fatigue of the pipe is only likely to happen during pipe laying operations. Thus, future work should seek to investigate the effect of bending fatigue on the pressure handling capability.

Torsion analysis, neither numerical nor experimental, of the composite pipe was successfully executed. Future work should seek to investigate this loading mode more carefully. Pressure handling capability should also be investigated following torsional loading.

Numerical analysis tools for fatigue analysis of composite pipes should be sought. Using the work by Shokrieh[27] and Lessard[27] as basis, a module for, for example ABAQUS could be developed.

Future numerical analysis should be executed using three-dimensional analysis capable elements, for example 8 node orthotropic soild for linear analysis, and a 20 node orthotropic for non-linear analysis. Numerical analysis work should also be performed in several stages, with initial analysis being done using an isotropic material formulation to enable optimisation of the mesh.

The mathematical relations for fatigue analysis of composites as presented by Shokrieh[37] should be investigated with respect to cases where the induced stresses are very small or any of the properties is higher in compression than in tension.

APPENDIX A Composite Materia l Properties

Table 25 Material Properties used in Analytical and Numerical Analysis Work

Property		Value	Unit
Longitudinal Elastic Modulus	E_x	45.50	GPa
Transverse Elastic Modulus	E_y	8.0	GPa
Shear Elastic Modulus (In-plane)	E_s or G	3.5 – 5.0	GPa
Longitudinal Tensile Strength	X_t	1100	MPa
Longitudinal Compressive Strength	X_c	610	MPa
Transverse Tensile Strength	Y_t	50	MPa
Transverse Compressive Strength	Y_c	120	MPa
In-Plane Shear Strength	S	60	MPa
Longitudinal Ultimate Tensile Strain	ε_{xt}	2.4	-
Longitudinal Ultimate Compressive Strain	ε_{xc}	1.6	-
Transverse Ultimate Tensile Strain	ε_{yt}	0.6	-
Longitudinal Ultimate Compressive Strain	ε_{yt}	1.5	-
In-Plane Ultimate Shear Strain	ε_s	1.8	-
Poisson's Ratio	ν_{xy}	0.3	-

APPENDIX B Equivalent Enginee ring Bending Stiffness (EI)of Laminated Composite Pipe

By assuming the composite structure at hand to satisfy all assumptions made for simple beams, and to satisfy the equilibrium equations as follows

Equation 37

$$\frac{\partial N_1}{\partial x_1} = 0$$

and

Equation 38

$$\frac{\partial^2 M_1}{\partial x_1^2} + q(x_1) + N_1^0 \frac{\partial^2 w}{\partial x_1^2} = 0$$

where:

N_1	Force in the x1-direction (in-plane load)
M_1	Bending moment
x_1	Element in x1-direction
$q(x_1)$	Distributed load lateral load
w	Element in downward direction (deflection)

Also by assuming Kirchhoff's assumption to be valid (small deflection), and by determining the moment deflection relations for laminated tubes

Equation 39

$$M_1 = \int_A \sigma_1 \times x_3 dA = \int_0^{2\pi} \int_{r_i}^{r_0} \sigma_1 x_3 r dr d\theta$$

where:

A	Area
σ_1	Stress in the 1-directionof the pipe
x_3	Downward motion/deflection
r	Radius of pipe
r_i	Inner radius of pipe
r_0	Outer radius of pipe

Working through this eventually gives

Equation 40

$$M_1 = B_x e_1^0 + D_x k_1$$

where:

B_x	Shear coupling term
D_x	Equivalent bending stiffness of composite pipe
k_1	Curvature
e_1^0	Strain in 1-direction

For cylindrical tubes, B_x reduces to zero[40(pp273)]. This reduces Equation 40 to

Equation 41

$$M_1 = D_x k_1$$

Where D_x can be expressed as

Equation 42

$$D_x = \frac{\pi}{4} \sum_{k=1}^{M} Q_{11}^k \left[(r_i + t_k)^4 - (r_i + t_{k-1})^4 \right]$$

where:

k	Number of layers or plies
Q_{11}^k	Stiffness element (11) in the ply stiffness matrix for ply k
r_i	Inner radius of pipe
t_k	Thickness of ply k
t_{k-1}	Thickness of ply k-1

To find Q_{11}^k, the material properties for a unidirectional ply must be determined (APPENDIX A). These material properties are then used to find the compliance matrix [S], and then the stiffness matrix [S] (relates to on-axis properties). Note that plane stress is assumed.

By transforming the on-axis stiffness matrix to off-axis format, the Q_{11} values can be found. The figures following this paragraph outlines this work. A comprehensive description on this can be found in reference 40, chapter 3, with a summary in table 3.9, and details in equation 3.29 in the same.

The stiffness Q_{11} of a ply is found using the following set of equations and the material properties given in APPENDIX A. Relationships described in Table 26 and Table 27 can easily be found by knowing the material properties of a given composite material.

Table 26 On-Axis Strain-Stress for Uni-Directional Ply in Terms of Engineering Constants

	σ_x	σ_y	σ_s
e_x	$\frac{1}{E_x}$	$-\frac{\nu_{yx}}{E_y}$	
e_y	$-\frac{\nu_{xy}}{E_x}$	$\frac{1}{E_y}$	
e_s			$\frac{1}{E_s}$

Table 27 Compliance Matrix (On-Axis Strain-Stress for Uni-Directional Ply in Terms of Compliance)

	σ_x	σ_y	σ_s
e_x	S_{xx}	S_{xy}	
e_y	S_{yx}	S_{yy}	
e_s			S_{ss}

By viewing the tables above as matricies, stress-strain relationships can be obtained by inverting the matricies.

Table 28 Modulus Matrix (On-Axis Strain-Stress for Uni-Directional Ply in Terms of Modulus)

	e_x	e_y	e_s
σ_x	Q_{xx}	Q_{xy}	
σ_y	Q_{yx}	Q_{yy}	
σ_s			Q_{ss}

We have that

Equation 43

$$Q_{xx} = mE_x$$

Equation 44

$$Q_{yy} = mE_y$$

Equation 45

$$Q_{yx} = m\nu_{xy}E_y$$

Equation 46

$$Q_{xy} = m\nu_{yx}E_x$$

Equation 47

$$Q_{ss} = E_s$$

Equation 48

$$m = \left(1 - \nu_{xy}\nu_{yx}\right)^{-1}$$

m can be found by assuming that the material is orthotropic, hence the relationship

Equation 49

$$\frac{\nu_{xy}}{\nu_{yx}} = \frac{E_x}{E_y}$$

holds, as well as

Equation 50

$$S_{xy} = S_{yx}$$

and

Equation 51

$$Q_{xy} = Q_{yx}$$

In order to transform the calculated properties from "on-axis" to an "off-axis" system, the angle between the on-axis (local or material) and the off-axis (global) system must be known. Given the angle θ, we have that $z = \cos\theta$ and $n = \sin\theta$. Eventually, the relationship between on-axis and off-axis modulus is found (Table 29) to be

Equation 52

$$U_1 = \frac{1}{8}\left[3Q_{xx} + 3Q_{yy} + 2Q_{xy} + 4Q_{ss}\right]$$

Equation 53

$$U_2 = \frac{1}{2}\left[Q_{xx} - Q_{yy}\right]$$

Equation 54

$$U_3 = \frac{1}{8}\left[Q_{xx} + Q_{yy} - 2Q_{xy} - 4Q_{ss}\right]$$

Equation 55

$$U_4 = \frac{1}{8}\left[Q_{xx} + Q_{yy} + 6Q_{xy} - 4Q_{ss}\right]$$

Equation 56

$$U_5 = \frac{1}{8}\left[Q_{xx} + Q_{yy} - 2Q_{xy} + 4Q_{ss}\right]$$

Table 29 Relationship Between On-Axis and Off-Axis Modulus (Stiffness) Given in Multiple Angle Functions

	1	U_2	U_3
Q_{11}	U1	$\cos 2\theta$	$\cos 4\theta$
Q_{22}	U1	$-\cos 2\theta$	$\cos 4\theta$
Q_{12}	U4		$-\cos 4\theta$
Q_{66}	U5		$-\cos 4\theta$
Q_{16}		$\frac{1}{2}\sin 2\theta$	$\sin 4\theta$
Q_{26}		$\frac{1}{2}\sin 2\theta$	$-\sin 4\theta$

Using this method, the equivalent bending stiffness of the SSI pipe was found to be 31143 Pa*m^4.

INPUT

Ex	45.5	GPa
Ey	8	MPa
Es	3.5	MPa
nux	0.3	-
Xt	1100	MPa
Xc	610	MPa
Yt	50	MPa
Yc	120	MPa
S	60	MPa
ext	2.4	
exc	1 6	
yet	0.6	
eyc	1.5	
es	1.8	
alfax	0.0000071	
alfay	0.00003	
alfaz	0.00003	
rho	2055	
nuy	=C6*C4/C3	

Angle	0
	=C23*2*PI()/180
	78
	=C25*PI()/180
	-78
	=C27*PI()/180

ID	69.5	mm
	=C32*0.001	m
ri	=C33/2	m
OD	91	mm
	=C35*0.001	m
ro	=C36/2	m
tlam	=C37-C34	m
	=(C39-to)/8	
0 deg ply	2.3	mm
	=C41*0.001	m
78 degree plies	1.0563	mm
	=C40	m

Figure 48 Input Material Properties and Values for Calculation of Equivalent Bending Stiffness of Composite Pipe

APPENDIX C Equivalent Engineering Shear Modulus (G) of Laminated Composite Pipe

Laminate theory is used to find the shear modulus (G) of the laminate making up the composite pipe[40(Chapter 4)]. Exact description of equations can be found in the reference[40].

It was assumed that the in-plane shear modulus could be set equal to the equivalent engineering shear modulus

Equation 57

$$E_6^0 = \frac{}{a_{66}h}$$

By using the Us found in APPENDIX B (Equation 52 to Equation 56) and four geomtrical factors denoted V_1 through to V_4, it is possible to determine the in-plane modulus of a laminate [A]. Having found [A] and inverted it to obtain [a], the in-plane shear modulus was calculated. Each ply orientation has a $V_{1\to4}$ and by summing these over their thicknesses within the laminate we get the following relationship

Equation 58

$$V_{[1,2,3,4]} = \int_{-h/2}^{h/2} [\cos 2\theta, \cos 4\theta, \sin 2\theta, \sin 4\theta] dz$$

Table 30 In-Plane Modulus of Laminates

	h	U_2	U_3
A_{11}	U_1	V_1	V_2
A_{22}	U_1	$-V_1$	V_2
A_{12}	U_4		$-V_2$
A_{66}	U_5		$-V_2$
A_{16}		$1/2V_3$	V_4
A_{26}		$1/2V_3$	$-V_4$

h here is defined as laminate thickness.

V_1, for example, was found by summing the different ply groups within the laminate (0° and ±78°) as shown in Equation 59 below.

Equation 59

$$V_1 = \sum_{i=1}^{m} \cos 2\theta_i h_i$$

h_i is the thickness of ply group i, and with i is referenced to the mid-plane. Similar summations was performed for V_2, V_3 and V_4.

With [A] now fully defined, a simple matrix inversion yields the [a] matrix. Using the value for a_{66}, the equivalent engineering shear modulus was found.

Uni-directional ply material properties are the same as listed in Figure 48.

The shear modulus Es (or G) was found to be 4.65 GPa. This value found for G (Es) is larger than the shear modulus for the uni-directional ply (Table 25 and Figure 48). This is not entirely unexpected, as large parts of the composite laminate consists of ±78° plies, and a much thinner 0° ply. Hence, the contribution from the ± plies is large, and the apparent modulus when loaded to induce shear follows.

Torsional stiffness is given by

Equation 60

$$GJ = G_{equiv.} * \frac{\pi}{2} * \left(r_o^4 - r_i^4\right)$$

where

G_{equiv}	Engineering equivalent shear modulus
J	Polar second moment of area

Using composite pipe dimensional values (Table 1) and the equivalent engineering shear modulus, we find the torsional stiffness to be 20670.0 Pa*m^4.

APPENDIX D Goodness of Curve Fit

R_{fit}^2

Excel indicates the quality of a curve fit by an R_{fit}^2 value. This number has a value between 0 and 1. A value of 1 indicates a perfect correlation between the data and the least squares line fit through the same data points. For more information, please refer to Microsoft® Excel 97 help function.

R_{fit}^2 is a function of the Y-values and the number of data points as follows:

Equation 61

$$R_{fit}^2 = \frac{\Sigma\left(Y_i - \tilde{Y}_i\right)^2}{\left(\Sigma Y_i^2\right) - \frac{\left(\Sigma Y_i\right)^2}{n}}$$

Y_i	Y-value i
$\tilde{Y}$	Average Y-value
n	Number of data points (Y-values)

APPENDIX E Definitions

Off-Axis Axial Stress	Stress acting along the longitudinal axis of the pipe.
Off-Axis	Relates to global co-ordinate system of the/a structure
Epoxy	Thermosetting Polymer
Thermosetting Polymer	Polymer supplied as two or more liquids that are subsequently mixed and heated according to given specifications in order to obtain a solid material with given properties
Polymer	Chain of organic molecules organised to give solid material properties
Fatigue test start	The fatigue test is defined as having started on the first cycle where the pre-decided constant applied load is registered
First fatigue cycle	First cycle where the pre-determined applied load is reached
Fatigue life	Defined as the point where the stiffness – or registered MTS cross-head displacement drops more than 5% over two registered values or 10 cycles
Initial damage sequence	100 to 400 cycles from first registered fatigue cycle

δ	Non-linearity parameter (value material dependent and should be measured). If equal to zero linearity is assumed
α	Curve fitting parameter
β	Curve fitting parameter
σ	Magnitude of applied maximum stress
λ	Curve fitting parameter
γ	Curve fitting parameter
θ	Angle of twist, given in radians/m (degrees/m are also used for presentation purposes)
γ	Shear strain (-)
τ	Shear stress (MPa)
δ_d	Mid-point deflection (m)
ε_1	Assumed to be surface strain on the outer surface of the SSI pipe in the axial direction of the pipe (off-axis 1 direction of the surface ply)
σ_1	Off-Axis axial stress in pipe at the external pipe surface due to bending
σ_1^k	Stress in the off-axis axial 1 direction of the pipe in ply k
σ_a	Alternating stress
σ_c	Compressive strength
ε_f	Average strain to failure, assumed to be independent of n and σ
σ_m	Mean stress

σ_{max}	Maximum stress
σ_{min}	Minimum stress
σ_t	Tensile strength
σ_{xx}	On-axis stress in x-direction (along fibre axis)
σ_{xy}	On-axis stress in xy-direction (in-plane shear direction)
σ_{xz}	On-axis stress in xz-direction (out-of-plane shear direction)
σ_{yy}	On-axis stress in y-direction (transverse to fibre axis)
σ_{yz}	On-axis stress in yz-direction (out-of-plane shear direction)
σ_{zz}	On-axis stress in z (normal)-direction (normal to the xy plane)
a	Distance from guided end of pipe to point of load application
D	Bending diameter of the pipe (m)
D_x	Equivalent engineering constant for bending stiffness EI from Table 3
E	Young's Modulus (Pa)
$E(n, \sigma, \kappa)$	Residual stiffness for arbitrary number of cycles, state of stress and stress ratio of a unidirectional ply
e_1^0	In-plane strain
e_F^{-}	Failure parameter. If equal to or larger than 1, failure has occurred in fibre compression
e_F^{+2}	Failure parameter. If equal to or larger than 1, failure has occurred in fibre tension
e_{FM}^{-}	Failure parameter. If equal to or larger than 1, failure has occurred in defines fibre-matrix shearing
e_M^{+2}	Failure parameter. If equal to or larger than 1, failure has occurred in matrix tension.
e_M^{-2}	Failure parameter. If equal to or larger than 1, failure has occurred in matrix compression
e_N^{+2}	Failure parameter. If equal to or larger than 1, failure has occurred in normal tension
e_N^{-2}	Failure parameter. If equal to or larger than 1, failure has occurred in normal compression
E_s	Static stiffness
E_{xx}	On-axis stiffness in x-direction (along fibre axis)
E_{xy}	Shear stiffness in xy-plane (in-plane shear direction)
E_{xz}	Shear stiffness in xz-plane (out-of-plane shear direction)
f	Curve fitting constant, assumed to be 1.06
F	Applied load/force – using Newton (N)
G	Shear modulus (GPa)
I	Second moment of inertia
J	Polar moment of inertia

K	Load or Stress ratio
k_1	Inverse of pipe radius of curvature or curvature along the 1 axis (1/R)
l	Distance from centre of pipe (guided end) to simply supported end of pipe
L	Length of pipe section investigated (m)
M	Bending moment (Nm)
M_1	Bending moment
M_A	Bending moment at point A found by Equation 6 equal to M_1
n	Number of applied cycles
N_f	Number of cycles to failure (or fatigue life) at σ and a given κ
P_{max}	Maximum applied load
P_{min}	Minimum applied load
Q_{11}^k	Off axis stiffness of ply k in the 11 direction
R	Radius of curvature or bending radius of the pipe assumed to measured along the central neutral axis of the pipe
r	Distance from centre of pipe to outer "outer fibre" of pipe wall in Equation 29 on page 47 (m)
$x_3 \times k_1$	Flexural deformation
$R(n, \sigma, \kappa)$	Residual strength for arbitrary number of cycles, state of stress and stress ratio of a unidirectional ply
R_s	Static strength
S_{xy}	In-plane shear strength
S_{xz}	Out-of-plane shear strength
S_{yz}	Out-of-plane shear strength
T	Torsional moment (Nm)
t	Laminate wall thickness (m)
W	½ of MTS applied load
x	Distance from guided end to point of interest. This case: $x = a$
x_3	Distance from centre of pipe (neutral axis) to a point on/in the pipe wall where stress is sought determined. Direction in this case is defined to be down with the movement of the pipe as it is bent.
X_c	Fibre compressive strength
X_t	Fibre tensile strength
Y	Distance from the assumed neutral axis of the pipe to the point where the strain is measured
Y_A	Deflection (maximum) at the guided end of the pipe
Y_a	Deflection at point x, in this case point of load application, a
Y_t	Matrix tensile strength
Z_t	Normal tensile strength

APPENDIX F Shift in Neutral Axis

Shift in the neutral axis is apparent from the difference in measured strain on the compressive and tensile pipe surfaces. Tensile strain is higher, as can be seen in Figure 49 and Figure 50 below. The strain values used in Figure 49 are calculated from Equation 32 and Equation 33.

Figure 49 is drawn to scale, and as is clearly visible, the neutral axis shifts towards the top face of the pipe (the compressive face). The shift is found, from the graphical representation, to be about 7.2 mm.

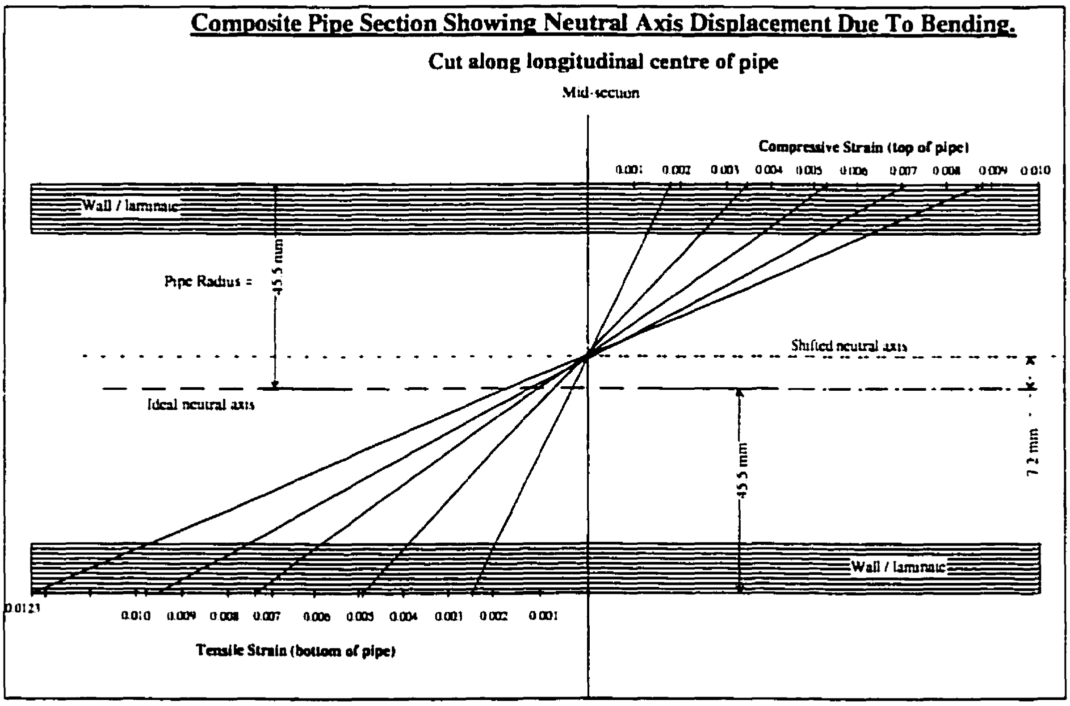

Figure 49 Shift in Neutral Pipe Axis as Would be Seen from the Side of the Pipe

Looking at Figure 50, and sketching in the new neutral axis as found in Figure 49, it can be seen that the area of the pipe section retained in compression is reduced. In order for the structure to remain in stable equilibrium, the bending stiffness of the part of the pipe held in compression must equal the bending stiffness of the part of the pipe held in tension. By inspection of Figure 50, it is obvious that the second moment of inertia (I) of the pipe sections A (top / compressive face) and B (bottom / tensile face) must be different. But, from the statement requiring the structure to be stable, we can then deduce that there must be a difference in compressive and tensile modulus.

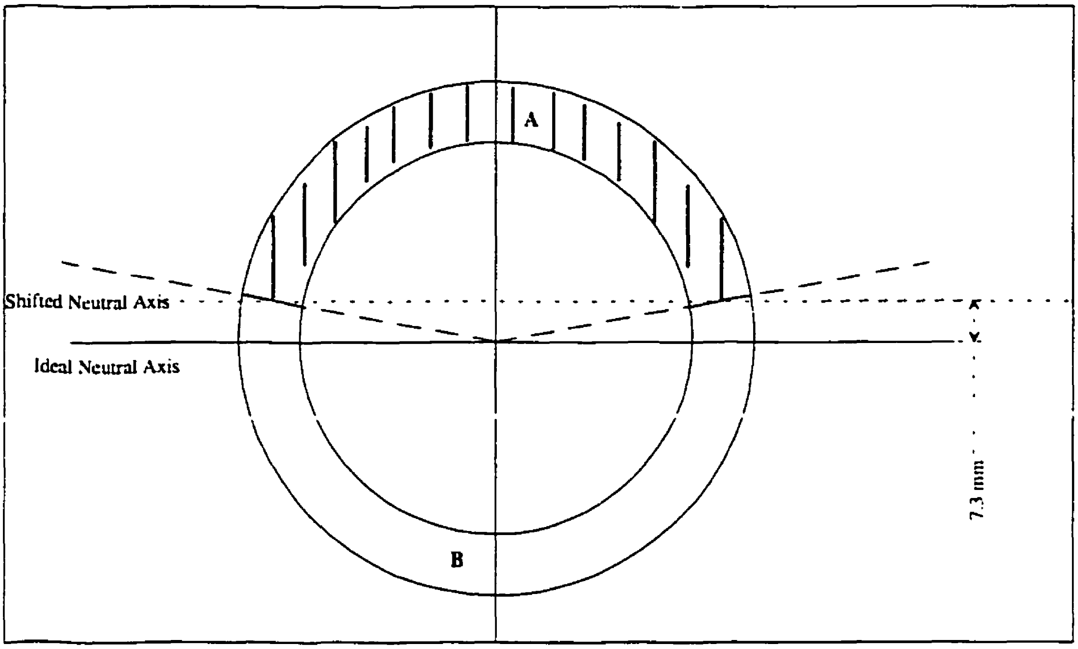

Figure 50 Shift in Neutral Axis as Would be Seen Through a Transverse Pipe Section

The shift in neutral axis represented graphically is about 8%.

From reference 42, table 1, rows 20 and 22, it is possible to estimate the moment of inertia for the pipe section with a displaced neutral axis. It will not provide an entirely accurate answer, but give a reasonable indication of the situation.

From observation and previous experience, it is known that the pipe has matrix and /or matrix-fibre shearing cracking initiated in the laminate as a result of spooling. These cracks mean that the laminate has lost most of its stiffness properties in the tensile matrix direction. The compressive properties however, are to a certain extent intact. Of the compressive properties it is a fair assumption that compressive stiffness is retained to some percentage. Thus, as part of several factors, matrix cracking and the residual properties following contributes towards the measured differences in surface strain.

The observed final failure, as apparent through-thickness (normal) tensile de-lamination on the compressive side is somewhat more difficult to explain. Again, initiated matrix cracks may play a role, but inherent material properties may also be important.

Explanations other than a difference in material properties, in this case stiffness, includes:

Measurement errors throughout the experimental phase.	Not very plausible, as some pipes where turned 180 degrees between each bending, hence moving the extensiometer and/or strain gauges from compressive to tensile faces (or vice versa)

without interfering with calibration devices. Calibration of equipment may not have been as good as one would hope for. However, the consistency and repeatability of the readings from both extensiometer and strain gauges indicates this type of error to be small.

Some experimental errors will be present

- The experimental set-up may have inherent flaws giving rise to, if not faulty, so at least inaccurate readings. However, again the consistency and repeatability of all results indicates a reasonably good experimental set-up to be in place.

REFERENCES

[1] Advanced Materials AS together with among others Conoco, Amoco, Saga Petroleum, Elf, Statoil, Enterprise Oil, Shell in several Joint Industry Projects (JIP) between 1988 and 1995. Continuation through Compipe AS from 1995

[2] NAT Compipe, product qualified as of 1997, first commercial contract January 1999 in co-operation with Statoil

[3] Troll Onshore Gas Terminal facilities at Kollsnes, Bergen, Norway, completed 1996. Composite access structures. NAT Compipe documentation.

[4] Valhall Wellhead Platform, North Sea 1996. Composite deluge fire water system. NAT Compipe documentation

[5] Mars Platform, Gulf of Mexico. Top side structures, accumulator bottles, hydraulic pistons etc. Total composite usage exceeding 250 metric tonnes. 1998. Private communication with Douglas Johnson of Lincoln Composites

[6] T.J. Corbishley "Installation Methods Including Towed Pipeline Bundles" Lecture 15, Lecture notes on Subsea and Pipeline Engineering presented at University College London, 26 – 28 October 1993, page 15.5

[7] A. Sas-Jaworsky "Coiled Tubing Operations", 1993

[8] P. Odru "paper from 1979, could not find the title", Institute Francais du Petrolier, 1979

[9] M M. Salama, "Some Challenges and Innovations for Deepwater Developments", SPE, Conoco, OTC 8455, 1997

[10] N.L. Newhouse, D.B. Johnson, D.D. Baldwin, "Design and Qualification of Advanced Composites for Marine Applications", Lincoln Composites, OTC 8568, 1997

[11] D.D. Baldwin & N.L. Newhouse, Lincoln Composites, K.H. Lo, Shell Oil Products Company, R.C. Burden, Hydril Company, "Composite Production Riser Design" OTC 8431, 1997

[12] M.D. Drey, Lincoln Composites, M.M. Salama, SPE, Conoco, Inc, J.R. Long, Stress Engineering Services, Inc, M.G. Abdallah, Hexcel Corp, S.S. Wang, CEAC/University of Houston, "Composite Production Riser - Testing and Qualification", OTC 8432, 1997

[13] W.F. Andersen, J.J. Anderson, C.S. Mickelson, Northrop Grumman Marine Systems, T.F. Sweeney, ABB Vetco grey, "The Application of Advanced Composite Technology to Marine Drilling Riser Systems: Design, Manufacturing and Test", OTC 8433, 1997

[14] Alex. Y. Lou, Phillips Petroleum Company, Chris Lundberg, Summit Composites Corporation, "Composite Drill Pipe for Extended Reach Horizontal Drilling" OTC 8434, 1997

[15] Fikry Botros, Jerry Williams, Conoco Inc, Edward Coyle, DuPont, "Application of Composite Materials in Deep Water Offshore Platforms", OTC 8500, 1997

[16] NAT Compipe AS and Stena Coflexip Offshore, Spoolable composite pipe and unbonded flexible polymer, fibre and metal pipes respectively. Development efforts and commercialisation from late 1980s, to today and further into the future.

[17] Hydril Joint Industry Project, Fiberspar, Lincoln Composite: Spoolable composite pipe, continuous for injection line, flowline and/or coiled tubing applications and segmented for riser systems both production and drilling. Ongoing projects

[18] P.A. Quigley, S.C. Nolet, Fiberspar Inc, J.G. Williams, Conoco Inc, A. Sas-Jaworsky, SAS Industries Inc, "Development and Application of a Novel Coiled Tubing String for Concentric Workover Services", OTC 8456, 1997

[19] A.B. Hansen, B.Asdal, Compipe AS, T. Meland, I.O. Grytdal, Statoil, "Qualification and Verification of Spoolable High Pressure Composite Service Lines for the Åsgard Field Development Project", OTC 8436, 1997

[20] K.L. Reifschnider Ed. "Damage in Composite Materials" ASTM STP 775, 1982

[21] D.S. Saunders, G. Clark, Department of Defence, Aeronautical and Maritime Research Laboratory, Melbourne, Australia, "Fatigue Damage in composite Laminates", Materials Forum (1993) 17, pp 309-331

[22] K.L. Reifsnider, D.A. Dillard, A.H. Cardon (editors), "Progress in Durability Analysis of Composite Systems", Proceedings of the Third International Conference on Progress in Durability analysis of Composite Systems, Blacksburg, Virginia, USA, 14-17 September 1997. A.A.Balkema, Rotterdam, NL (Publishers)

[23] Z. Gao, "Numerical modeling of damage, property degradation and life prediction in fatigue of composite lamiantes", from "Numerical Analysis and Modelling of Composite Materials" edited by J.W. Bull, Blackie Academic & Professional, 1996

[24] S.W. Tsai and H.T. Hahn " Introduction to Composite Materials" Technomic Publishing Co., Inc., Westport, CT, 1980

[25] J. Lee, B. Harris, D.P. Almond, F. Hammett, School of Materials Science, University of Bath, UK, " Fibre composite fatigue-life determination", Composites Science and technology, 1997, Elsevier

[26] J. Botsis, D. Zhao, Dept of Civil and Materials Engineering, University of Illinois at Chicago, "Fatigue fracture process in a model composite", Composites Science and technology, 1997, Elsevier

[27] M.M. Shokrieh, L.B. Lessard, Dept. of Mech. Engineering, McGill University, Canada, "Residual Strength and Fatigue Life of Unidirectional Composite Plies under Multiaxial Fatigue Loading"

[28] S.R. Frost, A. Cervenka, "Glass fibre-reinforced epoxy matrix filament-wound pipes for use in the oil industry", Composites Manufacturing, vol 5, No 2, 1994, Butterworth-Heinemann Ltd.

[29] P.M. Jelf, N.A.Fleck, Cambridge University Engineering Department, "The failure of composite tubes due to combined compression and torsion", Journal of Materials Science 29 (1994), p. 3080 - 3084, Chapman & Hall

[30] A. Khdeir, J.N. Reddy, "An Exact Solution for the Bending of Thin and Thick Cross-ply Laminated Beams", Composite Structures 1997, V.37, no.2, p.195

[31] M.S. Bhalerao, T.j. Moon, "Micromechanics of Local Viscoelastic Buckling in Thick Composites", Composites - Part B - Engineering 1996

[32] C.Kim, S.R. White, "Analysis of Thick Hollow Composite Beams under General Loading", Composite Structures 1996, V.34, no.3, p.263

[33] A.W. Leissa, J-D. Chang, "Elastic Deformation of Thick Laminated Composite Shells", Composite Structures 1996, V.35, no.2, p153

[34] I.M. Daniel, H-M. Hsiao, S-C. Wooh, "Failure Mechanisms in Thick composites under Compressive Loading", Composites - Part B - Engineering 1996, V.27, no.6, p.543

[35] L. Kroll, W. Hufenbach, "Physically Based Failure criterion for Dimensioning of Thick Walled Laminates", Applied Composite Materials 1997, V.4, no.5, p.34

[36] I-DEAS finite element analysis software, Structural Dynamics and Research Corporation, 1998

[37] Mahmood M. Shokrieh, Dept. of Mech. Engineering, McGill University, Canada, "Progressive Fatigue Modeling of Composite Materials", Ph.D. Thesis, February 1996

[38] Compipe, internal research 1998

[39] Compipe spoolable composite service and injection line pipe qualification data

[40] Larry B. Lessard "Mechanics of Composite Materials", McGill course 305-561B (Mechanical Engineering), Spring 1997, pp 265 to 279

[41] P.P. Benham & R.J. Crawford "Mechanics of Engineering Materials", 5th ed.1991, Longman Scientific and Technical. Chapters 6 and 7 for bending, and chapter 5 for torsion

[42] Warren C. Young "Roark's Formulas for Stress and Strain", 6th ed 1989 ,McGraw-Hill Book Company, start on p 93 and table 3 for bending. And start on p 345 for torsion

[43] Warren C. Young "Roark's Formulas for Stress and Strain", 6th ed 1989 ,McGraw-Hill Book Company, p 101, table 3, column no.2.

[44] Jocelyn M. Seng, PhD, Owens Corning Science and Technology Center. Privat communication, "S-2 Glass Fiber. Enhanced properties for demanding applications", table in back of brochure.

[45] Larry B. Lessard "Mechanics of Composite Materials", McGill course 305-561B (Mechanical Engineering), Spring 1997, table C.3

[46] M.W. Hyer "Stress Analysis of Fiber-Reinforced Composite Materials" McGraw-Hill, 1998, pp348 - 386

[47] Klaus Jurgen Bathe "Finite Element Procedures", Prentice Hall, 1996

[48] T.Adam, N. Gathercole, H. Reiter, B. Harris, , School of Materials Science, University of Bath, UK., "Fatigue Life Prediction for Carbon Fibre Composites", Advanced Composites Letters, 1(1992) pp.23-26

[49] N. Gathercole, H. Reiter, T.Adam, B. Harris, School of Materials Science, University of Bath, UK, "Life Prediction for Fatigue of T800/524 Carbon-Fibre Composites: I Constant Amplitude Loading", International Journal of Fatigue, Vol 16 (nov. 1994), pp. 523-532

[50] M.M. Shokrieh, L.B. Lessard, Mechanical Engineering, McGill University, "Fatigue Behaviour of Composite Pinned/Bolted Joints – Part II Users Guide", Structures and Materials Research, Institute for Aerospace Research, National Research Council, Contract # 31946-1-0008/01-SR

[51] Privat communication with NAT Compipe ASA, phone +47 51 53 76 00

[52] Bent Asdal, 'Internal Documentation', Compipe AS, Norway, phone +47 51 53 76 00

[53] P.P.Benham, R.J. Crawford "Mechanics of Engineering Materials", Longman Scientific & Technical, 1987, pp 187 - 188

[54] P.A. Haug (NAT Compipe AS) and K I. Ekeberg (Alcatel Kabel Norge AS) "Dynamic Umbilical with Composite Tube (DUCT)", OTC 8887, 1998, May 4th – 7th, Houston, Texas

[55] S.S. Wang, X.Lu & Z.Q.Gong, CEAC, University of Houston, Houston, Texas, "Composite Production Riser Reliability Assessment: The Influence Of Probabilistic Fiber-Composite Strength", OTC Proceedings, 1998, OTC 8667

[56] D.Perreux, E.Joseph, Laboratoire de Mechanique Applique R.Chaleat, URA04 CNRS, UFR Sciences et Techniques, Besancon, France, "The Effect of Frequency on the Fatigue Performance of Filament-Wound Pipes under Biaxial Loading: Experimetnal Rersults and Damage Model", Composites Science and Technology 57 (1997) p. 353 - 364

[57] J.E. Shigley and L.D. Mtichell "Mechanical Engineering Design", McGraw-Hill Series in Mechanical Engineering, 4th edition, 1983, p 74.